



HAL
open science

Fischer Tropsch synthesis on conductive silicon carbide based support

Benoît De Tymowski

► **To cite this version:**

Benoît De Tymowski. Fischer Tropsch synthesis on conductive silicon carbide based support. Other. Université de Strasbourg, 2012. English. NNT : 2012STRAF019 . tel-00855282

HAL Id: tel-00855282

<https://theses.hal.science/tel-00855282>

Submitted on 29 Aug 2013

HAL is a multi-disciplinary open access archive for the deposit and dissemination of scientific research documents, whether they are published or not. The documents may come from teaching and research institutions in France or abroad, or from public or private research centers.

L'archive ouverte pluridisciplinaire **HAL**, est destinée au dépôt et à la diffusion de documents scientifiques de niveau recherche, publiés ou non, émanant des établissements d'enseignement et de recherche français ou étrangers, des laboratoires publics ou privés.

ÉCOLE DOCTORALE DES SCIENCES CHIMIQUES

UMR 7515

THÈSE

présentée par

Benoît de TYMOWSKI

soutenue le : **14 Septembre 2012**

pour obtenir le grade de

Docteur de l'université de Strasbourg

Discipline / Spécialité : Chimie

**Fischer Tropsch synthesis on conductive
silicon carbide based support**

**Synthèse de Fischer Tropsch sur support conducteur
à base de carbure de silicium**

THÈSE dirigée par :

M. PHAM-HUU Cuong

Directeur de recherches, UDS, Strasbourg

RAPPORTEURS :

M. KHODAKOV Andrei

Directeur de recherches, USTL, Lille

M. RONNING Magnus

Professeur, NTNU, Université de Trondheim, Norvège

MEMBRES DU JURY :

M. GARIN François

Directeur de recherches, UDS, Strasbourg

Mme PHAM Charlotte

Directeur Technique, SICAT, Willstätt

M. LUCK Francis

Directeur scientifique, TOTAL, Paris

Remerciements

Ce travail de thèse a été effectué à l'Ecole Européenne de Chimie, Polymère et Matériaux (ECPM) à l'Université de Strasbourg (UDS), au sein du Laboratoire des Matériaux Surfaces et Procédés pour la Catalyse (LMSPC), sous la direction de Cuong Pham-Huu, directeur de recherche au CNRS.

Tout d'abord, je tiens à remercier Cuong de m'avoir accueilli dans son équipe et de m'avoir guidé lors de ce travail.

Merci aussi à Charlotte Pham et Patrick Nguyen de la société SiCat pour les conseils et leur aide dans la réalisation de ce travail.

Je remercie la société TOTAL pour le financement de ce travail et plus particulièrement Francis Luck, directeur scientifique à Total et responsable de ce projet.

Je remercie également les membres du jury, Andrei Khodakov Directeur de recherches du CNRS à l'USTL de Lille, Magnus Ronning Professeur à l'Université de Trondheim NTNU en Norvège, François Garin, Directeur de recherche CNRS au LMSPC, Charlotte Pham, Directeur Technique, SICAT, Francis Luck Directeur scientifique de TOTAL.

Je remercie également mes prédécesseurs sur la synthèse Fischer-Tropsch, Maxime Lacroix et Lamia Dreibine pour m'avoir ouvert le chemin et m'avoir mis sur de bons rails pour la suite de mes travaux.

Je tiens également à remercier mes collègues et amis du LMSPC et tout particulièrement les membres de l'équipe « carbure et nanostructure ». Dominique Bégin, Izabela Janowska, Jean-Mario Nhut, Matthieu Houllé, Adrien Deneuve, Kambiz Chizari, Yu Liu, Shabnam Hajiesmaili, Ouanassa Guellati, Yuefeng Liu, Fabrice Vigneron, David Edouard. Je remercie également les ITAs du laboratoire à savoir Véronique Verkruysse, Thierry Romero, Alain Rach, Michel Wolf, Pierre Bernhardt et Thierry Dintzer.

Résumé – Abstract.....	1
1. Chapitre 1 : Introduction	
2. Chapitre 2 : Silicon Carbide Foam Composite Containing Cobalt as a Highly Selective and Re-Usable Fischer-Tropsch Synthesis Catalyst	
3. Chapitre 3 : Co-Ru/SiC impregnated with ethanol as an effective catalyst for the Fischer-Tropsch synthesis	
4. Chapitre 4 : Fischer-Tropsch Synthesis with Improved Active-Site Availability on a Large Pore Silicon Carbide Microspheres Containing Cobalt Catalyst	
5. Chapitre 5 : Titania-Doped Silicon Carbide Containing Cobalt Catalyst for the Fischer-Tropsch Synthesis	
6. Conclusion	
7. Perspectives	
Chapter 1: introduction.....	23
1. Introduction.....	24
1.1 driver.....	24
1.2 history.....	27
1.3 Recent commercial developments.....	30
2. Fischer-Tropsch synthesis.....	31
3. Fischer-tropsch Technology.....	31
3.1 synthesis gas preparation.....	31
3.2 Reactor.....	33
3.3 Catalyst.....	34
3.4 Supports.....	35
4. Scope and outline of this thesis	42
Chapter 2: Silicon carbide foam composite containing cobalt as a highly selective and re-usable Fischer-Tropsch synthesis catalyst	49
1. Introduction.....	50
2. Experimental.....	54
2.1 Silicon carbide foam synthesis and characterization	54
2.2 Al ₂ O ₃ and Al ₂ O ₃ -SiC foams.....	56
2.3 Catalyst preparation	56

2.4	Characterization techniques.....	56
2.5	Fischer-Tropsch reaction.....	57
3.	Results and discussion	58
3.1	Support characteristics.....	58
3.2	Catalysts characteristics	61
3.3	Catalytic performance.....	64
3.4	Support and active phase recovery	73
4.	Conclusion	75

Chapter 3: Co-Ru/SiC impregnated with ethanol as an effective catalyst for the Fischer-Tropsch synthesis.....83

1.	Introduction.....	86
2.	Experimental section.....	88
2.1	Support.....	88
2.2	Catalyst preparation.....	88
2.3	Characterization technique.....	90
2.4	Fischer-Tropsch synthesis reaction.....	91
3.	Results and discussion.....	91
3.1	catalyst characteristics.....	91
3.2	FTS performance as a function the GHSV and temperature.....	95
3.3	⁵⁹ Co zero field NMR.....	103
3.4	SiC surface wetting.....	108
4.	Conclusion	109

Chapter 4: Fischer-Tropsch Synthesis with Improved Active-Site Availability on a Large Pore Silicon Carbide Microspheres Containing Cobalt Catalyst.....115

1.	Introduction.....	117
2.	Experimental section.....	119
2.1	SiC support characteristics.....	119
2.2	Co/SiC catalysts.....	119
2.3	Characterization technique.....	119
2.4	Fischer-Tropsch synthesis reaction.....	120
3.	Results and discussion.....	121
3.1	Support characteristics.....	121
3.2	Co/SiC catalyst characteristics.....	123
3.3	Fischer-Tropsch synthesis (FTS)	126
4.	Conclusion.....	131

Chapter 5: Co / TiO₂-SiC	135
1. Introduction.....	138
2. Experimental section.....	140
2.1 TiO ₂ doped SiC support synthesis and characterization.....	140
2.2 Catalyst preparation.....	141
2.3 Characterization techniques.....	141
2.4 Fischer-Tropsch synthesis reaction.....	143
3. Results and discussion.....	144
3.1 Physicochemical properties of the supports and catalysts.....	144
3.2 Reduction behavior of catalysts.....	147
3.3 Morphological and microstructural characteristics of Co/SiC and Co/TiO ₂ -SiC catalysts.....	149
3.4 Fischer-Tropsch synthesis (FTS) catalytic performance.....	152
3.5 Chain growth factor (α) from the linear portion of the hydrocarbon.....	159
3.6 Influence of the cobalt loading.....	160
4. Conclusion.....	162
Conclusion and Perspectives.....	168

Résumé

1. Chapitre 1 : Introduction

Le pétrole est devenu, au cours du siècle dernier et reste encore aujourd'hui la principale source de matière première pour la production de carburant et de produit de base de synthèse organique. Aujourd'hui, la découverte de nouvelles réserves n'est pas aussi rapide que l'augmentation de la consommation en énergie. Depuis 10 ans les prix ont beaucoup augmenté, par exemple le prix du baril à 25\$ en janvier 2001 dépassait les 145\$ en juillet 2008. Ceci est dû à plusieurs facteurs: l'épuisement des réserves, l'augmentation des besoins en énergie des pays émergents tels que la Chine ou l'Inde, ainsi que la consommation énergétique élevée des pays industrialisés. Cet épuisement des réserves, conduit à la nécessité de trouver de nouvelles sources de matières premières pour la production de carburant et plus spécialement dans le domaine des transports. De plus, le pétrole qui est extrait, perd également en termes de qualité et nécessite des traitements de purification coûteux en temps et en énergie.

A l'heure actuelle il existe plusieurs produits de remplacement pour les carburants tels que le diméthyle éther (DME), le gaz de pétrole liquéfié (GPL) ou le gaz naturel liquéfié (GNL), les éthers d'huiles végétales (biodiesel) et le bioéthanol, mais ils ont tous leurs inconvénients. C'est pourquoi de nombreuses recherches sont menées sur le développement des carburants de synthèse dont les propriétés physico-chimiques sont similaires à celles des carburants traditionnels obtenus par distillation du pétrole. Ces nouveaux carburants sont en général obtenus par transformation d'une matière première carbonée en hydrocarbures par l'intermédiaire de procédés catalytiques dénommés XTL (X to liquide où X=G (gaz naturel), C (charbon) et B (biomasse)). Ces procédés sont composés de trois étapes (i) la gazéification ou le reformage catalytique en présence de vapeur d'eau, dépendant de la source carbonée afin d'obtenir le mélange de gaz de synthèse ($nH_2 + CO$), (ii) la synthèse de Fischer-Tropsch commune à tous pour l'obtention des hydrocarbures et des cires, et enfin (iii) l'hydrocraquage et l'hydro-isomérisation des coupes lourdes issues de la synthèse de Fischer-Tropsch pour l'obtention des coupes spécifiques qui seront utilisées ensuite dans les différents domaines d'application.

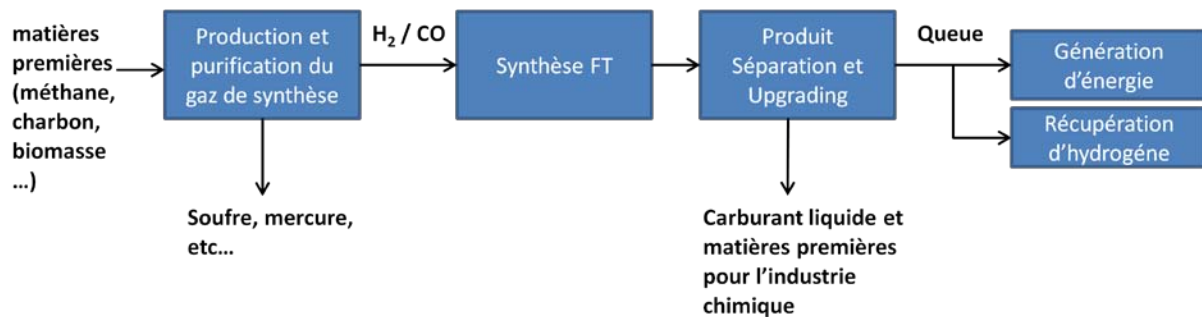
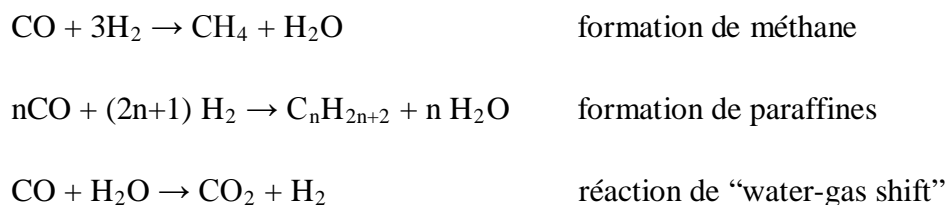


Figure 1. Schéma simplifié d'une unité XTL intégrant les différentes étapes du procédé

C'est en 1923 que les allemands Franz Fischer et Hans Tropsch ont découvert la synthèse qui porte leurs noms et qui consiste à convertir le mélange de gaz de synthèse sur un catalyseur à base de fer afin d'obtenir un mélange d'hydrocarbures. Le procédé de synthèse de Fischer-Tropsch sera industrialisé en 1936 par Ruhrchemie et ensuite intensément utilisé durant la seconde guerre mondiale par l'Allemagne afin de produire du carburant pour les besoins de la guerre.

La synthèse de Fischer-Tropsch (SFT) est un processus complexe en raison de la large gamme de produits obtenus. Les principales réactions sont les suivantes :



Les métaux de transition du groupe 8 sont actifs pour la SFT. Cependant, pour une application commerciale, seuls le cobalt et le fer sont utilisés, car ils présentent une activité et une sélectivité suffisante ainsi qu'un prix de base raisonnable. En raison de son coût relativement élevé, le cobalt doit être dispersé sur un support approprié afin de maximiser sa surface effective par unité de masse. Afin d'obtenir une bonne dispersion de ces particules de métal, il est nécessaire d'avoir un support poreux à haute surface spécifique présentant une forte interaction métal-support. Cependant, cette forte interaction peut entraîner la formation d'espèces difficilement réductibles qui ne participent pas à l'activité en SFT et de ce fait, induisent une perte de sites actifs par rapport à la quantité de métal déposé initialement sur le support. Les supports généralement utilisés de façon commerciale sont la silice, l'alumine, l'oxyde de titane, l'oxyde de zinc ou des combinaisons de ces oxydes [1, 2]. Le

développement d'un nouveau type de support combinant les avantages des supports traditionnels avec une meilleure réductibilité du précurseur de la phase active sera d'un intérêt non négligeable pour le procédé SFT en particulier mais aussi pour la catalyse hétérogène en générale.

Le carbure de silicium (SiC) est un matériau céramique, de structure tétraédrique avec une excellente stabilité thermique, une résistance mécanique élevée, une excellente résistance à l'oxydation et à la corrosion, un faible coefficient de dilatation thermique et une conductivité thermique élevée. La méthode permettant la synthèse du SiC à moyenne et haute surface spécifique ($>20 \text{ m}^2 \cdot \text{g}^{-1}$), eg. méthode de synthèse à mémoire de forme, a été découverte dans les années 80 par Ledoux et ses collaborateurs [3,4]. La synthèse industrielle de β -SiC a été développée par la suite dans les années 90, les matières premières et le processus ont été modifiés afin de faire face aux exigences d'une production industrielle [5,6].



Figure 2. Différentes formes, mousses alvéolaires, extrudés et anneaux, de carbure de silicium synthétisé par la méthode de synthèse à mémoire de forme (SICAT).

2. Chapitre 2 : Silicon Carbide Foam Composite Containing Cobalt as a Highly Selective and Re-Usable Fischer-Tropsch Synthesis Catalyst

L'un des supports de catalyseurs les plus utilisés pour la synthèse de Fischer-Tropsch est l'alumine sous forme gamma présentant une surface spécifique relativement élevée de l'ordre de $200 \text{ m}^2 \cdot \text{g}^{-1}$. Cependant, sa faible conductivité thermique est en partie responsable

des problèmes d'emballlement thermique et de la formation de points chauds près des sites actifs, ce qui peut compromettre la sécurité des installations, et diminuer la sélectivité à l'égard des hydrocarbures à longue chaîne. La perte de sélectivité est plus marquante lorsque la conversion du CO est élevée à cause de la forte chaleur dégagée par unité de masse du catalyseur.

Dans ce chapitre, le carbure de silicium sous forme de mousse alvéolaire est utilisé comme support de catalyseurs à base de cobalt (Co/SiC) pour la synthèse de Fischer-Tropsch en mode lit fixe. Ses performances catalytiques ont été comparées avec celles obtenues sur des catalyseurs à base de mousse alvéolaire d'alumine et de mousse de SiC recouverte par une couche d'alumine.

Le carbure de silicium (β -SiC) sous forme de mousse a été synthétisé par la réaction gaz-solide entre la vapeur de SiO et du carbone solide [7]. La synthèse détaillée des matériaux à base de SiC est résumée dans une revue [8]. La mousse alvéolaire de SiC ainsi obtenue possède une surface spécifique de l'ordre de $25 \text{ m}^2 \cdot \text{g}^{-1}$ et un réseau poreux essentiellement constitué de méso- et de macropores. Les mousses alvéolaires à base de SiC peuvent être fabriquées avec des formes définies et aussi une porosité variable en fonction des applications ultérieures. Les images optiques (fig. 3A) et MEB (fig. 3B et C) montrent les mousses alvéolaires avec différentes tailles de cellules ainsi que la microstructure des alvéoles et du pont de la cellule.

L'analyse par microscopie TEM à haute résolution du SiC présenté dans la figure 3D indique clairement la présence d'une couche mince amorphe sur la surface de SiC. Cette couche amorphe est composée d'un mélange de SiO_xC_y et SiO_2 d'après la littérature [9,10]. Ces espèces sont également confirmées par l'analyse XPS présentée dans la figure 3E. Cette couche de passivation contenant de l'oxygène devrait jouer le rôle de « wash-coat » naturel permettant l'ancrage de la phase active sur la surface de SiC.

Les mousses commerciales à base d' α - Al_2O_3 de faible surface spécifique ($1 \text{ m}^2 \cdot \text{g}^{-1}$) ne permettent pas un ancrage efficace des particules métalliques sur leur surface. De ce fait, une couche de « wash-coat » à base de γ - Al_2O_3 de grande surface spécifique a été déposée sur la surface de la mousse avant le dépôt de la phase active. La phase de cobalt est déposée sur les supports au moyen du procédé d'imprégnation à humidité naissante en utilisant une solution aqueuse de nitrate de cobalt. La charge de cobalt est fixée à 30% en masse.

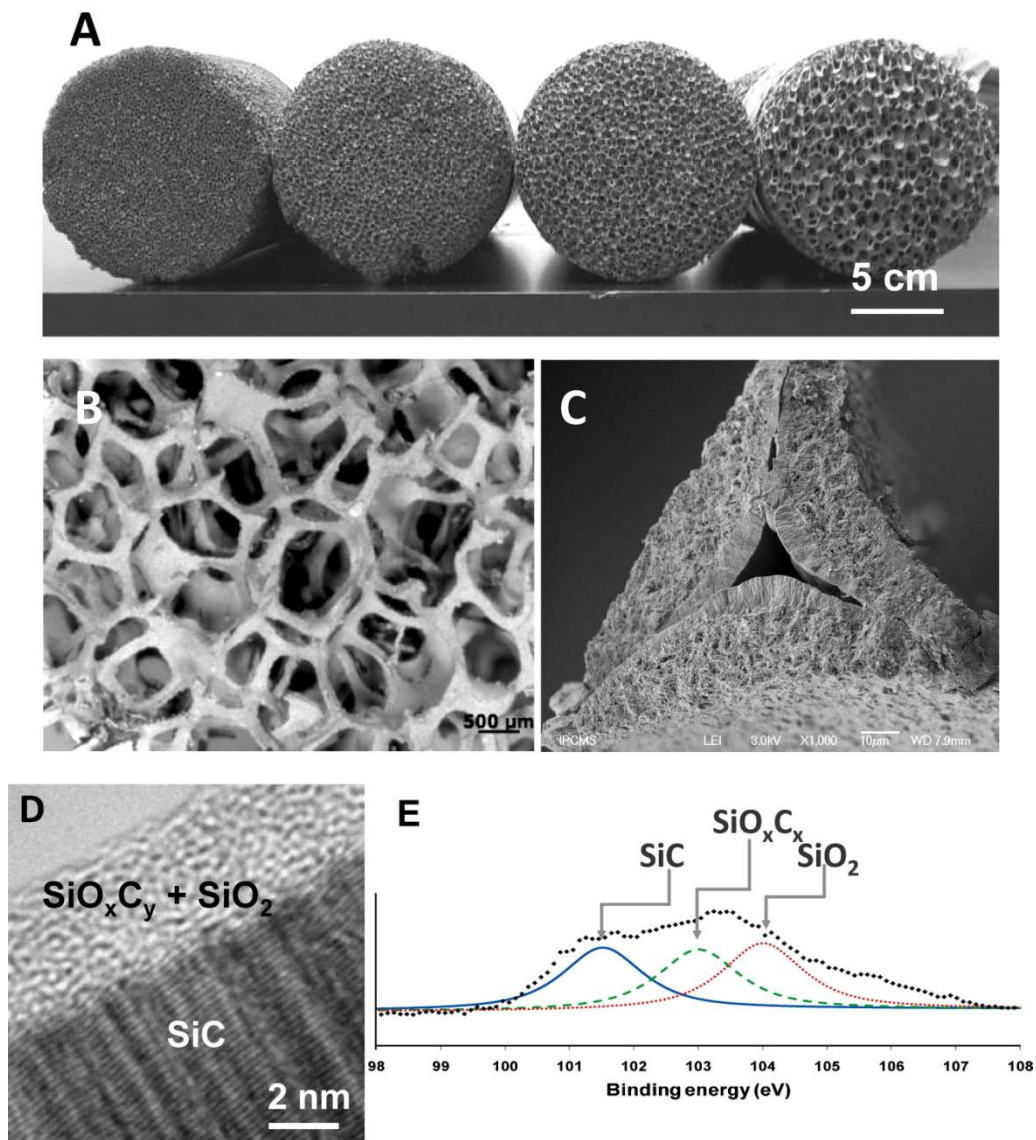


Figure 3.

(A) Exemple de mousse de SiC avec différentes tailles d'alvéoles (Sicat). (B) Image MEB à faible résolution montrant l'empilement des fenêtres pentagonales dans la matrice de mousse. (C) Image MEB à haute résolution montrant la microstructure d'un pont. (D) Image MEB à haute résolution mettant en évidence la présence d'une fine couche de phase amorphe de SiO₂ et SiO_xC_y. (E) Spectre XPS Si2p du SiC montrant les différentes espèces présentes en surface.

La réaction de Fischer-Tropsch est effectuée dans un réacteur opérant en mode lit fixe, en acier inoxydable (ID = 25,4 mm) avec une circulation d'huile de silicone comme source de chauffage. Les produits gazeux issus de la réaction sont analysés en ligne par chromatographie en phase gazeuse tandis que les hydrocarbures liquides et cires sont piégés dans deux pièges haute pression maintenus à 85 et 15 °C puis sont analysés post-réaction.

Les résultats catalytiques obtenus sur un catalyseur à base de cobalt sur une mousse alvéolaire à base de SiC ont été comparés avec ceux obtenus sur un catalyseur Co/Al₂O₃ à base de mousse alvéolaire de caractéristiques physiques similaires. A conversion moyenne (<50%), les deux catalyseurs affichent des sélectivités C5+ similaires, ce qui indique que les sélectivités intrinsèques entre les deux catalyseurs sont proches. Toutefois, lorsque la conversion du CO est augmentée à 70%, une différence significative en terme de sélectivité en C5+ est observée entre les deux catalyseurs, 80% sur le Co/SiC et 54% sur la Co/Al₂O₃, ce qui indique que, sous conditions réactionnelles sévères, le support SiC semble être plus approprié que l'alumine. Il est également intéressant de noter que, dans ces conditions de réaction, la probabilité de croissance de chaînes α , obtenue sur le catalyseur à base de SiC est de 0,91 et la formation de cires est particulièrement favorisée. L'amélioration de la sélectivité en C5+ observée sur le catalyseur SiC a été attribuée à sa grande efficacité pour évacuer la chaleur générée au cours de la réaction en raison de sa conductivité thermique plus élevée. La porosité, essentiellement méso- et macroporeuse du support SiC joue également un rôle important dans l'évacuation des produits intermédiaires liquides formés lors de la réaction favorisant ainsi une meilleure diffusion des réactifs vers les sites actifs.

Des tests catalytiques additionnels ont été également effectués sur un support hybride, à savoir une mousse de SiC recouverte d'une couche de wash-coat de γ -Al₂O₃, et les résultats obtenus confirment de nouveau la haute sélectivité en C5+ dans les mêmes conditions réactionnelles mais avec une activité légèrement plus élevée. Il semblerait que la présence d'une structure de SiC en-dessous de la couche d'alumine joue le rôle de diffuseur de chaleur ce qui permet de réduire la formation des points chauds sur la surface du catalyseur, néfastes pour la sélectivité de la réaction. Les résultats obtenus ci-dessus indiquent que l'ajout d'une couche de « wash-coat » à base d'alumine, présentant une interaction métal-support plus élevée que celle du SiC, a probablement permis une meilleure dispersion des particules de la phase active conférant ainsi au catalyseur une meilleure activité en SFT. Cette idée sera

développée par la suite dans ce mémoire de thèse en introduisant un dopant, à base de TiO_2 , dans la matrice du support SiC afin d'améliorer la dispersion des particules de la phase active.

En outre, l'inertie chimique du support à base de SiC permet également d'effectuer une récupération facile à la fois de la phase active et du support par un simple lavage acide à température ambiante, ce qui n'est pas le cas pour des catalyseurs à base d'alumine ou de silice où les traitements à haute température sont nécessaires. Le support de SiC récupéré est ensuite re-testé en SFT après avoir été imprégné avec une nouvelle phase de cobalt. Les résultats catalytiques sont comparés à ceux du catalyseur frais. Un rendement identique en produits de réaction a été obtenu, ce qui confirme le potentiel du SiC utilisé comme un support réutilisable.

3. Chapitre 3 : Co-Ru/SiC impregnated with ethanol as an effective catalyst for the Fischer-Tropsch synthesis

Ho et al. [11] et Tsubaki et al. [12,13] ont rapporté que la nature du solvant d'imprégnation, à savoir l'éthanol par rapport à l'eau, induit une forte modification de la phase active et une meilleure dispersion de cette dernière menant à une amélioration significative de l'activité FTS, tout en gardant une sélectivité en hydrocarbures liquides semblable dans un réacteur à lit agité. Dans ce chapitre, nous testons l'influence de la nature du solvant d'imprégnation sur l'activité en SFT des catalyseurs à base de cobalt, promus avec des traces de ruthénium, supporté sur des supports à base de SiC. Les catalyseurs seront ensuite testés pour la réaction de SFT en mode lit fixe. La stabilité des catalyseurs en fonction du temps sous flux sera également évaluée.

Les catalyseurs ont été préparés par imprégnation du volume poreux en utilisant soit l'eau (catalyseur noté Co-Ru/SiC-**W**), soit l'éthanol (catalyseur noté Co-Ru/SiC-**E**) comme solvant. La charge de cobalt a été fixée à 30 % en masse. Le ruthénium 0,1 % a été ajouté par imprégnations successives. Le ruthénium permet une meilleure réduction des particules de cobalt à basse température et une meilleure dispersion de la phase active sur la surface du catalyseur. Les tests catalytiques ont été réalisés dans un réacteur en lit fixe tubulaire de diamètre interne de 6 mm muni d'une double enveloppe dans laquelle circule de l'huile de

silicone. Les systèmes analytiques sont identiques à ceux déjà décrits dans le chapitre précédant.

Les surfaces spécifiques des catalyseurs après réduction sont de $23 \text{ m}^2 \cdot \text{g}^{-1}$ (Co-Ru/SiC-E) et $22 \text{ m}^2 \cdot \text{g}^{-1}$ (Co-Ru/SiC-W) respectivement. Par rapport à la surface spécifique du support SiC de départ ($29 \text{ m}^2 \cdot \text{g}^{-1}$) la surface BET a légèrement diminué après dépôt du cobalt. Ce résultat a été attribué à la présence de mésopores dans le support SiC permettant de bien disperser les particules de cobalt sans boucher les entrées de pores permettant ainsi de maintenir une surface acceptable pour la réaction. Les diagrammes DRX après réduction ne montrent pas de pics de diffraction correspondant aux oxydes de cobalt, ce qui montre que le cobalt est totalement réduit grâce à sa faible interaction avec le SiC contrairement aux autres supports tels que l'alumine ou la silice. Ces résultats ont été également confirmés par les analyses par réduction en température programmée (TPR) montrant la réduction des phases oxydes de cobalt à des températures plus basses que celles nécessaires pour un catalyseur supporté sur de l'alumine. La taille moyenne des particules de cobalt, déterminée par la formule de Scherrer, est rapportée dans le Tableau 1 et indique qu'il existe deux populations de particules, des particules hexagonales (*hcp*) de petites tailles et des particules cubiques faces centrées (*cfc*) de tailles plus importantes.

Tableau 1. Tailles moyenne de particules de cobalt déterminées par la formule de Scherrer.		
	Plan de diffraction <i>cfc</i> (111)	Plan de diffraction <i>hcp</i> (101)
Co-Ru/SiC-W	54 nm	17 nm
Co-Ru/SiC-E	70 nm	17nm

L'activité SFT et la sélectivité C5+ obtenues sur les catalyseurs Co-Ru/SiC-E et Co-Ru/SiC-W en fonction de la température de réaction et une vitesse spatiale horaire (GSHV) relativement élevée, 2850 h^{-1} , sont présentées sur la figure 4.

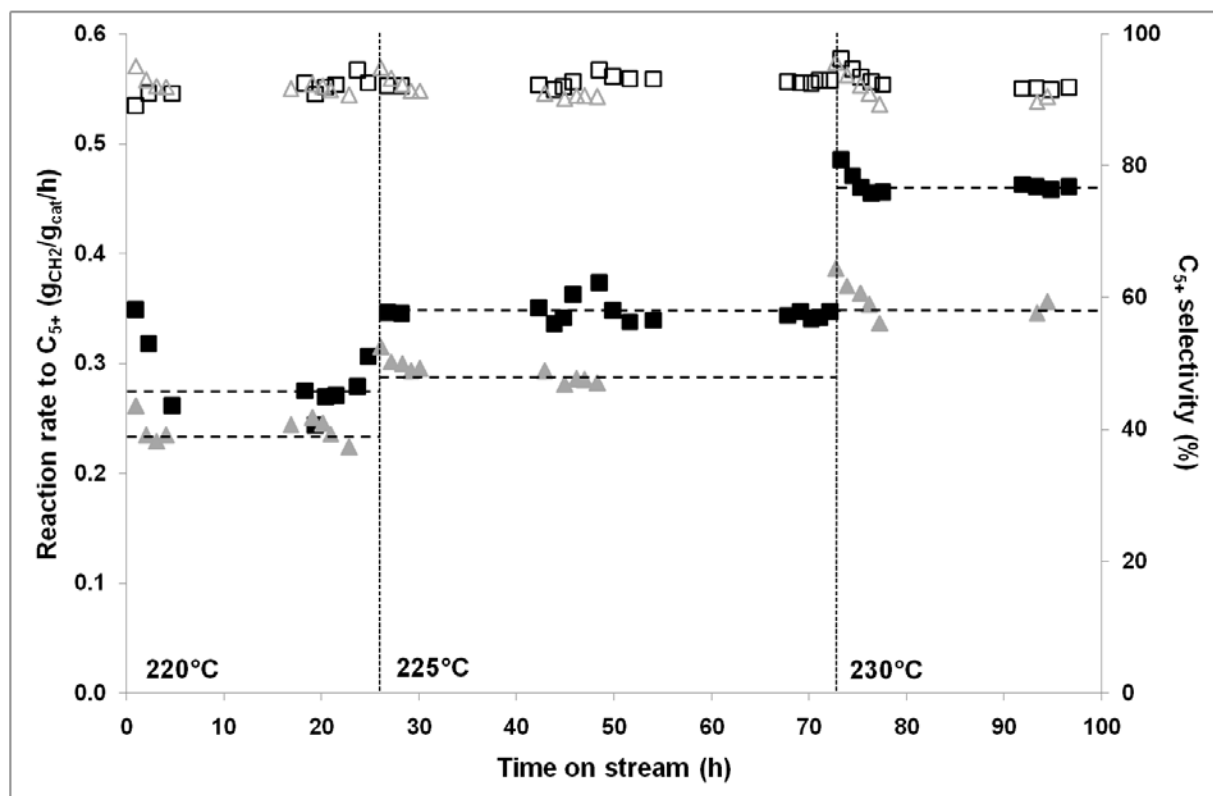


Figure 4. Performances catalytiques de Co-Ru/SiC-W et Co-Ru/SiC-E en fonction de la température de réaction. Conditions réactionnelles: P= 4 MPa, GHSV=2850 h⁻¹, masse catalyseur= 5 g. Les catalyseurs ont déjà été testés à 215°C à une GHSV de 1900 h⁻¹ durant environ 200 hrs.

Le catalyseur préparé avec de l'éthanol présente un rendement plus élevé comparé à celui préparé avec de l'eau même à température de réaction élevée, soit 230 °C. Les performances du catalyseur imprégné avec l'éthanol sont même améliorées, si l'on augmente la température de réaction et la vitesse spatiale, jusqu'à atteindre 0,54 g_{CH₂}·g_{cat}⁻¹·h⁻¹ pour une température de réaction de 235 °C et une vitesse spatiale de 3800 h⁻¹, tout en gardant une sélectivité C₅₊ relativement forte soit 90 %. En outre, le catalyseur présente également une stabilité relativement élevée en fonction du temps en service.

Afin d'obtenir une meilleure idée de l'activité SFT des catalyseurs Co-Ru/SiC-E, une analyse RMN à champ nul du ⁵⁹Co a été réalisée. Le spectre RMN ⁵⁹Co enregistré à 4,2° K (figure 5) indique la présence de plusieurs espèces de cobalt dans le catalyseur: hexagonal compact (hcp), cubique à faces centrées (cfc) et des défauts d'empilement, soit à partir de la fcc ou des phases hcp [14,15].

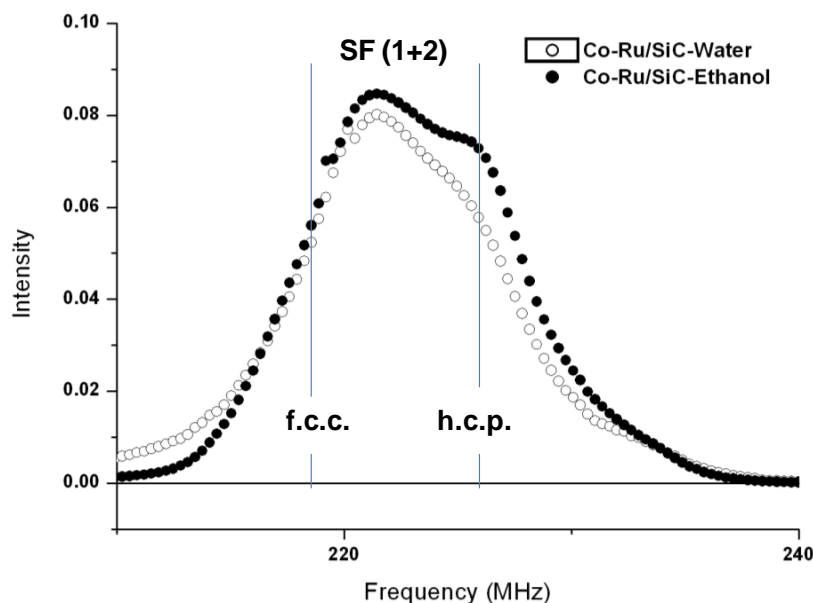


Figure 5. Spectres RMN ^{59}Co des catalyseurs Co-Ru/SiC-E et Co-Ru/SiC-W, enregistrés à 4.2 K, montrant la présence de plusieurs espèces de cobalt: Co (f.c.c.), Co (h.c.p.) ainsi que des fautes d'empilement (SF (1+2)) avec $56 \pm 1 \%$ pour le Co-Ru/SiC-E et $52 \pm 1 \%$ pour le Co-Ru/SiC-W.

Les analyses RMN ^{59}Co à champ nul indiquent que la proportion d'atomes de cobalt engagés dans les petites particules de cobalt h.c.p. ($< 8 \text{ nm}$) est plus élevée pour le catalyseur imprégné à l'éthanol. Les analyses montrent aussi une meilleure dispersion, plus homogène des atomes de ruthénium dans le réseau de cobalt formant l'alliage entre les deux phases.

Le catalyseur cobalt utilisant l'éthanol comme solvant présente une activité très élevée ainsi qu'une haute sélectivité $S_{\text{C}_5^+}$ dans des conditions sévères de SFT, c.à.d. à haute température ($235 \text{ }^\circ\text{C}$) et à une vitesse spatiale élevée ($3800 \text{ environ h}^{-1}$). La forte activité a été liée à la grande taille des pores du catalyseur qui permet une meilleure diffusion des réactifs et des produits de réaction, réduisant le problème de bouchage des pores par les hydrocarbures liquides lourds formés au cours de la réaction, et facilite l'accès du réactif aux sites actifs situés à l'intérieur des pores. Les analyses RMN du ^{59}Co à champ nul réalisées sur les catalyseurs indiquent que la population globale de Co f.c.c. par rapport Co h.c.p. ne change pas de manière significative selon le solvant utilisé ; en revanche le solvant éthanol semble favoriser la formation d'une plus grande quantité de particules de Co de petites tailles (moins de 8 nm).

Ces petites particules ont un large rapport surface sur volume et pourraient être responsables de l'activité accrue en SFT observée.

4. Chapitre 4 : Fischer-Tropsch Synthesis with Improved Active-Site Availability on a Large Pore Silicon Carbide Microspheres Containing Cobalt Catalyst

Dans ce chapitre, l'influence de la taille des pores du support sur l'activité en SFT est étudiée. Les supports utilisés sont à base de SiC sous forme de grains donc la porosité a été modifiée. La réaction de SFT a été testée en mode lit fixe.

La porosité du support des différents SiC, mesurée au moyen de l'intrusion de mercure, est présentée sur la figure 6. La distribution de taille des pores du SiC est comprise entre 0,01 et 10 μ m. Dans le cas du support à forte porosité, la taille des pores s'étalant entre 0,1 et 10 μ m est plus importante par rapport au support à faible porosité. La surface spécifique mesurée par adsorption N₂ est respectivement de 30 m² • g⁻¹ et 40 m² • g⁻¹ pour les supports à faible et à forte porosité.

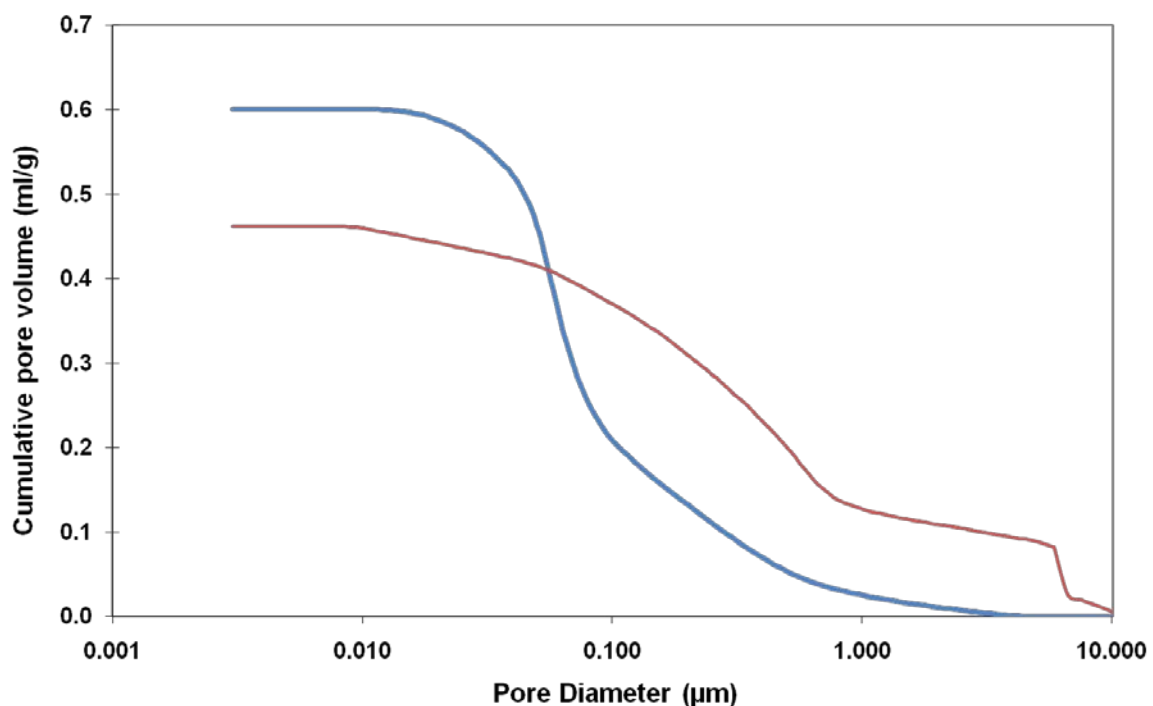


Figure 6. Distribution des tailles de pores des différents SiC déterminée par intrusion de mercure: mesoporeux (SiC-LP) and haute porosité (SiC-HP).

La diffraction des rayons X montre la complète réduction de la phase oxyde sur les catalyseurs confirmant ainsi la faible interaction entre le SiC et la phase active. Le profil de réduction d'après les résultats TPR semble être également indépendant de la taille des pores du support. Ces résultats confirment que la réductibilité des phases oxydes ne dépend que de la nature du support comme discuté ci-dessus.

Les résultats FTS, conversion et sélectivité en C5+, obtenus sur les catalyseurs sont résumés dans le Tableau 2. L'activité FTS reste stable pendant la durée du test, soit environ 100 heures, ce qui indique qu'aucune désactivation n'est produite dans les conditions réactionnelles utilisées. Dans le cas des catalyseurs faiblement chargés en cobalt, 10 % en poids, l'activité en SFT demeure similaire tandis que pour les catalyseurs plus chargés en cobalt, 30 % en poids, une forte amélioration en activité SFT a été observée sur le catalyseur à haute porosité. Ce phénomène pourrait être expliqué par le fait que pour les catalyseurs à faible charge, la quantité de cobalt déposée ne suffit pas à boucher les pores du support et de ce fait, l'ensemble des sites actifs est disponible pour la réaction et ce, quelque soit la taille des pores du support. Dans le cas d'une charge de cobalt plus importante, il est possible qu'une partie des pores du support à basse porosité soit bouchée par les particules de la phase active donnant ainsi une activité en SFT plus faible. Dans le cas du catalyseur à forte porosité, le phénomène de bouchage des pores par les particules de cobalt est plus faible et de ce fait, une plus grande partie des sites actifs est accessible aux réactifs d'où une activité en SFT plus importante.

Tableau 2. Distribution des produits à l'équilibre sur les catalyseurs Co/SiC-LP et Co/SiC-HP. Conditions réactionnelles: Charge de Co = 10-30 % massique, H₂:CO = 2, température = 215°C, pression total = 40 atm., GHSV = 1900 h⁻¹.

Catalyseur	CH ₄ (%)	CO ₂ (%)	C ₂ -C ₄ (%)	C ₅₊ (%)	ASM
10 Co/SiC-LP	2.5	0	1.8	95.7	0.14
10 Co/SiC-HP	2.9	0	1.6	95.5	0.15
30 Co/SiC-LP	4.2	0.09	3.1	92.6	0.17
30 Co/SiC-HP	5.1	0.05	3.6	91.3	0.2

L'influence de la température de réaction a également été étudiée en gardant les autres conditions de réaction similaires (Tableau 3). L'activité en FT sur le Co/SiC-HP est nettement améliorée en augmentant la température de réaction de 215 ° C à 220 ° C et enfin, à 225 ° C, sans qu'aucun changement significatif de la sélectivité C₅₊ n'ait été observé. Il est à noter que l'activité reste stable et qu'aucune désactivation appréciable n'a été observée sur le catalyseur.

Tableau3. Distribution des produits à l'équilibre sur le catalyseur Co/SiC-HP en fonction de la température de réaction. Condition réactionnel: Charge de Co= 30%, H₂:CO = 2, pression totale = 40 atm., GHSV = 1900 h⁻¹.

temperature	CH ₄ (%)	CO ₂ (%)	C ₂ -C ₄ (%)	C ₅₊ (%)	ASM
215°	5.4	0.06	3.4	91.2	0.2
220°	5.9	0.1	4.2	89.8	0.26
225°	6.7	0.16	4.4	88.8	0.31

La taille des pores du support joue un rôle important dans la dispersion des particules de cobalt pour la réaction SFT. La porosité élevée du support limite les phénomènes de bouchage des pores lorsque la charge du cobalt est importante et permet ainsi une meilleure accessibilité de la phase active permettant l'obtention d'une activité en SFT plus importante.

5.Chapitre 5 : Titania-Doped Silicon Carbide Containing Cobalt Catalyst for the Fischer-Tropsch Synthesis

Dans ce chapitre, nous rapportons le développement d'un nouveau support hybride composé d'un carbure de silicium dopé avec du titane possédant une surface spécifique élevée et des interactions métal-support plus fortes.

L'introduction du TiO₂ dans la matrice en SiC augmente de manière significative la surface spécifique du support dopé, soit 101 m²·g⁻¹, par rapport à celui non dopé, à savoir 40 m²·g⁻¹. Le TiO₂-SiC contient également une quantité relativement importante de micropores. Ceci explique la forte augmentation de la surface spécifique du support après oxydation. Le dépôt de cobalt affecte différemment la surface des deux supports: la surface du SiC non dopé diminue légèrement de 40 à 33 m²·g⁻¹, tandis que la surface du SiC dopé est considérablement réduite de 101 à 25 m²·g⁻¹, ce qui est principalement due à l'obturation des micropores par les particules de cobalt.

Les diagrammes DRX et TPR montrent la réduction complète du cobalt. La taille moyenne des particules de cobalt déterminée par la formule de Scherrer est rapportée dans le Tableau 1. Les résultats indiquent que l'introduction de la phase de TiO₂ dans la matrice en SiC diminue sensiblement la taille des particules de cobalt, probablement en générant une interaction plus élevée avec le précurseur de sel métallique tout en permettant une réduction facile et complète de la phase active. Ce résultat est similaire à celui déjà observé dans le Chapitre 2 sur les catalyseurs cobalt supportés sur du SiC recouvert par une couche d'alumine.

Tableau 4. surface BET et volume poreux du support SiC dope et non dopée avant et après dépôt de cobalts. La taille de particule correspondante, avant et après sous H₂ a 300 °C pendant 6 h, est déterminé par la formule de Scherrer est aussi présenter.

Sample	Surface area (m ² /g)	Total pore volume (cm ³ /g)	BJH pore diameter (nm)	Co ⁰ particle size ^(a) (nm)	Co ⁰ particle size ^(b) (nm)
SiC	40	0.120	12.8	-	-
TiO ₂ -SiC	101	0.123	4.4	-	-
10Co/SiC	33	0.139	17.1	42 ± 5	51 ± 5
10Co/TiO ₂ -SiC	25	0.082	13.0	22 ± 5	14 ± 5

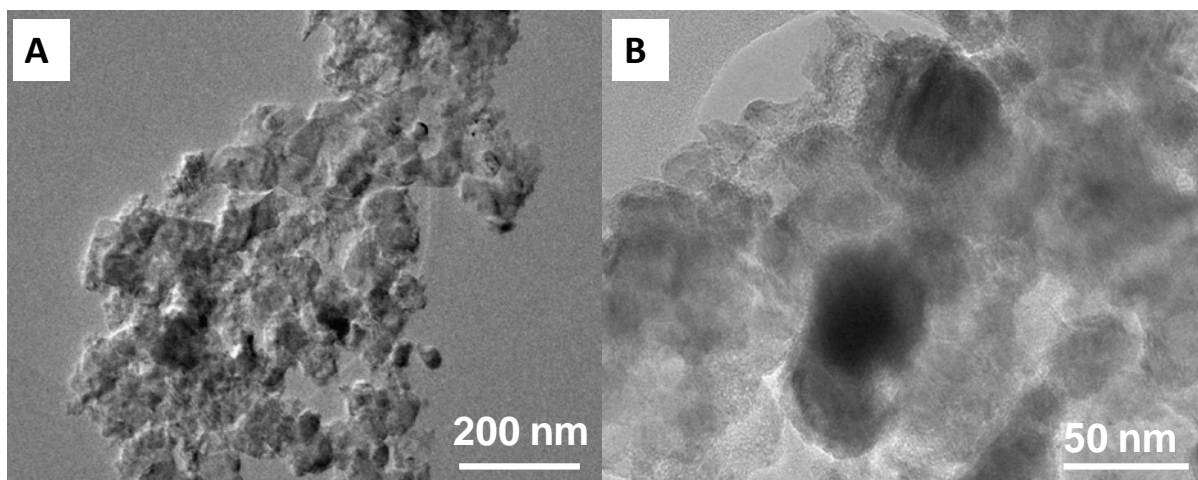
$$(a) d(\text{Co}^0) = 0.75 \times d(\text{Co}_3\text{O}_4)$$

$$(b) d(\text{Co}^0) = k \cdot \lambda / (\tau \cos \theta), \text{ The sample was reduced by H}_2 \text{ at 300 } ^\circ\text{C for 6h}$$

La taille des particules de cobalt sur les catalyseurs de SiC et TiO₂-SiC dopé a été évaluée par TEM et EFTEM et les résultats sont présentés sur la figure 7. Les micrographies

TEM du catalyseur Co/SiC indiquent la présence d'une taille de particules de cobalt relativement homogène avec une taille moyenne d'environ 40 nm (figure 7A et B) dispersées sur toute la surface de support. Cette taille de particules est en bon accord avec les résultats déjà reportés dans le cas d'un support à base de SiC non dopé et est attribuée à une interaction faible entre le support et le précurseur de la phase active.

Dans le cas du catalyseur supporté sur du SiC dopé avec du TiO₂ les images EFTEM indiquent que la taille des particules de cobalt change de manière significative en fonction de la surface sur laquelle ils sont en contact, soit 5 à 15 nm pour les particules de Co en contact avec TiO₂ et 30 à 50 nm pour les particules de Co directement en contact avec la surface de SiC. Un tel résultat est relativement proche de ceux obtenus par la formule de Scherrer. Selon les résultats observés, on peut dire que la phase TiO₂ incorporée dans le support de SiC présente une plus forte interaction avec la phase active conduisant à la formation de particules de cobalt avec une taille beaucoup plus petite par rapport à ceux obtenus sur le support de SiC non dopé. Néanmoins, cette interaction n'est pas trop forte pour permettre une réduction complète de la phase active à des températures de réduction relativement basse contrairement à un support à base d'alumine ou de silice.



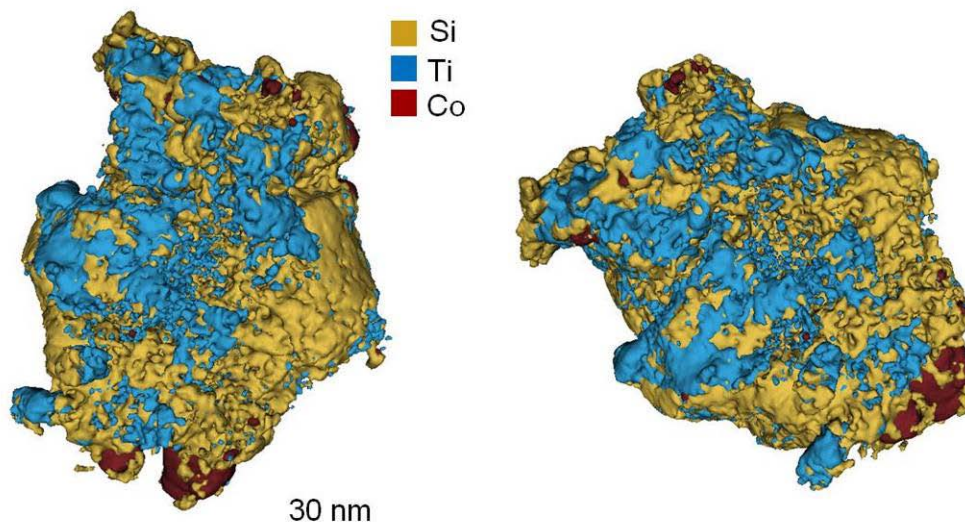


Figure 7.(A, B) images MET du 10Co/SiC. (C, D) images EFTEM du 10Co/TiO₂-SiC montrant l'interaction des particules de cobalt avec les différents composants du support :Ti (bleu), Si (jaune), Co (rouge). Le catalyseur a été calciné à 350 °C pendant 2 h suivi d'une réduction sous H₂ à 300 °C pendant 6 h.

L'activité FTS et la sélectivité en C₅₊ obtenues sur les catalyseurs en fonction de la température de réaction sont présentées dans le tableau 5. On peut remarquer que la sélectivité en C₅₊ reste relativement élevée même à des températures de réaction élevées, 230 °C. Les résultats obtenus montrent une augmentation significative de l'activité SFT sur le catalyseur dopé au TiO₂. Cette augmentation de l'activité en SFT sur le catalyseur dopé pourrait être directement liée à la présence de petites particules de cobalt en contact avec la phase TiO₂.

Tableau 5.Résultats obtenue sur catalyseur de cobalt à base de SiC dopé et non dopé. Conditions réactionnel : H₂/CO = 2, syngas pur, pression totale = 40 atm.

Catalyst	T(°C)	GHSV (h ⁻¹)	CO Conversion (%)	Product selectivity (%)				CTY ^a (10 ⁻⁵ mol _{co} /g _{Co} /s)	ASM ^b
				CO ₂	CH ₄	C ₂ -C ₄	C ₅₊		
10Co/SiC	215	2850	26.9	0	2.9	1.6	95.5	4.0	0.19
	220	2850	28.8	0	3.7	2.0	94.3	4.3	0.21

Résumé

	225	2850	32.3	0	4.5	2.4	93.1	4.8	0.23
	230	2850	35.4	0.1	5.4	2.9	91.6	5.3	0.24
	215	2850	33.9	0	3.2	1.5	95.3	5.0	0.24
10Co/TiO ₂ -SiC	220	2850	37.0	0	3.9	1.7	94.4	5.5	0.26
	225	2850	43.4	0	4.5	1.9	93.6	6.5	0.30
	230	2850	50.5	0.2	5.9	2.2	91.7	7.5	0.35
	215	2850	57.7	3.1	4.7	0	92.2	2.9	0.40
30Co/TiO ₂ -SiC	220	2850	68.3	2.7	4.7	0	92.5	3.4	0.47
	230	3800	61.8	3.1	6.2	0.1	90.6	4.1	0.56
30Co-Ru/SiC-E	230	3800	47	3.0	5.5	0.0	91.5	2.9	0.43

Les résultats obtenus dans ce chapitre ont montré que le dopage du support SiC par du titane, en l'occurrence du TiO₂, a permis une meilleure dispersion des particules de cobalt sur la surface du support grâce à une interaction métal-support plus élevée entre la phase TiO₂ et le précurseur du cobalt. La meilleure dispersion des particules de cobalt entraîne une augmentation significative de l'activité en SFT par rapport aux catalyseurs à base de SiC non dopés.

6. Conclusion

Les résultats obtenus dans ce mémoire de thèse portent sur l'utilisation d'un nouveau type de support à base de carbure de silicium (SiC) possédant une surface spécifique allant de 20 à 100 m²/g dans la réaction de synthèse de Fischer-Tropsch (SFT). Nous étudions également dans ce travail l'influence de différents paramètres tels que la nature du solvant

d'imprégnation, la porosité du support et le dopage sur les performances des catalyseurs à base de cobalt pour cette réaction des plus demandées à l'heure actuelle.

Nous avons constaté que la nature du solvant d'imprégnation a un effet non négligeable sur les performances en SFT du catalyseur à base de Co/SiC. L'éthanol utilisé comme solvant d'imprégnation permet une meilleure dispersion des particules de la phase active dans l'ensemble du support et aussi une meilleure incorporation du promoteur, en l'occurrence du ruthénium, dans les particules de cobalt. Cette forte dispersion permet une augmentation significative de l'activité en SFT tout en gardant une sélectivité en hydrocarbures liquides élevée (90 %).

L'influence de la porosité du support sur les performances catalytiques en SFT a été également étudiée. Les résultats obtenus indiquent que l'augmentation de la taille des pores du support permet une meilleure accessibilité des sites actifs aux réactifs, et plus spécialement lorsque la charge en phase active est élevée (30 % en poids), et par conséquent, une meilleure activité en SFT est obtenue. La porosité n'influe par contre en aucune manière sur la sélectivité en hydrocarbures liquides du catalyseur par rapport à son homologue ayant une taille de pores de plus faible diamètre.

Le dernier paramètre étudié concerne l'influence du dopage du support avec du titane présentant une meilleure interaction métal-support. En effet, la présence d'une phase de TiO_2 sur la surface du SiC permet de réduire d'une manière significative la taille des particules de cobalt déposées. Il a été observé par microscopie électronique à transmission en mode image filtrée que les particules de cobalt se trouvant en contact avec la phase TiO_2 possèdent une taille de particule moyenne de l'ordre de 5 à 15 nm alors que celles en contact direct avec le SiC ont une taille plus élevée, 30-40 nm. Cette forte dispersion des particules de la phase métallique permet une amélioration significative de l'activité catalytique en SFT tout en maintenant une sélectivité en hydrocarbures liquides élevée (90-92 %).

7. Perspectives

Les perspectives découlant des résultats obtenus dans ce travail sont relativement nombreuses et parmi elles on peut citer :

- l'influence de promoteurs sur l'activité catalytique en SFT avec des supports à base de SiC dopés avec du titane.

- l'influence d'une superstructure à base de nanofibres de carbone déposée sur la surface du support SiC qui a pour effet une augmentation significative de la surface spécifique tout en évitant la formation de micropores qui sont facilement bouchées par les particules de la phase active.

- l'influence de la morphologie du support

Référence

-
- [1] R. Oukaci, A. H. Singleton, J. G. Goodwin Jr. *Appl. Catal. A* 281 (1999) 129-144
- [2] M.E. Dry Chapter 7 Fischer-Tropsch Reactors, *Studies in Surface Science and Catalysis*, Elsevier, (2004), Volume 152, Fischer-Tropsch Technology, Pages 533-600
- [3] M. J. Ledoux, S. Hantzer, C. Pham-Huu, J. L. Guille, M. P. Desaneaux, *J. Catal.* 114 (198) 176-185.
- [4] M. J. Ledoux, C. Pham-Huu, J. L. Guille, H. M. Dunlop, S. Hantzer, S. Marin, M. Weibel, *Catal. Today* 15 (1992) 263-24.
- [5] Website : www.sicatcatalyst.com
- [6] P. Nguyen, Ch. Pham, *Appl. Catal. A* 391 (2011) 443-454.
- [7] M. J. Ledoux, S. Hantzer, C. Pham-Huu, J. L. Guille, M. P. Desaneaux, *J. Catal.* 114 (1988) 176-185.
- [8] M. J. Ledoux, C. Pham-Huu, *CaTTech* 5 (2001) 226-246.
- [9] R. Pampuch, W. Ptak, S. Jonas, J. Stoch, *Mater. Sci. Monographs* 6 (1980) 435-448.
- [10] R. Moene, M. Makee, J. A. Moulijn, *Appl. Catal. A* 167 (1998) 321-330.
- [11] S. W. Ho, Y. S. Su, *J. Catal.* 168 (1997) 51-59.
- [12] Y. Zhang, Y. Liu, G. Yang, S. Sun, N. Tsubaki, *Appl. Catal. A* 321 (2007) 79-85.
- [13] Y. Zhang, Y. Liu, G. Yang, Y. Endo, N. Tsubaki, *Catal. Today* 142 (2009) 85-89.
- [14] H. Karaca, J. Hong, P. Fongarland, P. Roussel, A. Griboval-Constant, M. Lacroix, K. Hortmann, O. V. Safonova, A. Y. Khodakov, *Chem. Commun.* 46 (2010) 788-790.
- [15] O. Ducreux, B. Rebours, J. Lynch, M. Roy-Auberger, D. Bazin, *Oil&GasSci. Technol.* 64 (2009) 49-62.

CHAPTER I

I INTRODUCTION

1. Introduction

1.1 Driver

During the last century, petroleum, due to its cheap price, has become the principal source of raw material for transportation fuel and for basic organic compounds supply. Since the beginning of the 21th century the situation has been changing. Indeed, it has been observed that over the past ten years a durable increase in the price of petrol has occurred (*Figure 1*), this is due to multiple factors like the expected depletion of oil reserves, the increasing demand of petrol due to the development of emerging countries like China and India and the still high consumption of industrial countries and also the political exploitation of oil reserves. According to these facts new ways for producing fuel must be found in order to avoid petroleum shortage.

There is a few promising compounds replacement for motor fuel [1] such as methanol, dimethyl ether (DME), liquefied petroleum gas (LPG) or liquefied natural gas (LNG), ethers of vegetable oils (biodiesel) and bioethanol, but the major drawback of these fuels excepted biodiesel is that they need a change in the design of the engine. Biodiesel is interesting because of its potential to reduce greenhouse gas emissions, but it also has a very different chemical structure compared with conventional diesel, containing much more oxygen leading to a lower power per volume compared to traditional fuel. Though it does not contain high concentrations of aromatics, it contains other cyclic species with a similar effect and it still contains sulfur. So the preference is going to synthetic fuels with physico-chemical properties similar, after post-synthesis up-grading, to the petroleum fuel for the automotive transportation, chemical market or the use as fuel for electricity production. These synthetic fuels are obtained by the transformation of natural gas, coal or biomass through the XTL process (GTL = Gas-to-Liquids, CTL = Coal-to-Liquids and BTL = Biomass-to-Liquids). These processes have received an ever increasing interest in the last decade due to the convergence of several factors: (i) the rising price of crude oil and legislative constraints on fuel quality as discussed above, (ii) the policy of some countries to reduce their dependence on crude oil supply such as the United States, which has the largest coal reserve in the world estimated at about 260 billion recoverable tons[2], China and India¹, and (iii) new legislations

¹ China and India represent a third of the world's population and are experiencing a large economic development for the last decade and will face an unprecedented demand for energy supply in a near future. Similar to the

regarding the production of synthetic fuels with renewable sources such as biomass. All these factors seem to indicate that the XTL technology has a significant role to play in the global energy landscape.

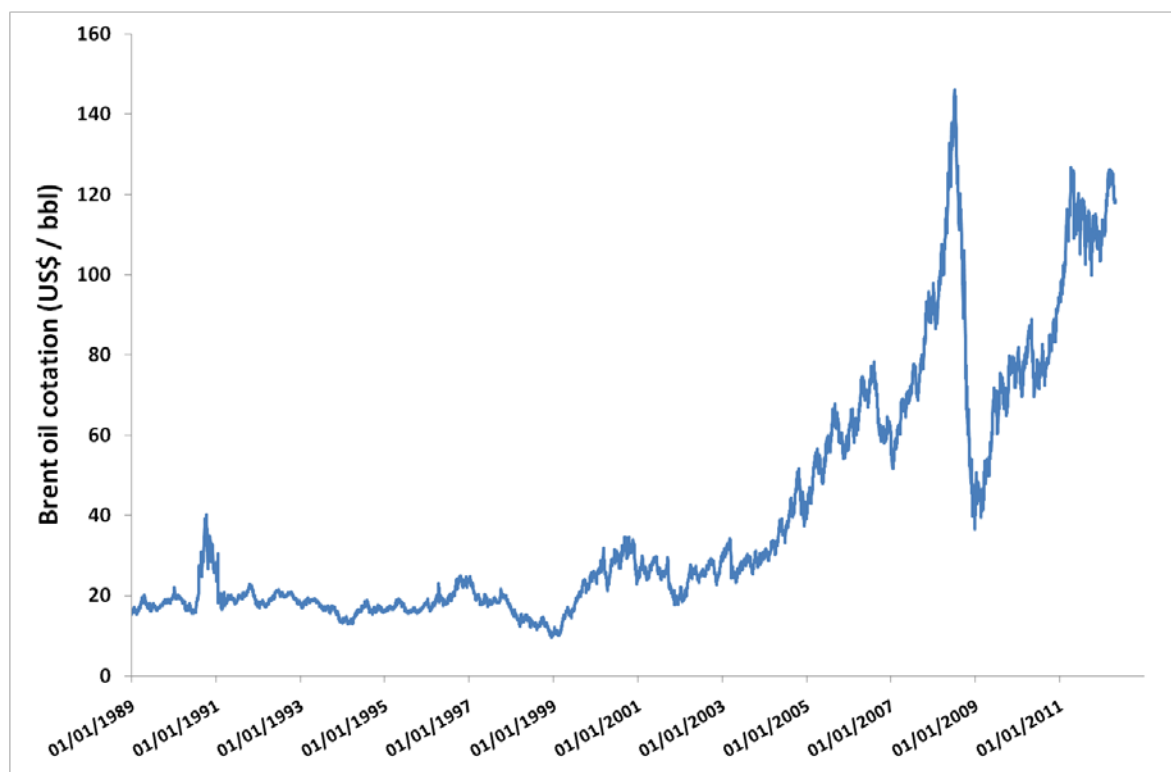


Figure 1. Brent oil cotation from 1989 to 2011.

The XTL processes consist of three main transformation steps: (i) syngas production through reforming to produce synthesis gas mixture or syngas ($\text{CO} + n\text{H}_2$), (ii) Fischer-Tropsch synthesis (FTS) to get liquid hydrocarbons and waxes from the syngas, and (iii) FTS products upgrading to obtain the required fractions for downstream applications. The simplify scheme of the XTL process is presented in Figure 2.

United States these countries have also at hand large amounts of reserves of coal that can be converted to synthetic fuels in order to reduce as much as possible their external crude oil supply.

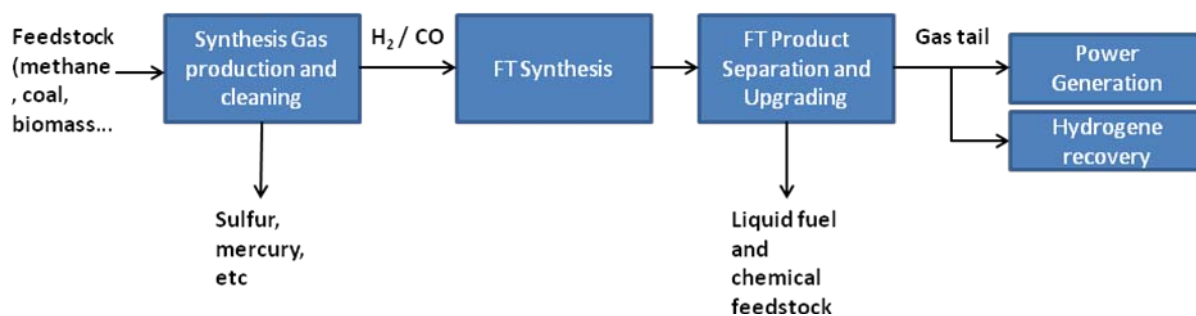


Figure 2. Simplified linear scheme of the principle of the XTL unit.

Among the different XTL processes GTL seems to be the most developed up to date (see below). Indeed, the continuous increase in the known reserves of natural gas along with the environmental pressure to reduce as much as possible the flaring of associated gas push ahead the natural gas to become the second energy source before coal in 2030. GTL diesel (as produced) is completely free of sulfur and aromatics, and has a cetane number of 77. The GTL diesel is almost colorless compared to the traditional diesel with a yellow pale color due to the presence of sulfur (Figure 3). As such in its pure form GTL diesel is considered as an ideal fuel for both advanced diesel engines with advanced emissions control technology and for fuel cells. GTL diesel will probably be blended with conventional diesel in order to reduce the sulfur content down the limit fixed by the European legislations.

Figure 3. Optical photos showing the difference in colour between sulphur-free synthetic fuel (colourless) and the traditional fuel containing sulphur (yellow pale).

1.2 History

The first synthesis of hydrocarbon through hydrogenation of carbon monoxide was carried out by Senderens and Sabatier [3] in 1902 over nickel or cobalt catalyst to form methane. Twenty years later Franz Fischer and Hans Tropsch [4] obtained a mixture of aliphatic oxygenated compounds from a synthesis gas on alkalized iron catalyst under a relatively high pressure (> 100 bar). In 1923 they made some progress in the FTS and heavy hydrocarbons were the main products of the reaction using Fe/ZnO and Co/Cr₂O₃ catalysts. The process was licensed by Rührchemie in 1936. Even though it was discovered early in the last century the development of the Fischer-Tropsch technologies has been hampered by the lack of market pull and was driven only by political situation like Germany during the Second World War or during the embargo on oil product in south Africa in the 70's. Indeed, Germany had no oil and the Fisher-Tropsch process was one of the two processes with the Bergius process that allowed them to reach energies independence during the war. After the war, due to the cheap price of crude oil this process has lost interest. In the 1980s, FT process has known a renewed interest driven by the need of diversification of source of fossil fuel, the utilization of stranded gas and environmental concern and in the last decade the interest had also been driven by the price of crude oil.

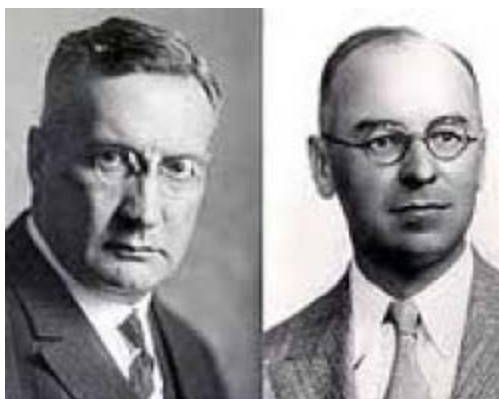


Figure 4. Franz Fischer and Hans Tropsch who discovered the Fischer-Tropsch process.

1.3 Recent commercial developments

The Fischer-Tropsch Synthesis (FTS) has received an ever-increasing interest in the last decades (Figure 5) [5,6,7,8]. The final market for the liquid fuels produced by the FTS process is the transportation and chemical intermediates markets where sulphur free fuels are

highly demanded. The FTS process also allows the reduction of natural gas flaring which is environmental prohibited due to the formation of CO₂ which is a greenhouse gas. In addition, the synthetic fuels derived from the FTS process are free of nitrogen, sulfur, aromatics and metal, have a high cetane number and could be further be blended with others to meet the environmental requirements of the diesel fuel.

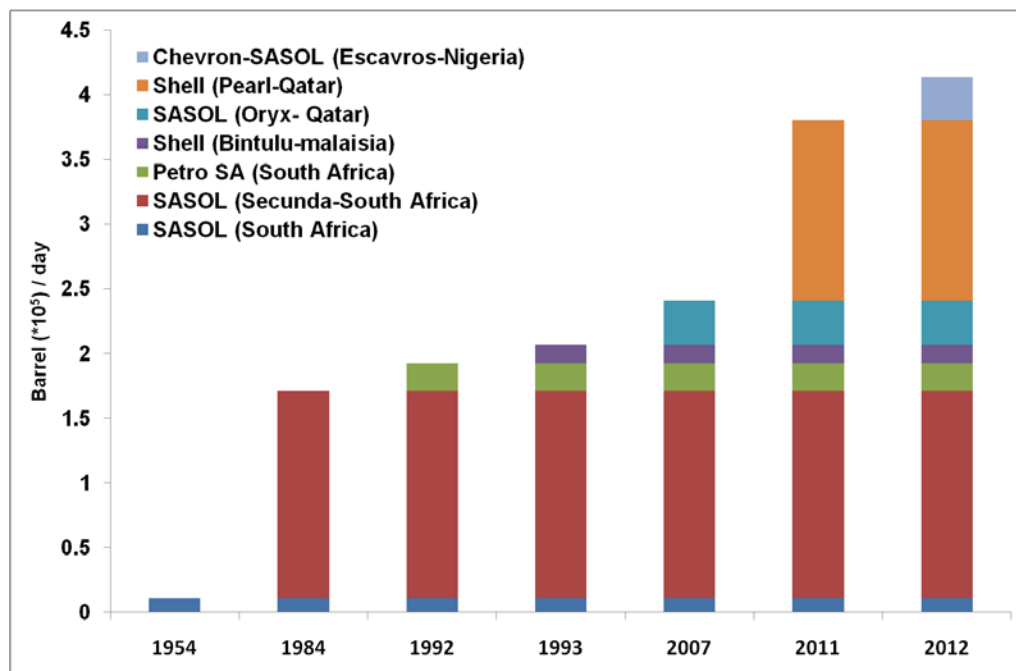


Figure 5. Industrials development of synthetic fuels based on the Fischer-Tropsch process. New FT plants with more important capacity have been developed during the last decade².

Due to the large capital investment and high operation and maintenance costs, only a few large scale FT plants exist.

- SASOL has three production units in South Africa. Their first CTL production units were built in Sasolburg, started operating in 1954 and has a production capacity of 11,000 barrels per day from 2004 the plant use methane as feed. The two other production unit are based in Secunda and have a total production capacity of 160,000 barrels per day.
- Petro SA has a GTL plant in Mossel Bay, South Africa, operating with a high temperature iron fluidized bed reactor. It is the first operating GTL plant, the production started in 1992 and has a GTL production capacity of 22,000 barrels per

² Escravos is still under construction

day. In 2004 Petro SA with Statoil/Hydro started a semi-commercial scale unit with a cobalt slurry bed reactor with a production capacity of up to 1000 barrels per day [9].

- Shell is operating a GTL plant in Bintulu, Malaysia with a cobalt fixed bed reactor and a production capacity of 14,000 barrels per day the production started in 1993.

Figure 6. Shell Bintulu plant.

- SASOL operates the GTL Oryx plant in Ras Laffan, Qatar: the production started in 2007 and the process is based on a cobalt slurry reactor. The production capacity is 34,000 barrels per day.
- The Pearl GTL project of Shell in Qatar the production started in 2011 and will reach full production 140,000 barrels per day in 2012. It will be the largest GTL plant[10]

Figure 7. Bird-view photo of the Pearl GTL plant operated by Shell in Qatar with a capacity of about 140,000 barrels per day.

- Chevron, the Nigerian National Petroleum Corporation and SASOL are building 33,000 barrels per day plant in Escravos, Nigeria. The Escravos GTL (EGTL) project

was 76% complete by June 2011 and is expected to be expanded to a 120,000 bpd capacity within ten years of its completion [11,12].

At present day there is no BTL plant in operation but UPM [13] a Finnish paper and pulp manufacturer has a project to build a BTL plant in Europe using waste biomass resulted from paper and pulp manufacturing as a feedstock.

2 Fischer-Tropsch synthesis

Fischer-Tropsch synthesis is a complex process because of the large range of product obtained including paraffin, olefin and oxygenate compounds. This large range of products was obtained from the various reactions that takes places during the reaction resulted from elementary bond-breaking and bond-formation steps. The Fischer-Tropsch reaction is generally regarded as a polymerization reaction and can be summarized into a few general equations:

Methane formation

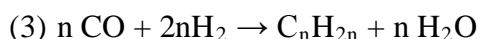


Paraffin formation



Methane and paraffins are the main products obtained during the FTS and their formation are highly exothermic reactions as indicated by the reaction's enthalpy but other reactions can occur during the process like the formation of olefin and oxygenated compounds.

Olefin formation



Oxygenated compound formation



Other unwanted side reaction can occur during the process. The water gas shift (WGS) reaction (5) and the Boudouard reaction (6) leading to the formation of CO₂ and carbon deposit.



Despite the fact that the reaction is known since the 1920s the exact mechanism of this reaction is still under debate. Although it is regarded as a polymerization reaction the main difference is the monomer responsible for the chain growth. The first mechanism proposed by Fischer and Tropsch [14] is a carbide mechanism where CH_x is the monomer. Storch et al [15] proposed a mechanism where oxymethylene (HCOH) is the species responsible for the chain growth and Pichler and Schulz [16] proposed the CO insertion into the metal-methyl bond.

3 Fischer-Tropsch Technology

3.1 Synthesis gas generation

The synthesis gas preparation section is an important part of XTL plant. It is the most expensive part of the plant. Synthesis gases are prepared from a carbonaceous feedstock. The feedstock should also contain hydrogen which is needed to produce hydrocarbons. For the preparation of synthesis gas there are two main technologies, gasification and reforming. Gasification is used to convert solid or heavy liquid feedstocks into synthesis gas while reforming is the term used to describe the conversion of gaseous or light liquid feedstocks. The most common feeds are coal and natural gas.

Gasification involves the reaction of a carbon source with a source of hydrogen usually steam. The solid will be converted into raw synthesis gas containing hydrogen, carbon oxide, carbon dioxide, methane and other unwanted product. Once the feedstock has been converted into gas, undesirable products like sulfur, mercury, arsenic, etc. will be removed from the gas by different techniques.

In an oxygen and steam fed gasifier the reactions are summarized below: (7) steam/carbon reaction and (8) partial oxidation.



In addition to these reactions total combustion can also occur. Other reaction may occur such as methanation (9) and WGS (5)



The water gas shift (WGS) reaction can be used to tune the H₂/CO ratio.

Before reforming the natural gas must be treated to remove or recover higher hydrocarbon (NGL or LPG) and also to remove sulfur compounds because sulfur is a poison for both synthesis gas catalyst and for the FT synthesis catalyst. The synthesis gas can be prepared in various ways, steam reforming or autothermal reforming.

Steam reforming involves the reaction of methane with water in vapor form. This reaction is usually catalyzed by nickel on alumina, although other metals can be used.



Steam can be partially substituted by carbon dioxide to perform CO₂ reforming.



Steam and CO₂ reforming are accompanied by the WGS reaction. The steam reforming of methane is highly endothermic and need a high temperature, i.e. from 600 to 1000°C. This process produces a synthesis gas rich in hydrogen which is subsequently adjusted for the Fischer-Tropsch process.

Autothermal reforming (ATR) combine combustion with a catalytic process. The first part of ATR is the combustion at fuel-rich conditions of a mixture of natural gas and steam and the final conversion into syngas over a catalytic fixed bed. The reactions are combustion (12), reforming (10) and WGS (5).



ATR can produce H₂/CO within a wide range of ratio which could find use in different processes.

3.2 Reactor

There are four types of Fischer-Tropsch reactors in commercial use [17], which are:

- Fluidized bed reactor
- Circulating fluidized bed
- Tubular fixed bed reactor
- Slurry phase reactor

Figure 8. Different types of reactors which operated in the Fischer-Tropsch process [18]

Because the formation of a liquid phase in the fluidized bed will lead to particle agglomeration and loss of fluidization, the fluidized bed reactors are used for high temperature Fischer-Tropsch synthesis (HTFT). Indeed, the temperature level to operate fluidized bed is in the range 320-350 °C. The catalyst, generally iron in a metallic state and

operating conditions are selected to obtain the desired products. HTFT reactors are generally used to produce light alkenes or gasoline.

Slurry phase and tubular fixed-bed reactors operate in the temperature range from 220 to 250 °C and hence they are called low temperature Fischer-Tropsch (LTFT) reactor. In this type of reactor heavy hydrocarbons in the form of liquid waxes are obtained which will be further upgraded to yield the valuable fractions. Both iron and cobalt are used in those reactors. For slurry phase reactors the advantages are (i) cost of the reactor, i.e. 25 % of the cost of a multi-tubular reactor, (ii) absence of pressure drop, and (iii) easy control of the reaction temperature due to the high heat exchange between the catalyst particles and the liquid medium. The disadvantages are the difficulty in the separation between the wax and the catalyst, due to the problem of fine formation during the operation, and the sensibility to poisoning.

For the fixed bed reactor the operating conditions are easier but there are some disadvantages. Because of the high exothermicity of the reaction the preferred fixed bed reactor configuration is constituted by multi tubular reactors to narrow the distance between the catalyst particle and the reactor walls where the heat exchange with the external medium is performed. A short distance between the catalyst particles and the reactor walls and a high gas linear velocity will improve the heat transfer inside the catalyst bed and to prevent hot spot formation which is detrimental to the reaction selectivity. To achieve higher conversion small catalyst pellets or extrudates are needed but it increases the pressure drop along the tubes so compromises are needed between the size of the particle and the activity of the catalyst. However, multi-tubular reactors consist of thousands of tubes and thus, result in high construction cost. The advantages of the fixed-bed reactor compared to the slurry phase reactor are the following:

- They are easy to operate, because the waxes simply trickle out of the bed there is no need to separate the wax from the catalyst;
- Large scale reactor performance can easily be extrapolated starting from pilot consisting of one single tube.
- In addition, if some poisons pass through the purification process only the top of the catalyst bed will be damaged.

3.3 Active phase

It is a well known fact that Group 8 transition metals are active for the FTS. However the CO hydrogenation activity is a key parameter for a commercial application and only Ni, Co, Fe and Ru have a sufficient activity. Unfortunately Ni has a high selectivity toward methane and for this reason it is not a suitable catalyst to produce long chain hydrocarbon. Ruthenium is the most active metal for FTS and is also working at the lowest temperature [19], however the scarce availability and the high cost of Ru prevents its commercial use in large scale FT applications (Table1). The choice of active metal, between iron and cobalt for commercial application, depends on a number of parameters, the source of carbon used for syngas and the end-product. For syngas deficient in hydrogen, as those obtained from coal and biomass, iron is generally preferred because of its high WGS activity reaction, the lack of hydrogen is compensated by the WGS but more CO₂ is produced. But with new environmental concerns, including the greenhouse effect, carbon dioxide is becoming more and more an unwanted byproduct and the high WGS is becoming a major drawback for iron.

Metal	Relative cost
Fe	1
Ni	250
Co	1000
Ru	50000

Table 1: Approximate relative cost of active metals for FT reaction.

Cobalt is preferred for performing FTS with an almost stoichiometric ratio of hydrogen and carbon monoxide, i.e. syngas produced from natural gas. Because of the relatively high cost of cobalt, the use of bulk cobalt as a catalyst is not economically viable. To obtain a high exposed cobalt metal surface per mass unit of cobalt, cobalt needs to be dispersed on an appropriate support. To have a well dispersed metal particle a suitable high area porous material is required.

3.4 Supports

Supports material typically used in commercial FT are silica, alumina, titania, zinc oxide or combinations of these oxides [20,21]. In the literature numerous example of mesostructured material [22,23,24] like MCM41 and SBA-15 can be found and there is also

some publications on carbon supports [25,26,27]. The ideal support for the Fischer-Tropsch synthesis should have the following properties:

- Appropriate specific surface area.
- Adequate mean pore diameter, preferentially large mesopores (for fixed bed).
- Medium metal-support interactions.
- High attrition resistance and bulk crush strength (for slurry).
- Chemical inertness.
- Moderate and/or high thermal conductivity (for fixed bed).
- Appropriate size and shape regarding the scaling up to industrial process.

The surface area is one of the most important parameter, because a high surface will help the dispersion of the metal. However, high surface area materials generally possess narrow pores which could affect mass transfer and in turn, the selectivity in liquid hydrocarbons. Several studies [28 ,29,30 ,31 ,32 ,33] have shown that the support pore size affects the particle size of cobalt. Crystallites are formed from the droplets during the drying of the cobalt precursor and the pores size will affect the size of this liquid hence affect the size of the cobalt particle. They also found that the reduction is easier on large pore support's and attributed this effect to the cobalt cluster size. Because FTS depends on the number of active site when increasing the pore size there is a competition between the dispersion and the degree of reduction of cobalt cluster. Saib et al [29] also observed that support with very small average pore diameter face some problem of pore plugging. Khodakov [34] observed a lower activity and selectivity on narrow pore cobalt catalyst and attributed them to a lower reducibility of the active phase. But recent studies [35,36] point out the effect on the diffusion of the reactant and product. When small pores are present the diffusion of reactant will be hampered which induces a higher H₂/CO ratio and decreases the selectivity toward higher hydrocarbons. Xiong [37] observed on alumina that the activity and selectivity were differently affected by the support pore size and attributed the lower activity to the lower number of active sites and the higher selectivity to the re-adsorption of olefins due to the long residence time of products in micro-pores. Witoon [36] found that with increasing mesopore diameter the cobalt crystallite size and C₅+ selectivity increase, whereas CO₂ and methane selectivities decrease and the presence of macropores will affect selectivity only for large catalyst particles.

The synthesis of small cobalt crystallites requires a strong metal-support interaction to stabilise the metal particles and prevent sintering [38]. But strong metal interactions induce formation of hardly reducible species that need high reduction temperature which lead to extensive sintering of the active phase particles. According to Jacobs [39] the extent of cobalt oxide reduction follows the trend $\text{Al}_2\text{O}_3 < \text{TiO}_2 < \text{SiO}_2$ and increases with the cobalt loading while the average particle size follows the reverse trend. There is a competition between dispersion and extent of reduction of the cobalt crystallite. Among the different supports cited above, alumina has the strongest interaction with cobalt, resulting in a good dispersion of the metal particles but a lower reducibility due to the diffusion of cobalt ions into the alumina structure, while the interaction with silica is lower resulting in larger particles but a higher degree of reduction [40,41].

The formation of cobalt surface phase which strongly interacts with the support is a major drawback especially for alumina because of the reduction of the number of cobalt available for the reaction. Jongsomjit [42] observed an increase in activity upon zirconia-modified alumina and attributed this effect to an increase in reducibility due to a stabilisation of the alumina support by blocking the defects site thus blocking the aluminates formation. But Hong [43] observed that on large pore SBA-15 zirconia modification did not result in change in reducibility hence did not change the activity, while on smaller pore MCM-41 increasing the zirconia loading led to lower dispersion. Jean-Marie et al [44] have shown that doping alumina with silica enhances cobalt reducibility and reduces the amount of hardly reducible cobalt aluminate which leads to higher conversion. Sun et al [45] arrive to the same conclusion: the reduction degree increases with increasing SiO_2 loading while the cobalt particle size slightly increases; they also observed that addition of Al_2O_3 to SiO_2 has the reverse promotional effect.

Alumina is the most used support for FT catalysts, however, the low thermal conductivity of alumina renders it more sensitive to the problems of temperature runaway and hot spots formation, which compromise the plant security and decrease the selectivity towards liquid hydrocarbons. In addition, the FTS is generally carried out with a relatively low space velocity in order to increase the α -olefins intermediate insertion to improve chain growth. The low space velocity favours the catalyst temperature runaway as generally the hot spot extent is unlikely to appear at high space velocity which causes high turbulence that ensures high heat transfer between the catalytic bed, the gas flow and the reactor wall. One should also note that in some cases the hot spots which are generated on the catalyst surface are at a nanometer size

and thus, the extra-heat removal by the gas phase is not sufficient compared to that generated by the reaction itself, i.e. nanoscopic hot spot.

According to the results presented above dealing with the difficulty to reduce the active phase precursor on the oxidic supports, some projects dealing with the use of carbon-based catalysts in FTS have been initiated, such as , activated carbon (AC) [46,47], carbon nanotubes (CNT) [47,48,49], carbon nanofiber (CNF) [49,50,51] and carbone sphere (CS) [27]. Among these carbon supports, CNTs and CNFs have been especially studied for Fischer-Tropsch synthesis due to their exceptional physical properties for being used as catalytic support [52]. Yu et al [53] have shown that CNFs-based catalysts show the same conversion as high surface area γ -Al₂O₃-based catalysts but with a higher selectivity. Bezemer et al [54] have shown that SiO₂-based catalysts need higher reduction temperature than CNF-based ones and as a consequence, have larger metal particles due to sintering. Due to the low metal support interaction, Bezemer et al [50] have been able to use nanofibers to study the cobalt particle size effects. The nanoscopic morphology of the supports complicates the transport and handling, as well as the scaling up to an industrial process, hence carbon nanotubes and carbon nanofibers are up to now mostly studied as model catalysts. It is expected that the macroscopic shaping of these nanoscopic materials could allow them to be efficiently employed as catalyst support in the future.

The strong metal-support interactions between the deposited phase and the oxidic supports, i.e. Al₂O₃ and SiO₂, and the chemical reactivity of these later also complicate the recovery of the metal and the support after the end-life of the catalyst. On the other hand, carbon-based catalysts are more sensitive to oxidation during the regeneration process. It is therefore interesting to develop new support materials that can effectively replace those mentioned above, mainly in terms of physical properties, which could provide an easy reducibility of the deposited active phase leading to a higher available exposed metallic fraction for catalytic reaction which contributes to the improvement of the catalytic performance. New supports should also be cheap and readily available in the same shape as those usually employed in order to reduce the cost incentive linked to extra additional modifications of the plant itself.

New catalyst support materials are not frequently reported in the literature, with almost no new support materials being incorporated into commercial use since World War II. Silicon carbide (SiC) is a covalent material, with a tetrahedral structural unit with an excellent

thermal stability, high mechanical strength, excellent resistance to oxidation and corrosion, low thermal expansion coefficient and high heat conductivity. To be useful as a catalyst support, SiC must be prepared with a high surface area. This is not possible with the conventional Acheson synthesis and is consequently the limiting factor for its applications. The Acheson process as operated nowadays only yields materials with a surface area of 0.1 to 1 m²/g, too low to be used as catalyst supports. A simple gas-solid synthesis method (called Shape Memory Synthesis method, SMS) has been developed by Ledoux and co-workers at the beginning of the 80's to make silicon carbide (β -SiC) with medium specific surface area, 10-40 m². g⁻¹, which can be employed as catalyst support in heterogeneous catalysis [55,56]. The reactions sequence is described by the following equations (Eq. (13) and (14)):



Industrial synthesis of β -SiC was developed in the 90's and the raw materials and process were modified in order to cope with the industrial requirements [57,58]. In the typical synthesis, SiO vapour is generated by reaction between Si and oxygen contained in a solid resin, while the second step of the synthesis remains almost unchanged. It is noteworthy that the CO formed during the course of the synthesis was removed from the reaction zone by an argon flow at atmospheric pressure and thus shifting the reaction towards the right-hand side.

A high surface area support can provide a better dispersion which leads to a high active surface, but usually supports with a high surface area contain a large number of small pores limiting the diffusion of reactant and product. This diffusion limitation could lead to a decrease in the concentration of CO inside the pore and therefore change the ratio of CO to H₂ and lead to increase the selectivity toward lighter hydrocarbon. For this reason the meso-macroporous network of SiC is advantageous for the Fischer-Tropsch reaction.

The specific surface area and the pore volume of the silicon carbide depend on the physical properties of precursor materials [58] (particle diameter, specific surface area of the precursor). During the synthesis of the SiC, specific surface area and pore size can be tuned by changing some parameters like the particle size of the precursor material, the binder or by the addition of additive or pore former.

In catalytic lab-scale reactors filled with insulator supports, SiC is usually mechanically mixed with the catalyst in order to avoid hot spots formation within the catalyst

bed. To our knowledge SiC as catalyst support for industrial fixed-bed FTS reaction has never been reported so far in the literature apart of some patent applications [59,60,61,62]. It is thought that the intrinsic thermal conductivity of SiC can help in the heat dissipation throughout the catalyst body and thus, avoid the formation of local hot spots which could modify the overall selectivity of the reaction. Such an assumption has been verified in other exothermic reactions such as n-butane and H₂S selective oxidation reactions [63,64].

Silicon carbide synthesized by a gas-solid reaction also contains an appropriate porosity, mostly distributed in meso- and macro-pores, which significantly improve diffusion of the reactants to the active site and the release of the products from the catalytic bed and thus, reduces the problem linked to mass transfer limitations. Indeed, mass transfer limitation is a very important phenomenon in fixed bed Fischer-Tropsch synthesis due to the formation of liquids, i.e. liquid hydrocarbons and water during the course of the reaction, which slowly fill-up the pores of the catalyst. Diffusion of the gaseous reactants to the active sites localized within the pore covered with a thin liquid film is strongly enhanced and the reaction becomes mass transfer limited. The mass transfer limitations will mostly influence the reaction selectivity by modifying the H₂/CO ratio next to the active site, i.e. CO arrival limitation, and the escaping rate of the intermediate products.

Finally, it is worthy to note that the chemical inertness of the silicon carbide support also allows an easy recovery of both the active phase and the support by a simple acid or basic wash unlikely to the traditional catalysts based on alumina or silica where recovery needs a complex chemical treatment to be efficiently achieved.



Figure 9. Silicon carbide (SiC) with different shapes synthesized by the gas-solid reaction (courtesy by Sicat).

3.5. Deactivation

Deactivation in Fischer-Tropsch catalyst is a complex problem involving several mechanisms. The main causes of deactivation as they appear in the literature [65] are the following:

- Poisoning
- Oxidation of the cobalt active site
- Cobalt aluminate formation
- Carbon deposition
- Sintering
- Surface reconstruction
- Attrition

Sulphur and nitrogen are two main poisons for FT catalysts. Sulphur is a well known poison for cobalt because it adsorbs strongly on active sites leading to the physical blocking of the active sites. The poisoning by nitrogen compounds is rapid but reversible.

Re-oxidation of cobalt has been the most studied mechanism of deactivation in FT. But it is still a debated subject. Water which is the most important by-product of FTS is an oxidizing agent and may cause surface oxidation of the catalyst. But according to recent publications

only the smallest particles can be oxidized by steam during FT synthesis. Moodley [66] did not observe oxidation of crystallites with diameter $> 6\text{nm}$ but observed an extent of the reduction degree with time on stream.

Mixed oxides of cobalt and support are not active in Fischer-Tropsch so the formation of these mixed oxide during FTS may reduced the available quantity of cobalt for the reaction. But according to Moodley [66] during realistic FTS conditions the formation of cobalt aluminate resulted from the unreduced CoO species and so the formation of aluminates is not a cause of deactivation.

There are many ways for carbon to cause deactivation. Higher molecular weight hydrocarbons may accumulate in pore channels and slow down the diffusion of reactants. CO dissociation is an elementary step during FTS so carbon is present on the surface of the cobalt. Carbon oligomers can be formed followed by a coupling reaction between these oligomers to form polymeric carbon and lead to loss activity due to the geometric blocking.

Sintering is a common cause of deactivation for supported metal catalyst. But there are only a few publications reporting sintering during FTS.

Reconstruction of cobalt surface occurs during FTS and may lead in a change of the nature of active site which contributes to the activity loss.

Attrition is the breakdown of solid particle by erosion, abrasion or fracture. Attrition is more extreme for fluidized beds and slurry reactors.

3.6. Particle size effects

Metallic Co^0 sites are the active species in FTS. Lots of work have been done in order to improve the dispersion of the metal in order to enhance the amount of exposed metallic cobalt atoms. The particle size effect has been studied by several authors in the literature. Ho et al. [67] have found no influence of the particle size on CO hydrogenation turnover frequency for Co/SiO₂ with particle size in the range of 5 nm to 20 nm. Iglesia [68] shown that the turn over frequency (TOF) is not a function of the particle size for particle larger than 9 nm but for smaller particle a decrease in FT performance have been reported. Barbier et al [69] reported a decrease in TOF for particles smaller than 6 nm. Bezemer et al. [25] studied particle size on CNF and shown a decrease in TOF for particles smaller than 6 nm and an increase in methane

selectivity. Den Breejen et al [70] concluded with SSITKA experiment that the decrease in TOF and increase of methane selectivity is due to a change in the residence time of intermediates. Wang et al [71] have also studied the particle size effect on a series of Co/SiO₂ model catalysts and have only an effect of Co particle in the range 1.4-2.5 nm. Cobalt was easily oxidized leading to a decrease in the TOF.

4 Scope and outline of this thesis

The aim of the present work is devoted to the development of a new type of support based on silicon carbide with medium to high specific surface area and to study the influence of the different physical properties of the silicon carbide support, e.g. pore size distribution, specific surface area, nature of the dopant, etc., on the activity and the selectivity of the catalyst in the Fischer-Tropsch synthesis. The active phase is cobalt particles either pure or doped with trace amounts of ruthenium.

Chapter 2 presents the results obtained in the FTS on a cobalt-based catalyst supported on either silicon carbide or alumina foam structure. The FTS tests were also carried out on a hybrid SiC foam support coated with a thin layer of alumina. The results obtained showed that the liquid hydrocarbon selectivity (SC₅₊) was highly improved when the catalyst was constituted with supports with better thermal conductivity along with a mesoporous network, which facilitates both reactant and product diffusion. The catalyst recovery was also investigated in this chapter. The chemical inertness of the SiC support allows one to dissolve the cobalt active phase by a simple acid washing at room temperature. The treated support can be also re-used by depositing a new charge of cobalt. The results obtained indicate that the re-make catalyst exhibits a similar FT activity and selectivity as those obtained on the fresh one and confirms the high advantage of the ceramic support compared to other supports such as alumina, silica or activated charcoal.

Chapter 3 is devoted to the influence of ethanol as impregnation solvent on the FTS catalytic performance of the cobalt-based catalysts, doped with traces of ruthenium. The FTS activity significantly increases when the catalyst was impregnated with ethanol as solvent instead of water. The possible influence of the different cobalt species, i.e. face centered cubic (fcc) or hexagonal close packed (hcp), on the FTS performance was also investigated using a ⁵⁹Co zero field NMR technique. This is the first time this technique has been used in

catalysis. According to the NMR results one could state that the increase of the FT activity was linked on one hand to the presence of smaller hexagonal cobalt particles and on the other hand, to the complete incorporation of the ruthenium within the cobalt matrix forming an alloy.

Chapter 4 presents the effect of the porosity and the specific surface area of the support on the activity in FTS. For the tests, two SiC supports with different pore size were used. The results indicate that a higher activity was obtained with the sample having a higher porosity. It is expected that large pores favour the diffusion of reactant and the evacuation of product out from the catalyst porous network, and thus reducing the thickness of the wax layer on the pore surface, which could lead to a higher activity.

Chapter 5 concerns the doping of the support with titanium to modify the specific surface area and to change the surface chemistry of the support. The addition of titanium in the bulk of SiC significantly increases the specific surface area of the support which could help the dispersion of the active phase and increase the activity of the catalyst while keeping a good selectivity due to the presence of meso-macropores. The titania doping also improves the chemical interaction with the active phase leading to the formation of smaller cobalt particles with better FTS catalytic activity. The catalyst was characterized by several techniques including ^{59}Co NMR, Energy-filtered TEM with elemental volume reconstruction, etc.

Chapter 6 presents the general conclusion of this work and the outlook derived from the different results obtained.

-
- [1] P. Girard, A. Fallot, *Energy Sustain Develop*, 10, (2006), 92-108,
- [2] U.S. energy information administration www.eia.gov
- [3] P. Sabatier and J.B. Senderens, *Compt. Rend. Acad. Sci* 134 (1902) 514-516
- [4] F. Fischer and H. Tropsch, *Brennstoff-Chem.* , 4 (1923) 276-285
- [5] A. Y. Khodakov, W. Chu, P. Fongarland, *Chem. Rev.* 107 (2007) 1692-1744.
- [6] M. E. Dry, *Catal. Today* 71 (2002) 227-241.
- [7] A. Y. Khodakov, *Catal. Today* 144 (2009) 251-257.
- [8] R. Rostrup-Nielsen, *Science* 308 (2005) 1421-1422.
- [9] <http://www.petrosa.co.za/>
- [10] http://www.shell.com/home/content/aboutshell/our_strategy/major_projects_2/pearl/
- [11] <http://www.hydrocarbons-technology.com/projects/escravos/>
- [12] http://www.sasol.com/sasol_internet/frontend/navigation.jsp;jsessionid=UHVAQLGWNYOLDG5N4EZSFEQ?navid=21300011&rootid=2
- [13] <http://www.upm.com/EN/MEDIA/Press-kits/Business/Biofuels/Pages/default.aspx>
- [14] F. Fischer and H. Tropsch *Brennstoff-Chem* 104 (1926) 7-97
- [15] H.H. Storch, N. Golumbic, and R.B. Anderson. *The Fisher-Tropsch and related syntheses*, Wiley, New York
- [16] H. Pichler, H. Schulz, *Chem Ing Technol.* 42 (1970) 1162
- [17] A.P. Steynberg, M.E. Dry, B.H. Davis, B.B. Breman, Chapter 2 Fischer-Tropsch Reactors, in *Studies in Surface Science and Catalysis*, Elsevier, 2004, Volume 152, Fischer-Tropsch Technology, Pages 64-195
- [18] <http://www.zero.no/transport/biodrivstoff/fischer-tropsch-reactor-fed-by-syngas>
- [19] Vannice, M.A. J. *Catal* 37 (1975) 449-461
- [20] R. Oukaci, A. H. Singleton, J. G. Goodwin Jr. *Appl. Catal. A* 281 (1999) 129-144
- [21] M.E. Dry Chapter 7 Fischer-Tropsch Reactors, *Studies in Surface Science and Catalysis*, Elsevier, (2004), Volume 152, Fischer-Tropsch Technology, Pages 533-600

- [22] O. Gonzalez, H. Perz, P. Navarro, L.C. Almeida, J.G. Pacheco, M. Montes, *Catal. Today* 148 (2009) 140-147
- [23] G. Prieto, A. Martinez, R. Murciano, M.A. Arribas *Appl. Catal. A* 367 (2009) 146-156
- [24] M.K. Gnanamani, G. Jacobs, U.M. Graham, W. Ma, V.R.R. Pendyala, M. Ribeiro, B.H. Davis *Catal. Let.* 134 (2010) 37-44
- [25] G.L. Bezemer, J.H. Bitter, H.P.C.E. Kuipers, H. Oosterbeek J.E. Holewijn, X. Xu, F. Kapteijn, A. Jos Van Dillen, K.P. de Jong, *JACS* 128 (2006) 3956-3964
- [26] W. Ma, E.L. Kugler, J. Wright, D.B. Dadyburjor, *Energy Fuels* 20 (2006) 2299-2307
- [27] H. Xiong, M.A.M. Motchelaho, M. Moyo, L.L. Jewell N.J. Colville *J. Catal.* 278 (2010) 26-40
- [28] A.Y. Khodakov, A. Griboval-Constant, R. Bechara, F. Villain, *J. Phys. Chem. B* 105 (2001) 9805-9811
- [29] A.M. Saib, M. Claeys, E. van Steen, *Catal. Today* 71 (2002) 395-402
- [30] H. Xiong, Y. Zhang, K. Liew, J. Li, *Appl. Catal. A* 295 (2008) 68-76
- [31] Y. Liu, J. Chen, K. Fang, Y. Sun, *Stud. Surf. Sci. Catal.*, 165 (2007) 671-674
- [32] D. Song, J. Li *JMol. Catal. A* 247 (2006) 206-212
- [33] Ø. Borg, S. Eri, E.A. Blekkan, S. Storsæter, H. Wigum, E. Rytter and A. Holmen, *J. Catal.* 248 (2007) 89-100
- [34] A.Y. Khodakov, A. Griboval-Constant, R. Bechara and V.L. Zholobenko, *J. Catal.* 206 (2002) 230-241
- [35] C. Lesaint, W.R. Glomm, O. Borg, S. Eri, E. Rytter and G. Oye, *Appl. Catal. A* 351 (2008) 131-135
- [36] T. Witoon, M. Chareonpanich, J. Limtrakul, *Fuel Process. Technol.*, 92 (2011) 1498-1505
- [37] H. Xiong Y. Zhang S. Wang, J. Li, *Catal. Comm.* 6 (2005) 512-516
- [38] E. Iglesia *Appl. Catal. A* 161 (1999) 59-78
- [39] G. Jacobs, Y. Ji, B.H. Davis, D. Cronauer, A.J. Kropf, C.L. Marshall *Appl. Catal. A* 333 (2007) 177-191
- [40] M. Vob, D. Borgmann, G Weldler, *J. Catal.* 212 (2002) 10-21
- [41] G.Jacobs, T.K. Das, Y. Zhang, J. Li, G. Racoillet, B.H. Davis, *Appl. Catal. A* 281, (2002) 233-263

-
- [42] B. Jongsomjit, J. Panpranot, J.G. Goodwin Jr., *J. Catal.*, 215 (2003) 66-77
- [43] J. Hong, W. Chu, P.A. Chernavskii, A.Y. Khodakov, *Appl. Catal. A*, 382 (2010) 28-35
- [44] A. Jean-Marie, A. Griboval-Constant, A. Khodakov, F. Diehl, *C. R. Chim.* 12 (2009) 660-667
- [45] X. Sun, X. Zhang, Y. Zhang, N. Tsubaki, *Appl. Catal. A* 377 (2010) 134-139
- [46] W. Ma, E.L. Kugler, J. Wright, D.B. Dadyburjor, *Energy Fuels*, 20 (2006) 2299-2307.
- [47] M. Zaman, A. Khodadov, Y. Mortazavi, *Fuel Process. Technol.* 90 (2009) 1214-1219
- [48] A. Tavasoli, K.Sadagiani, F. Khorashe, A.A. Seifkordi, A.A. Rohani, A. Nakhaeipour, *Fuel Process. Technol.*, 89 (2008) 491-498.
- [49] Jung, A., Kern, C., Jess, A. DGMK Tagungsbericht, (2008) 263-268
- [50] G.L. Bezemer, J.H. Bitter, H.P.C.E. Kuipers, H. Oosterbeek, J.E. Holewijn, X. Xu, F. Kapteijn, A.J. Van Dillen, K.P.De Jong, *JACS* 128 (2006) 3956-3964
- [51] G.L. Bezemer, U. Falke, A.J. Van Dillen, K.P. De Jong, *Chem. Commun.*, (2005) 731-733
- [52] P. Serp, M. Corrias, P. Kalck, *Appl. Catal. A* 253 (2003) 337-358
- [53] Z. Yu, Ø. Borg, D. Chen, B.C. Enger, V. Frøseth, E. Rytter, H. Wigum, A. Holmen, *Catal. Lett.*, 109 (2006) 43-47
- [54] G.L. Bezemer, P.B. Radstake, V. Koot, A.J. Van Dillen, J.W. Geus, K.P. De Jong, *J. Catal.*, 237 (2006) 291-302
- [55] M. J. Ledoux, S. Hantzer, C. Pham-Huu, J. L. Guille, M. P. Desaneaux, *J. Catal.* 114 (198) 176-185.
- [56] M. J. Ledoux, C. Pham-Huu, J. L. Guille, H. M. Dunlop, S. Hantzer, S. Marin, M. Weibel, *Catal. Today* 15 (1992) 263-24.
- [57] Website : www.sicatcatalyst.com
- [58] P. Nguyen, Ch. Pham, *Appl. Catal. A* 391 (2011) 443-454.
- [59] S. Savin-Poncet, M. J. Ledoux, C. Pham-Huu, J. Bousquet, B. Madani, *Int. Pat. Appl. WO 2005/073345 A1*, assigned to TOTAL France (2005).
- [60] C. Pham-Huu, B. Madani, M. Lacroix, L. Dreibine, M. J. Ledoux, S. Savin-Poncet, J. Bousquet, D. Schweich, *Int. Pat. Appl. WO 2007/000506 A1*, assigned to TOTAL SA (2007).
- [61] M. Lacroix, PhD dissertation, University of Strasbourg (2008)

- [62] R. Philippe, M. Lacroix, L. Dreibine, C. Pham-Huu, D. Edouard, S. Savin, Fr. Luck, D. Schweich, *Catal. Today* 147 (2009) 305-312.
- [63] M. J. Ledoux, C. Crouzet, C. Pham-Huu, V. Turines, K. D. Kourtakis, P. L. Mills, J. J. Lerou, *J. Catal.* 203 (2001) 495-508
- [64] P. Nguyen, D. Edouard, J. M. Nhut, M. J. Ledoux, C. Pham-Huu, *Appl. Catal. B* 76 (2007) 300-310
- [65] N.E. Tsakoumis, M. Rønning, Ø. Borg, E. Rytter, A. Holmen, *Catal. Today*, 154 (2010) 162-182
- [66] D.J.Moodley, A.M. Saib, J. Van De Loosdrecht, C.A. Welker-Nieuwoudt, B.H. Sigwebela, J.W. Niemantsverdriet, *Catal Today*, 171 (2011) 192-200
- [67] S.-W. Ho, M. Houalla, D.M. Hercules, *J. Phys. Chem.*, 94 (1990) 6396-6399
- [68] E. Iglesia, *Appl. Catal. A*, 161 (1997) 59-78
- [69] A. Barbier, A. Tuel, I. Arcon, A. Kodre, G.A. Martin, *J. Catal.*, 200 (2001) 106-116
- [70] J.P. Den Breejen, P.B. Radstake, G.L. Bezemer, J.H. Bitter, V. Frøseth, A. Holmen, K.P. De Jong, *JACS* 131 (2009) 7197-7203
- [71] Z.-J. Wang, S. Skiles, F. Yang, Z. Yan, D.W. Goodman, *Catal Today*, 181 (2012) 75-81

CHAPTER II

SILICON CARBIDE FOAM COMPOSITE CONTAINING COBALT AS A HIGHLY SELECTIVE AND RE-USABLE FISCHER- TROPSCH SYNTHESIS CATALYST

Maxime Lacroix, Lamia Dreibine, Benoit de Tymowski, Fabrice Vigneron^a, David Edouard, Dominique Bégin, Patrick Nguyen, Charlotte Pham, Sabine Savin-Poncet, Francis Luck, Marc-Jacques Ledoux, Cuong Pham-Huu

Abstract

The Fischer-Tropsch synthesis was evaluated on cobalt based catalyst supported on a medium surface area SiC foam ceramic in a fixed-bed configuration. The catalytic results were compared with those obtained on a Co/Al₂O₃ foam catalyst. At medium conversion (< 50 %) the two catalysts display similar C₅₊ selectivity indicate that the intrinsic selectivity between the two catalysts is close from each other. However, when the CO conversion was increased to 70 %, a significant difference in terms of the C₅₊ selectivity was observed between the two catalysts, i.e. 80 % on the Co/SiC and 54 % on the Co/Al₂O₃, which indicate that under severe FTS reaction conditions the SiC seems to be more suitable support than alumina. It is also worth to note that under these reaction conditions the chain length probability, obtained on the SiC-based catalyst was 0.91 and wax formation was especially favoured. The improvement of the C₅₊ selectivity observed on the SiC catalyst was attributed to the high efficiency of the support to evacuate heat generated during the course of the reaction owing to its higher thermal conductivity. Additional catalytic test conducted on a hybrid support, i.e. Al₂O₃ coated SiC foam, again confirms the high C₅₊ selectivity under a similar severe reaction conditions in the presence of a SiC structure underneath of the alumina layer which play a role of heat disperser. In addition, the high chemical inertness of the SiC material also allows one to perform an easy recovery of both the active phase and the support by a simple acid washing. The recovered SiC support was further impregnated with a fresh cobalt phase and re-tested in the FTS and the catalytic results are compared with those of the former catalyst. The same product yield was obtained which confirms the potential of SiC to be employed as a re-usable support.

Keywords:

Silicon carbide – Alumina - Fischer-Tropsch synthesis – Catalyst recovery – Support recovery

1. Introduction

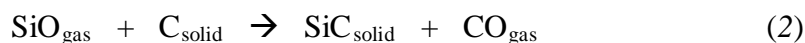
The Fischer-Tropsch Synthesis (FTS) which consists in the transformation of a synthesis gas mixture ($\text{CO} + n\text{H}_2$) into liquid hydrocarbons has received an over-increasing interest since the last decades (1-4). The final market for the liquid fuels produced by the FTS process is the transportation and chemical intermediates markets where sulphur free fuels are highly demanded. The FTS process also allows the reduction of natural gas flaring which is environmental prohibited due to the formation of CO_2 which is a green house gas. In addition, the synthetic fuels derived from the FTS process are sulphur free which could be further blended with others to meet the forwards environmental requirements about the sulphur content in the diesel fuel.

The FTS process is one of the most complex one, regarding the various reactions that take place during the gas-to-liquid transformation. Nowadays, the most employed active phase for the low-temperature FTS is cobalt, either pure or doped with trace amount of noble metal (5-11). Cobalt catalyst exhibits high stability, high activity and also is resistant towards oxidation. However, cobalt catalysts operate within a very narrow range of temperatures and pressures, and excursions out of the predicted temperature range leads to a huge increase in methane formation. Typically, an industrial state-of-the-art cobalt-based catalyst contains between 15 and 30 wt. % of cobalt supported on high specific surface area oxides, i.e. alumina, silica and titania, etc. The support could also be doped with foreign oxide, i.e. ZrO_2 , TiO_2 , etc. (12). Due to its relatively high price the cobalt is exclusively employed under a supported form. The support should have a high specific surface area in order to achieve a high dispersion of the active phase, a good mechanical and hydrothermal resistance and additionally, a high chemical inertness in order to reduce the fraction of hardly reducible phase during the thermal treatment steps. The metal-support interaction is also a parameter which needs to be taken into consideration, i.e. strong metal-support interactions give rise to the formation of the hardly reducible species leading to low active metallic sites, whereas too weak metal-support interactions induce metal particles sintering during the thermal treatment. Among the different supports, alumina is the most appropriate one to fulfil the requirements cited above. However, the low thermal conductivity of alumina renders it more sensitive to the problem of temperature runaway and hot spot formation which compromises the plant security and decreases the selectivity towards the liquid hydrocarbons. In addition, the FTS is generally carried out with a relatively low gaseous space velocity in order to increase the α -

olefins intermediate insertion and to improve the chain growth. The low gaseous space velocity favours the catalyst temperature runaway as generally the hot spot extent is unlikely to appear at high space velocity which causes high turbulence that ensures high heat transfer between the catalytic bed, the gas flow and the reactor wall. One should also note that in some cases, the heat generated on the catalyst surface cannot be effectively removed by the gas phase which leads to the formation of local hot spots on the catalyst surface. The heat release by the reaction could also be partly removed by the liquid hydrocarbons formed on and within the catalyst surface and porosity as well. However, it is worth mentioning that under severe reaction conditions, i.e. high CO conversion, the gaseous products inside the catalyst bed are significantly reduced and thus, part of the heat released by the reaction remains in the catalyst bed which could induce the temperature runaway. In this case, the use of support with higher thermal conductivity could be beneficial for maintaining a homogeneous temperature within the catalyst bed.

The metal-support interactions between the deposited phase and the alumina support also reduce the available fraction of metal for the reaction and also render difficult the recovery of the metal and support after the end-life of the catalyst. It is consequently of interest to develop new support materials that can efficiently replace those cited above, mainly in terms of physical properties, which could provide an improvement of the catalytic performance along with active phase recovery as well. The new support should also be cheap and be readily available in the same shape as those usually employed in order to reduce the cost incentive linked with extra additional modifications of the plant itself.

Silicon carbide (SiC) is a covalent material, with a tetrahedral structural unit with an excellent thermal stability, high mechanical strength, excellent resistance to oxidation and corrosion, low coefficient of thermal expansion and high heat conductivity. A simple gas-solid synthesis method (called Shape Memory Synthesis method, SMS) has been developed by Ledoux and co-workers at the beginning of 80's to make silicon carbide (β -SiC) with medium specific surface area, 10-40 m². g⁻¹, for use as catalyst support in heterogeneous catalysis field (13, 14). The reactions sequence is described by the following equations (1 and 2):



Industrial synthesis of β -SiC was developed in the 90s and the raw materials and process are modified in order to cope with the industrial requirements (15, 16). In the typical synthesis, the SiO vapour is generated by reaction between the Si and the oxygen contained in a solid resin while the second step of the synthesis remains almost unchanged. It is noteworthy that the CO evacuation by dynamic pumping used in the laboratory scale was replaced by a flushing with argon flow at atmospheric pressure.

In the catalytic reactor employing insulator support, SiC is usually mechanically mixed with the catalyst in order to avoid hot spots formation within the catalyst bed. To our knowledge SiC as catalyst support for fixed-bed FTS reaction has never been reported so far in the literature apart of some patent applications (17-20). It is thought that the intrinsic thermal conductivity of SiC can help in the heat dissipation throughout the catalyst body and thus, avoid the formation of local hot spots which could modify the overall selectivity of the reaction. Such assumption has been verified in other exothermic reactions such as n-butane and H₂S selective oxidation reactions (21, 22). In addition, the chemical inertness of the support also allows the easy recovery of both the active phase and the support by a simple acid or basic wash unlikely to the traditional catalysts based on alumina or silica where recovery needs a complex chemical treatment to be efficiently achieved.

The aim of the present article is to report the new development of an active and highly selective FTS catalyst consisted in a cobalt active phase supported either on a foam structure of silicon carbide (SiC) or on SiC support coated with a thin layer of γ -Al₂O₃. Alumina layer is expected to provide a surface having a higher interaction with the active phase and thus, to allow a reduction of the active phase particle size (23, 24). The results obtained are also compared with those obtained on a traditional γ -Al₂O₃ containing cobalt catalyst. The FTS performance will be discussed in the light of the catalytic results and physical characterization. Apparently, thermal conductor materials, i.e. SiC and Al₂O₃/SiC, provide a significant improvement of the liquid hydrocarbons selectivity compared to that obtained on an insulator support. The active phase and support recovery by a simple acid treatment was also carried out within the framework of the present article. The recovered SiC support was further re-impregnated with a new cobalt active phase and re-tested in the FTS reaction. The results will be compared with those obtained on the former catalyst.

2. Experimental section

2.1 Silicon carbide foam synthesis and characterization

Silicon carbide (β -SiC) in a foam shape was synthesized via a gas-solid reaction between the SiO vapour and dispersed solid carbon (13). The detailed synthesis of the SiC-based materials is summarized in a review (25). The starting polyurethane foam (PU foam) was infiltrated with a mixture of phenolic resin containing micrometric Si and carbon black at room temperature. After drying the obtained solid containing the resin, Si and carbon black was slowly heated up in flowing argon ($1^\circ\text{C. min}^{-1}$) from room-temperature to the carburization temperature (1350°C). During the heating from room-temperature to 700°C the resin underwent carbonization leaving behind a solid carbon skeleton containing oxygenated groups. At the carburization temperature, the oxygen issued from the resin reacted with Si to generated SiO vapour which further reacted with the carbon structure to form the SiC. The synthesis method allowed the complete conservation of the foam structure when passing from PU to carbon and finally SiC. All the geometry of the foam can be finely tuned by modifying the characteristics of the starting PU foam. The resulting SiC material was further calcinated in air at 800°C for 2 h in order to burn-off the residual un-reacted carbon material. Some examples of SiC foams with different window sizes are presented in Figure 1A. The microstructure of the used SiC foam is also presented in Figure 1B and C. The high-resolution TEM micrograph of the topmost surface of the SiC is presented in Figure 1D which clearly shows the presence of a thin amorphous layer on the SiC surface. Such amorphous layer consisted in a mixture of SiO_xC_y and SiO_2 according to the reports in the literature (26, 27). These species are also confirmed by the XPS analysis presented in Figure 1E. The amount of these SiO_x species present on the SiC surface, after synthesis and after calcination at 800°C , to remove the un-reacted carbon, was determined by submitting the sample to a NaOH (20 wt. %) treatment at 80°C which removed the SiO_2 and SiO_xC_y phases, is amounted to about 3.5 ± 0.5 wt. % (28). Such silicon containing oxygen phases was expected to play a role of natural wash-coat for anchoring the active phase onto the SiC surface. Indeed, on the SiC sample treated with NaOH at 80°C , the cobalt active phase is poorly dispersed resulting to the formation of aggregates with size of about micrometers due to the low interaction between the hydrophobic SiC surface and the precursor salt.

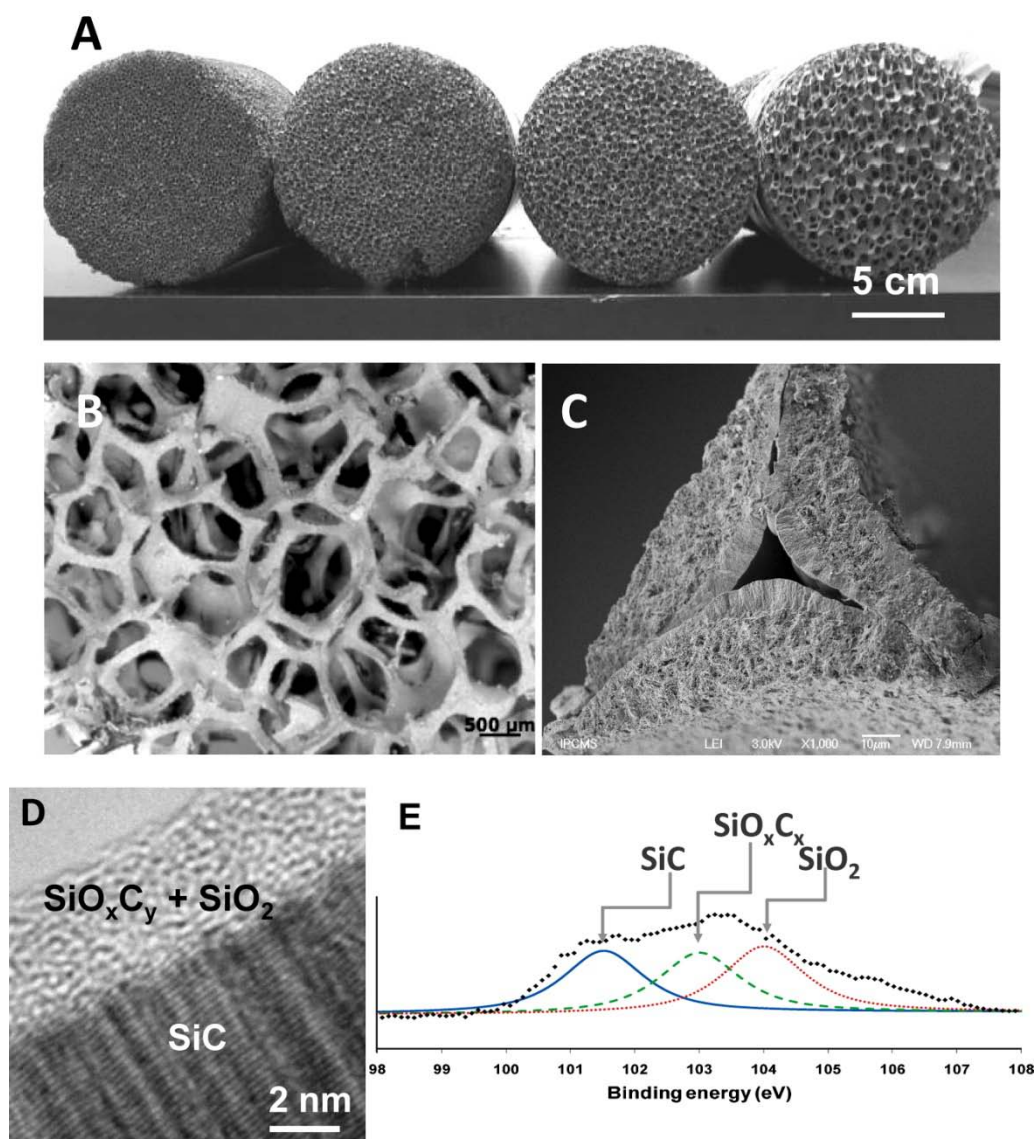


Figure 1. (A) Example of SiC foams with different window sizes, i.e. 850, 1100, 2700 and 4500 μm , synthesized according to the gas-solid reaction (Sicat courtesy). The representative SEM micrographs of the SiC foam support for cobalt in the FTS reaction. (B) Low magnification SEM micrograph showing the periodical stacking of pentagonal frames in the foam matrix. (C) High magnification SEM micrograph showing the detail microstructure of the strut containing mesoporous network. (D) High-resolution TEM micrograph evidences the presence of a thin layer of amorphous phase constituted by a mixture of SiO_2 and SiO_xC_y . (E) $\text{Si}2p$ XPS spectrum of the compounds present on the SiC surface. The XPS analysis evidences the predominant present of the Si-containing oxygen phases on the topmost surface of the SiC support which play a role of anchorage sites for the deposited metal active phase.

2.2 Al₂O₃ and Al₂O₃-SiC foams

The Al₂O₃ foam doped with zirconium was supplied by CTI (Salindres, France). The material has an extremely low specific surface area, 1 m². g⁻¹, and thus, a wash-coat is needed to ensure the active phase anchorage and dispersion on this material. The alumina wash-coat layer was prepared by immersing the low surface area Al₂O₃ foam into a solution of Disperal (aluminium hydroxide, Sasol) followed by a calcination step at 750°C 6h in order to form a layer of γ -Al₂O₃ on the foam surface.

The same process was further used to prepare the Al₂O₃-SiC foam hybrid support. The weight of the alumina was kept at 8 wt. % in order to obtain a similar surface area compared to the non coated SiC support. The Disperal coating was also favored by the presence of silicon containing oxygen species, i.e. SiO_xC_y and SiO₂, which are hydrophilic.

2.3 Catalyst preparation

The cobalt phase was deposited onto the supports via the incipient wetness impregnation method using an aqueous solution containing cobalt nitrate. The cobalt loading was set at 30 wt. % which is the upper range of cobalt loading according to the literature and patents surveys (29-31) and (11). The cobalt phase was loaded onto the support via a successive impregnation according to the patent recipes (32, 33). The catalyst after the first impregnation step was dried at 110 °C in air and calcined at 350 °C for 2 h in order to decompose the cobalt salt into its corresponding oxide. The catalyst was further impregnated a second time followed by a same thermal treatment to obtain the final catalyst. The oxidic form was further reduced in flowing hydrogen (300 ml. min⁻¹) at 300°C for 6 h. The reduced catalysts were passivated by contacting them with low oxygen containing mixture (1 vol. %) at room temperature before discharging in order to prevent as much as possible the bulk oxidation.

2.4 Characterization techniques

The nature and crystallinity of the cobalt phase, after calcination and after reduction, were characterized by means of the powder X-ray diffraction (XRD) technique. The analysis

was carried out on a Bruker D-8 Advance diffractometer with a Cu K α radiation. The sample was crushed into powder and deposited on a glass plate for analysis.

The morphology of the solid was examined by scanning electron microscopy (SEM) on a JEOL 6700-FEG microscope. The solid was fixed on the sample holder by a graphite paste for examination. Before analysis the sample was covered by a thin layer of gold in order to avoid the problem of charge effect.

The specific surface area measurements were carried out on a Tristar Micromeritics sorptometer using nitrogen as adsorbant at liquid nitrogen temperature. Before measurement the sample was outgassed at 250 °C for 3 h in order to desorb impurities and moisture on its surface.

Temperature-Programmed Reduction (TPR) was carried out in a Micromeritics Autochem II setup under diluted hydrogen flow (10 vol. % in argon) with a heating rate of 15°C. min⁻¹. The hydrogen consumption was continuously monitored with a thermal conductivity detector (TCD).

The XPS analysis of the support were performed on a MULTILAB 2000 (THERMO) spectrometer equipped with Al K α anode ($h\nu = 1486.6$ eV) with 10 minutes of acquisition in order to achieve a good signal-to-noise ratio. Peak deconvolution were made with the “Avantage” program from Thermoelectron Company. The C1s photoelectron binding energy was set at 284.6 +/- 0.2 eV relative to the Fermi level and used as reference for calibrating the other peak positions.

2.5 Fischer-Tropsch reaction

The Fischer-Tropsch synthesis reaction was carried out in a tubular fixed-bed stainless steel reactor (*I.D.* = 25.4 mm) with circulating silicon oil as heating source. The reduced catalyst (10 g of catalyst, the support in a foam form, containing 2.7 ± 0.3 g of cobalt) was deposited between quartz wool plugs in the centre of the reactor. The reactor pressure was slowly increased from 0.1 to 4 MPa (ramping rate of 1 MPa. h⁻¹) under argon. The total pressure was controlled by a back pressure regulator (MFI Ltd.). At 4 MPa the reactor temperature was raised from room temperature to the desired reaction temperature, 210°C (heating rate of 2°C. min⁻¹). Then, the argon flow was replaced by a 50:50 v:v mixture of

syngas and argon ($\text{CO:H}_2 = 1:2$). The catalyst was activated under a synthesis gas-argon mixture with different CO:H_2 concentrations, i.e. $\text{CO:H}_2/\text{Ar}$ of 50:50 vol. % for 24 h, 66:33 vol. % for an additional 24 h and pure synthesis gas condition. The gaseous hourly space velocity (GHSV) was calculated as follows: $\text{GHSV (h}^{-1}\text{)} = ((\text{Reactant flow (N cm}^3\text{/min)} \times 60)/\text{Catalyst apparent volume (cm}^3\text{)})$. The contact time was kept constant at 11 s for the whole activation period while the gas hourly space velocity was stepwise increased from 165 h^{-1} to 250 h^{-1} and finally to 330 h^{-1} . The space velocity is calculated based on the total apparent volume of the catalyst, foam structure with a porosity of 0.93, and thus, seems to be relatively low compared to those encountered with other fixed-bed reactor with lower porosity, i.e. 0.3-0.4. The catalyst bed temperature was monitored with a thermocouple ($\varnothing 0.3 \text{ mm}$) inserted inside a stainless steel finger ($\varnothing 1 \text{ mm}$) passing through the catalyst bed. The products were condensed in two high pressure traps maintained at 85°C and 15°C respectively. The exit gas was analyzed on-line, both by a Thermal Conductivity Detector (TCD) and a Flame Ionization Detector (FID), with a gas chromatography (GC Varian 3800 equipped with a Carbobond and DB-1 capillary column).

The liquid phase and water were condensed in the traps and analyzed off-line at the end of the test. The water was removed from the organic phase by decantation. A known amount (5 mg) of the organic phase, liquid hydrocarbons and waxy products, was dissolved in 3 ml of dichloromethane under sonication during 30 minutes. Then, 2 ml of CS_2 were further added to the solution in order to ensure the complete dissolution of the organic phase. For analysis, 10 μL of the solution was injected in a GC apparatus equipped with a Simdist column operated at 400°C which allowed the detection of hydrocarbons from C_9 to C_{70} . The weight of the solid hydrocarbons retained within the catalyst porosity and in the quartz wool plug was measured after reaction. The hydrocarbons were extracted with CS_2 at 40°C and analyzed.

3. Results and discussion

3.1 Support characteristics

The nature of the crystalline phases in the different supports in the foam form, i.e. SiC, Al_2O_3 and $\text{Al}_2\text{O}_3/\text{SiC}$, was analyzed by XRD and the corresponding XRD patterns are presented in Figure 2. On the $\text{Al}_2\text{O}_3/\text{SiC}$ composite only diffraction lines corresponding to the

SiC phase were visible. This result could be attributed to the fact that the alumina layer was too thin to be accurately detected by this technique. The small size of the alumina particle in the wash-coat could also be partly responsible for this. The introduction of the alumina layer on the SiC surface only slightly modified the specific surface area of the composite from 22 to 25 $\text{m}^2 \cdot \text{g}^{-1}$ and is comparable to that of the Al_2O_3 foam with a Disperal wash-coat, i.e. 24 $\text{m}^2 \cdot \text{g}^{-1}$.

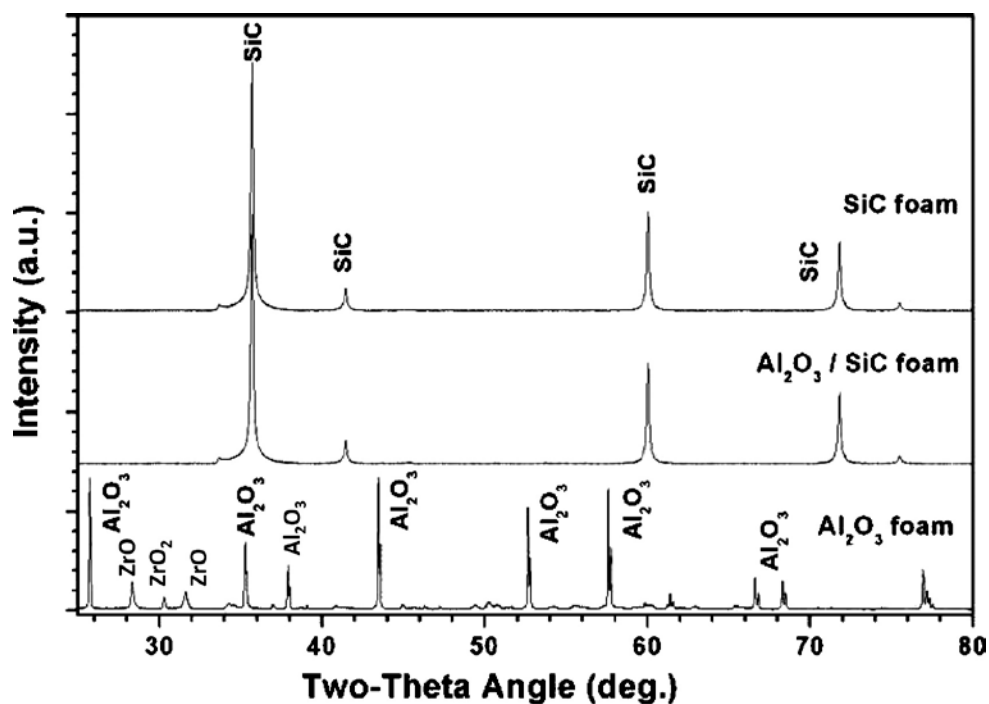


Figure 2. XRD patterns of the SiC, Al_2O_3 and $\text{Al}_2\text{O}_3/\text{SiC}$ foam supports. On the $\text{Al}_2\text{O}_3/\text{SiC}$ composite support no diffraction lines corresponding to the Al_2O_3 phase were observed due to the relatively thin layer of the alumina wash-coat.

SEM analysis indicates the relatively large difference between the different supports tested. The SiC morphology mostly consisted in small agglomerates (ca. 40 nm) of SiC nanoparticles (Fig. 3A) while the morphology of the $\gamma\text{-Al}_2\text{O}_3$ was more rough and contained faceted particles (Fig. 3B). The $\text{Al}_2\text{O}_3/\text{SiC}$ composite displays an intermediate morphology (Fig. 3C and D) which could be due to the nature of the precursor, i.e. Disperal.

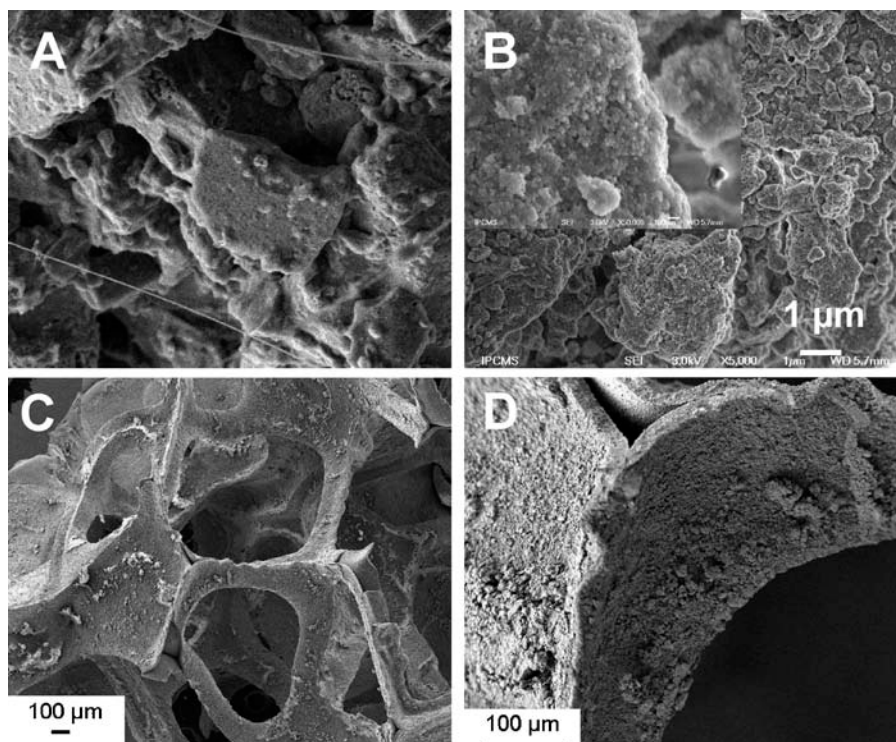


Figure 3. SEM micrographs of the different supports: (A) SiC. (B) Al₂O₃ foam with a thin layer of γ -Al₂O₃ on the top. The γ -Al₂O₃ layer was generated by deposition of thin layer of Disperal following by a calcination step at 750°C to transform the aluminium hydroxide into a γ -Al₂O₃. (C) Al₂O₃-SiC. The alumina layer was generated following the same process as for the Al₂O₃ foam described above. (D) High magnification SEM micrograph showing the homogeneous dispersion of the alumina particles on the SiC foam surface.

The SiC and Al₂O₃/SiC materials mostly contained meso- and macropores, centered at 40 and 100 nm, whereas the γ -Al₂O₃ mainly contained mesopores centered at 10 nm. The pore size distribution of the supports is deduced from adsorption branch of the N₂ isotherm obtained by N₂ adsorption at liquid N₂ temperature. In the case of the SiC support containing a large proportion of macropores, the pore size distribution was measured by mean of the mercury intrusion.

3.2 Catalysts characteristics

The XRD patterns were recorded ex situ on the reduced catalysts. The amount of the cobalt oxide formed during the transfer and during the XRD recording is monitored by temperature-programmed reduction (TPR). According to the TPR results, the cobalt oxide formed on the catalyst surface is relatively low at around 10 wt. %. However, this cobalt oxide, i.e. CoO, is rapidly reduced under the reaction conditions (see discussion below). The XRD patterns of the Co/SiC, Co/Al₂O₃ and Co/Al₂O₃-SiC catalysts are presented in Figure 4. On the Co/SiC and Co/Al₂O₃-SiC catalysts the XRD patterns only show the presence of a relatively well defined diffraction lines corresponding to the metallic cobalt phase whereas on the Co/Al₂O₃ diffraction lines corresponding to Co, CoO and Co₃O₄ were observed. Such results are in line with the literature results where reduction step leads to the formation of a stable CoO-Al₂O₃ compound (34). The low reducibility of the cobalt phase on Al₂O₃ was attributed to the presence of a strong metal-support interaction which prevents the complete reduction (6, 35). It was expected that, in this case, only the Co atoms not in direct contact with the support were reduced within each Co particle. The CoO will be further reduced under the FTS conditions which are well known to be a strong reductive medium (36, 37). The average Co particle size deduced from the XRD patterns by the Scherrer equation was the following: 49 nm for SiC, 33 nm for Al₂O₃/SiC, and 24 nm for Al₂O₃. The cobalt particle size on the alumina-based catalyst was deduced from the Co₃O₄ diffraction lines in the XRD pattern. The cobalt metal particle size was calculated according to the following formula: $d_{Co} \text{ (nm)} = d(\text{Co}_3\text{O}_4) \times 0.75$ (46). The smaller cobalt particle size observed on the Al₂O₃-based catalyst compared to those obtained on the SiC-based catalysts was directly attributed to the presence of a high metal-support interaction between the cobalt phase and the underneath alumina layer which led to a higher dispersion of the active phase.

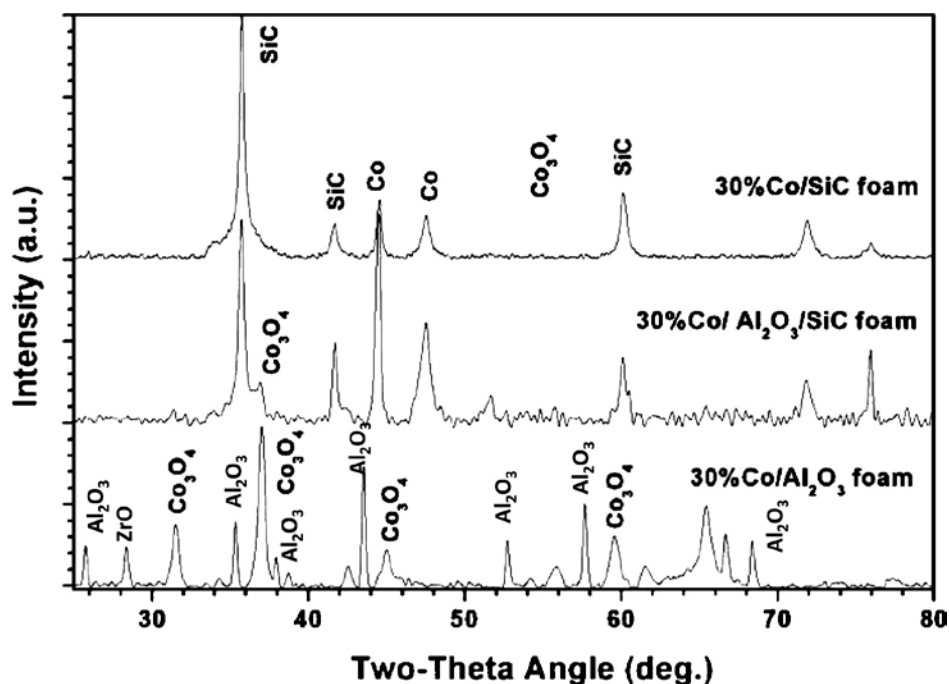


Figure 4. XRD patterns of the Co supported on SiC, Al₂O₃ and Al₂O₃/SiC catalysts. The catalysts were calcined at 350°C for 2 h followed by a reduction under H₂ at 300°C for 6 h.

Temperature-programmed reduction (TPR) was also carried out to analyze the reduction behaviour of the different catalysts (Fig. 5). The reduction of the cobalt oxide supported on the SiC-based catalyst was achieved at relatively low temperature, i.e. 380°C which indicated a low metal-support interaction and the absence of the formation of a hardly reducible cobalt-phase. On the other hand, the reduction of the Co/Al₂O₃ catalyst needed higher temperature to be completed with two distinct reduction peaks: the first one located at around 370°C and the large second one with a maximum centered at ca. 600°C, which corresponded to the following reduction sequence: Co₃O₄ → CoO then CoO → Co (38-40). These results confirmed the existence of a strong metal-support interaction between the cobalt phase and the alumina support which rendered difficult the complete reduction of the cobalt oxide phase at low temperature (41, 42). The Co/Al₂O₃-SiC catalyst exhibited an intermediate behaviour. The reduction temperature of the cobalt phase was slightly displaced to a higher temperature region compared to what was observed on the SiC-based catalyst. This temperature displacement was attributed to the presence of a metal-support interaction between the cobalt phase and the alumina layer. However, it is worth noting that the reduction behaviour observed on the Al₂O₃-SiC catalyst was far different from that observed on the

Al_2O_3 catalyst, which could be due to the presence of the SiC matrix underneath. Indeed, on the Al_2O_3 -SiC catalyst, most of the cobalt phase was reduced at 400°C whereas on the Al_2O_3 catalyst the main reduction part occurred at higher temperature, i.e. 600°C . The high-temperature TPR peak, at 600°C , observed on the Al_2O_3 -based catalyst could be attributed to the reduction of a cobalt aluminate phase (43, 44). The formation of this aluminate was easy because of the similarity of the crystalline structures between Co_3O_4 and $\gamma\text{-Al}_2\text{O}_3$ (45). The area of the high-temperature TPR peak was significantly reduced on the $\text{Al}_2\text{O}_3/\text{SiC}$ catalyst. This result could be explained by the fact that the SiC surface was not fully covered by the alumina wash-coat and that a part of the cobalt oxide could be located directly on the SiC with lower metal-support interactions and thus, leading to a lower reduction temperature.

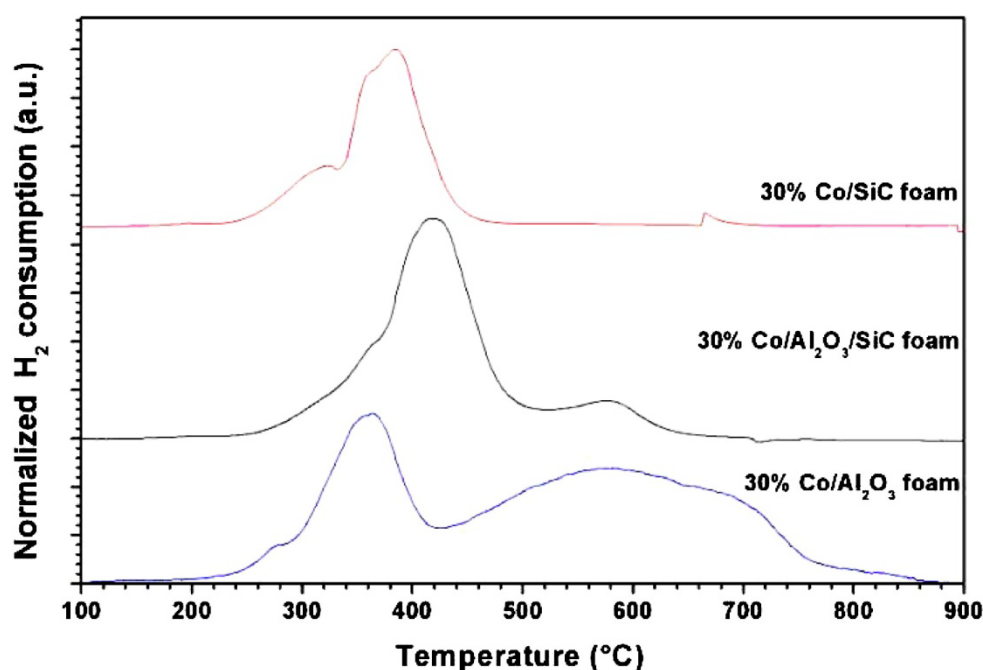


Figure 5. TPR spectra of the Co/SiC and the Co/ Al_2O_3 catalysts after calcination at 350°C for 2 h. Reduction conditions: heating rate of $15^\circ\text{C} \cdot \text{min}^{-1}$, hydrogen flow rate of $100 \text{ ml} \cdot \text{min}^{-1}$. The small peak observed above 600°C on the TPR spectrum of the Co/SiC corresponds to the formation of a small amount of CH_4 via the reaction $\text{Co} + 2\text{SiC} + 4\text{H}_2 \rightarrow \text{CoSi}_2 + 2 \text{CH}_4$ (39).

The morphology of the different catalysts was analyzed by SEM and the representative SEM micrographs are presented in Figure 6. The cobalt agglomerates significantly varied as a function of the support according to the following sequence: $\text{Co}/\text{Al}_2\text{O}_3 < \text{Co}/\text{Al}_2\text{O}_3\text{-SiC} <$

Co/SiC. According to this, one can state that the cobalt dispersion was enhanced by the presence of the alumina support layer generating a strong metal-support interaction with the active phase.

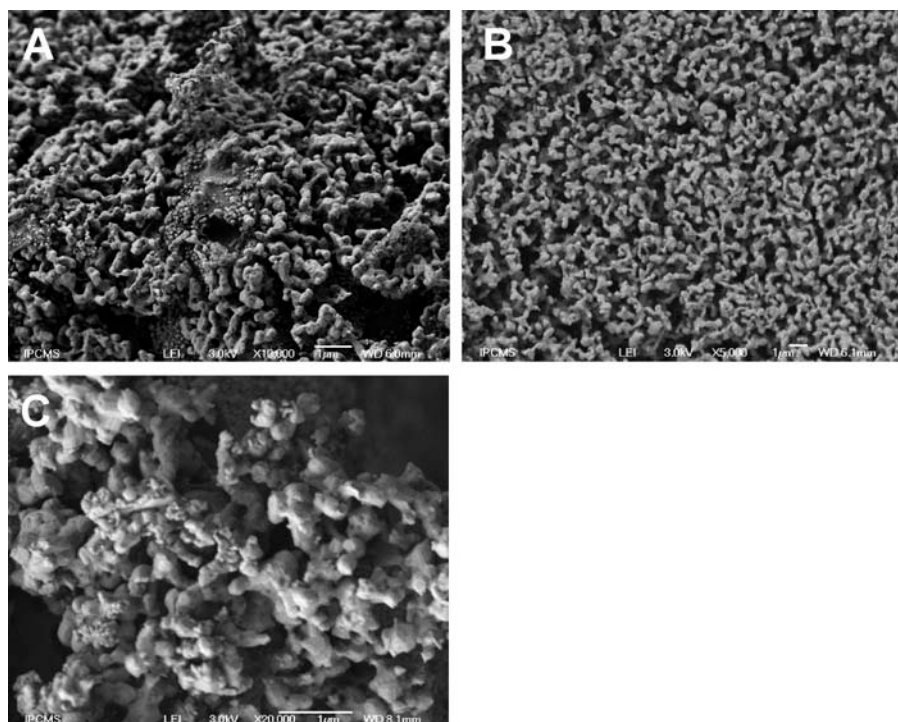


Figure 6. SEM micrographs of the different Co-based catalysts after reduction under H_2 at $300^\circ C$ for 6 h. (A) Co/SiC, (B) Co/ Al_2O_3 and (C) Co/ Al_2O_3 /SiC.

3.3 Catalytic performance

The FTS activity, expressed in terms of CO conversion, and C_{5+} selectivity obtained on the different Co-based catalysts as a function of time on stream is presented in Figure 7. On the Al_2O_3 catalyst the CO conversion at an external temperature of $220^\circ C$ (internal temperature of $238^\circ C$) is relatively high and stable at about 77% after 25 h on stream. It is worth noting that due to the problem of temperature runaway (the catalyst was tested as such without any use of heat disperser as usually encountered with FTS experiments) the FTS activity on the Co/ Al_2O_3 catalyst was obtained under diluted reactant mixture (CO: H_2 /Ar of 50:50 vol. %) and not under pure synthesis gas. The high CO activity observed on the Al_2O_3 -based catalyst could be attributed to the relatively high dispersion of the cobalt active phase

which leads to a high active surface for reactant. It is expected that under the reaction conditions used in the present work part of the cobalt active phase could undergo sintering and thus, the FTS activity observed is not an intrinsic activity without such deactivation due to the severe reaction conditions of the test. However on the Al_2O_3 -based catalyst, the C_{5+} selectivity, at the same level of CO conversion, was extremely low at around 54% and methane contributed to the main part of the light products. It is worth mentioning that during the activation period at lower reaction temperature, i.e. 210 °C, and low CO conversion, i.e. 40 %, the C_{5+} selectivity on the $\text{Co}/\text{Al}_2\text{O}_3$ catalyst was significantly improved from 54 % to about 84 %. Similar C_{5+} selectivity has also been obtained on the Al_2O_3 -based catalyst at medium CO conversion level by other groups, especially with large pore support, i.e. α - Al_2O_3 (46). The high C_{5+} selectivity obtained on the α - Al_2O_3 containing cobalt catalysts has been explained by the large pore size of the support (7, 47).

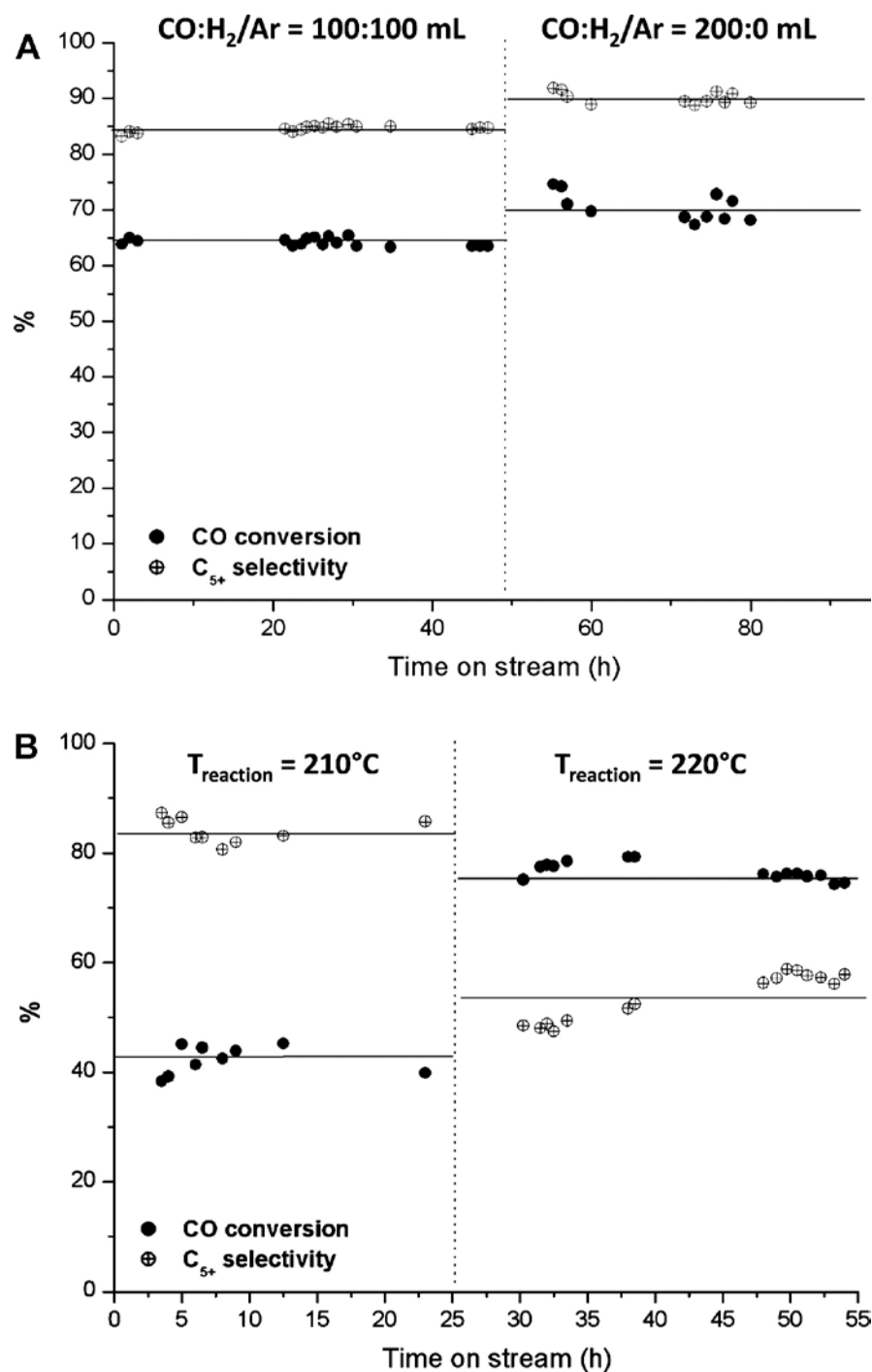


Figure 7. FTS activity and C₅₊ selectivity obtained on the Co/SiC (A) and Co/ Al₂O₃ (B) catalysts. (A) Co/SiC. Reaction conditions: H₂:CO molar ratio = 2, total pressure = 40 atm., reaction temperature = 220°C. The Co/SiC was tested both under a diluted and pure flow of synthesis gas. (B) Co/Al₂O₃. The tests were carried out under a diluted mixture at 210°C and 220°C in order to avoid the problem of temperature runaway. The catalytic results are obtained after a period of stabilization, i.e. 100 h, under diluted synthesis gas and argon mixture under the same reaction conditions.

Under similar reaction conditions, i.e. consigned temperature of 220 °C and internal temperature of 236 °C, the SiC catalyst exhibited a slightly lower CO conversion compared to the Al₂O₃ catalyst, i.e. 71% instead of 77% (Table 1). On the SiC-based catalyst, the C₅₊ selectivity was very high compared to that observed on the Al₂O₃ catalyst, i.e. 85% instead of 54%. The product distribution at steady-state, on both catalysts is reported in Table 2. The FTS results obtained on the Co/SiC under diluted reactant mixture was also presented in the same figure for comparison with that obtained on the Co/Al₂O₃ under similar reaction conditions. It is worth mentioning that the FTS performance on the Co/SiC was hardly influenced by the H₂ and CO partial pressures according to the results presented in Figure 7. Under diluted reactant mixture the CO conversion on the SiC-based catalyst was slightly lowered from 71 % to about 64 % while the C₅₊ selectivity remains high at about 85 % which is similar to that obtained on the Co/Al₂O₃ catalyst. However, it is worth mentioning that under the same reaction conditions and C₅₊ selectivity the CO conversion on the SiC-based catalyst is much higher than for the Co/Al₂O₃ catalyst, i.e. 71 % for the SiC instead of 42 % for the Al₂O₃. According to the observed results one can stated that on the alumina-based catalyst the CO conversion per pass should kept roughly under 50 % in order to maintain the C₅₊ selectivity at an acceptable level. At higher CO conversion the C₅₊ selectivity on the Co/Al₂O₃ catalyst was significantly decreased due to the problem of heat transfer. The intrinsic thermal conductivity measured on the SiC and alumina materials was 5.5 W. m⁻¹. K⁻¹ and 1.5 W. m⁻¹. K⁻¹, respectively. Recent work has shown that the thermal conductor SiC foam exhibits a relatively good effective radial thermal conductivity compared to that was obtained on the same material morphology, i.e. polyurethane foam, but with an insulator character (48). The high C₅₊ selectivity on the SiC-based catalyst is attributed to the low selectivity of the catalyst towards the formation of CO₂ and methane as encountered with the alumina-based catalyst. It is also worth mentioning that in the present work all the catalyst was tested without adding of any heat disperser as usually encountered with other works. It is expected that under these drastic reaction conditions the hot spot formation or some inhomogeneous temperature gradient are most likely to occur with significant impact on the C₅₊ selectivity.

Table 1. Representative FTS results obtained on the Co/SiC; Co/Al₂O₃ and Co/Al₂O₃-SiC catalysts.

Catalyst	T _{reactor} (°C)	T _{catalyst} (°C)	CO conv. (%)	C ₅₊ (%)	sel. STY ^(a) (h ⁻¹)	α ^(b)
Co/SiC	220	236	71	85	1.24	0.91
Co/Al ₂ O ₃	220	238	77	54	0.98	0.85
Co/Al ₂ O ₃ -SiC	220	234	75	79	1.40	0.89

(a) Cobalt-Time-Yield (molar CO conversion rate per g atom Co per hour)

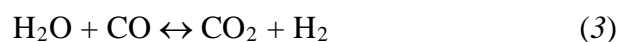
(b) Chain growth factor: The chain growth factor (α) calculated from the linear portion of the hydrocarbons, according to the following equation $W_n/n = (1-\alpha)^2\alpha^{(n-1)}$ where W_n is the weight fraction of hydrocarbon molecules containing n carbon atoms, α is the chain growth probability. When α is equal to 0 all the CO molecules are converted to CH₄ and when α is equal to 1 all the CO molecules are converted to liquid hydrocarbons.

Table 2. Product distribution at steady-state on the Co/SiC and Co/Al₂O₃ catalysts. Reaction conditions: Co loading = 30 wt. %, H₂:CO = 2, temperature = 220°C, total pressure = 40 atm.

Catalyst	CH ₄ (%)	CO ₂ (%)	C ₂ -C ₄ (%)	C ₅₊ (%)
Co/SiC	7	1	4	88
Co/Al ₂ O ₃	25	10	13	52
Co/Al ₂ O ₃ -SiC	5	1	7	87

It is also worth mentioning that on the SiC catalyst the CO₂ was extremely low compared to that observed on the alumina-based catalyst for the same level of CO conversion which indicated that the Water Gas-Shift contribution was negligible on the SiC-based catalyst. The low CO₂ formation on the SiC-based catalyst compared to that observed on the Al₂O₃-based catalyst could be attributed to the difference in terms of the porosity between the two supports. The relatively large pore size of the SiC allows the easy evacuation of the steam,

formed during the reaction toward the gas phase, and as a consequence, increases the available site for performing the FT reaction leading to a higher FTS activity and selectivity. The influence of the catalyst pore size on the FTS reactivity and selectivity has been well documented in the literature (49-51). On Al₂O₃, the small pore size could favour the steam condensation or retention which subsequently reacted with CO according to the water gas shift reaction, leading to the formation of CO₂ (3):



Steam condensation could also be favoured by the condensed liquid hydrocarbons which partly filled up the pores.

The representative FTS results obtained on the Co/SiC and Co/ Al₂O₃ catalysts are summarized in Table 1. Amongst the tested catalysts, the SiC-based catalyst is the most selective one under severe reaction conditions where hot spot is likely to occur. However, it is worth noting that the most active catalyst is the Co/Al₂O₃-SiC which combine medium dispersion and good thermal conductivity.

It was expected that the catalyst measured bed temperature was far lower compared to the real temperature inside the catalyst bed due to the poor contact between the thermocouple finger and the catalyst and thus, a higher internal temperature should be present on the catalyst surface.

The presence of local hot spots on the surface of the Al₂O₃-based catalyst can be indirectly viewed by SEM analysis on the used catalyst (not shown), i.e. cobalt phase morphology was greatly changed from well dispersed particles into a glassy shape. This modification is attributed to the presence of hot spots on the catalyst surface due to the inability of the alumina support to evacuate the local heat generated by the FTS reaction into the whole catalyst matrix.

The liquid hydrocarbon distribution on the Co/SiC and Co/Al₂O₃ catalysts is presented in Figure 8. The total amount of the liquid hydrocarbons recovered after the FTS test was around 105 ± 5 g. The solid wax retained on the catalyst after the FTS test is around 2 g (2 wt. % of the total hydrocarbon formed during the test). The weight of the hydrocarbons trapped within the quartz wool plug was amounted to 3 g by weighting the quartz wool plug before and after the FTS test which represents around 3 wt. % of the total hydrocarbon formed during the whole test.

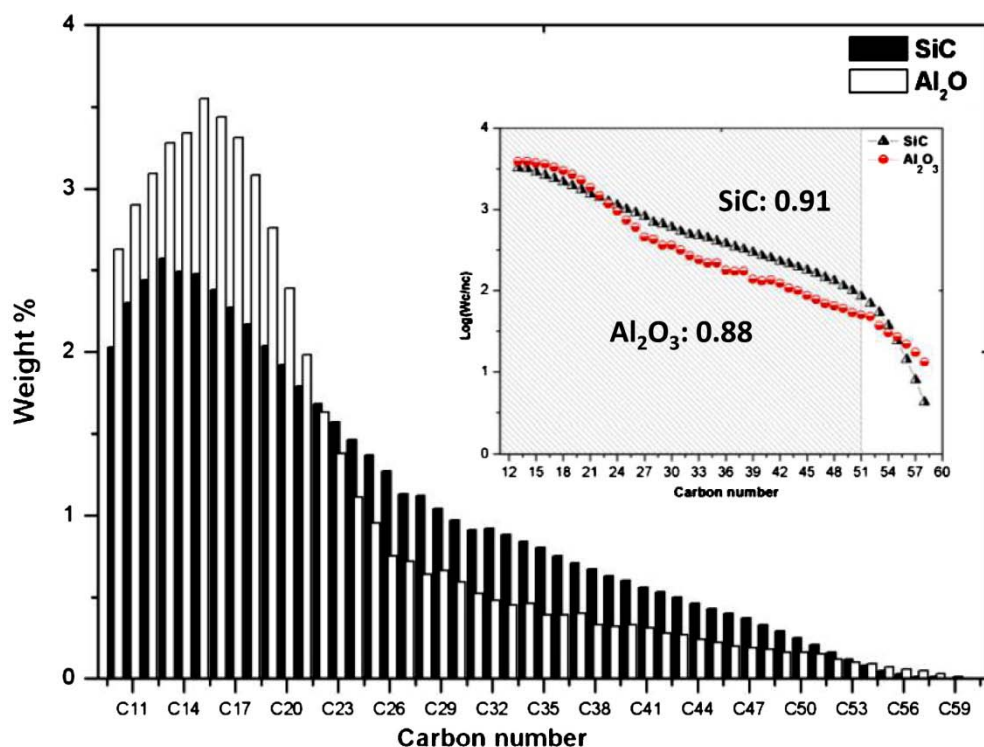


Figure 8. Liquid hydrocarbons distribution obtained on the Co/SiC and Co/Al₂O₃ catalysts. The results were obtained from the liquid hydrocarbons trapped in the high pressure and hot trap (85°C).

The difference in terms of C₅₊ selectivity on the Al₂O₃ catalyst could also be due to the different surface chemistry and/or intrinsic thermal conductivity between the two supports. In order to verify this assumption, a composite support was prepared which consisted in a SiC foam coated with a layer of γ -Al₂O₃ similar to that used in the case of the Al₂O₃ foam. The Al₂O₃ layer deposition and thermal treatment are similar to those employed for the Al₂O₃ foam. The cobalt active phase was deposited using the same impregnation method. The characteristics of the Co/Al₂O₃-SiC catalyst are presented in Figure 3C.

The FTS results obtained under similar reaction conditions on the Co/Al₂O₃-SiC catalyst are presented in Figure 9. The Al₂O₃-SiC catalyst displayed a constant CO conversion level along with a high stability as a function of time on stream. However, a large difference was observed regarding the C₅₊ selectivity between the Al₂O₃/SiC and the Al₂O₃ catalysts: on the Al₂O₃-SiC catalyst, the C₅₊ selectivity is extremely high compared to that observed on the Al₂O₃ catalyst which shared the same chemistry surface character, i.e. 79 % instead of 54 %, taken into account a similar CO conversion. This result indicated that the

high selectivity observed on the SiC catalyst was not solely due to the difference in terms of the support surface chemistry but mostly linked to other factors, namely intrinsic thermal conductivity of the support which favoured the temperature homogenisation throughout the catalyst body. The heat dissipation from the alumina layer coating the SiC structure was also favoured by the condensed liquid hydrocarbons within the support porosity, i.e. residual static hold-up liquid, which removes part of the heat generated during the reaction. It is expected that the SiC-based supports with porous structure have more facility to be filled with liquid hydrocarbons compared to the alumina catalyst where the large body is consisted by a non porous structure (see discussion above regarding the specific surface area of the alumina foam). Zhu *et al.* (52) have recently reported that for the FTS test the effective thermal conductivity increases with increasing the liquid wetting of the catalyst. Previous work by Edouard *et al.* (53) has shown that the static liquid hold-up on the SiC foam structure is relatively high compared to that occurred on the SiC extrudate. It is expected that for the SiC foam catalyst the high liquid wetting, i.e. high static liquid hold-up, could provided a more homogeneous temperature gradient within the catalyst bed and thus, participate in the improvement of the C_{5+} selectivity.

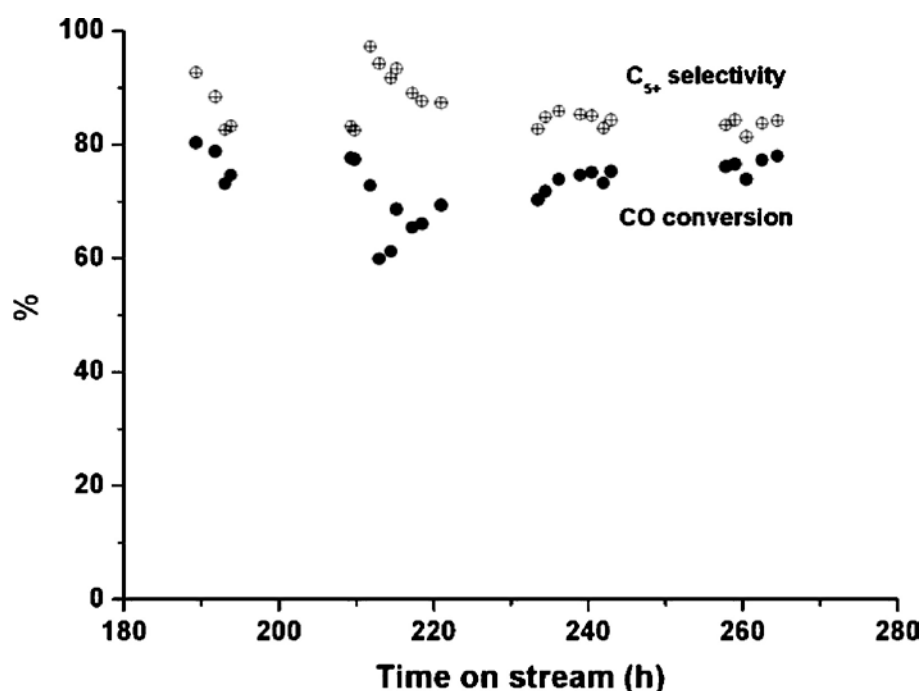


Figure 9. FTS activity and C_{5+} selectivity obtained on the Co/ Al_2O_3 -SiC catalyst. Reaction conditions: $H_2:CO$ molar ratio = 2, total pressure = 40 atm., pure synthesis gas, reaction temperature = 220°C.

The high C_{5+} selectivity obtained on the SiC and Al_2O_3 -SiC catalysts could also be linked with the porosity of the supports, i.e. meso- and macroporous, which favorize the reactants diffusion and the products escaping during the reaction. Such hypothesis has been recently confirmed by the work published by Holmen and co-workers (46) on the different alumina-supported cobalt catalysts with different pore size distribution. The same groups has observed that α - Al_2O_3 with larger pore size shows higher C_{5+} selectivity compared to the high surface area γ - Al_2O_3 (54, 55). Similar explanation could be used for the SiC-based catalyst where the porosity is larger compared to that of the Al_2O_3 -based catalyst.

It can be concluded that the FTS activity is linked to the active phase dispersion. Despite the difficulty to achieve a complete reduction of the cobalt active phase on the Al_2O_3 support, the cobalt particle size was smaller and thus, leading to a higher FTS activity per weight of catalyst. On the SiC catalyst, the lower cobalt dispersion, i.e. presence of large cobalt aggregates, led to the lowest FTS activity. The introduction of a thin alumina wash-coat layer on the SiC support slightly increased the cobalt dispersion with a concomitant improvement of the FTS activity. The influence of the cobalt particle size on the FTS activity was already reported in a well documented work from de Jong *et al.* using carbon nanofibers as catalyst support (56). Apparently, the interaction between the deposited cobalt and the natural SiO_2 - SiO_xC_y wash-coat layer on the SiC is not sufficient, due to the relatively high amount of metal, to allow a high dispersion of the cobalt phase.

A reverse trend was observed regarding the C_{5+} selectivity: the alumina catalyst exhibited the lowest C_{5+} selectivity among the tested catalysts despite the similarity in the CO conversion (Table 1 and Fig. 7). The difference in terms of C_{5+} selectivity between the Al_2O_3 and Al_2O_3 -SiC catalysts could not be solely explained by the difference in terms of the chemical surface as both alumina phases were derived from the same aluminium precursor and had received a similar thermal treatment. The following hypothesis could be advanced to explain this difference: (i) the surface temperature between the two catalysts which was linked to the thermal conductivity of the support. It was expected that in the Al_2O_3 -SiC support the heat release by the reaction could be partly dispersed by the underlying SiC whereas it was not the case for the insulator Al_2O_3 support. The presence of local hot spots on the insulator support, i.e. Al_2O_3 , most likely occurs in the present case because low space velocity was used and did not allow a good gas-solid heat removal. Wang *et al.* (57) have recently reported that the heat release by the FTS reaction cannot be properly evacuated to the entire body of

the alumina support and thus, leads to the formation of hot spots on the catalyst surface which favours the light product formation.

The support porosity, the absence of closed windows in the case of the Al_2O_3 -SiC also allowed a rapid evacuation of the products from the active site whereas the closed windows in the Al_2O_3 could favour the formation of reactant gradient within the catalyst porosity leading to the formation of light products and CO_2 by water gas shift reaction. Recent work published by Holmen and co-workers (46) on the alumina-based catalysts has also pointed out the strong influence of the support porosity on the C_{5+} selectivity as well.

3.4 Support and active phase recovery

Catalytic performance degradation as a function of time on stream is an important research topic for industrial catalyst development. Cobalt based catalyst deactivation has been the subject of two recent reviews (58, 59). The possibility of recovering both the active phase and the support is extremely important in the catalysis field as it avoids the solid waste disposal after the end-life of the catalyst and also reduces to a significant manner the cost investment of the process regarding the price of the FTS catalyst, i.e. 20,000 to 60,000 US\$ per ton of catalyst, i.e. cobalt phase doped with trace amount of noble metals, which depends on the intrinsic market value of the metal, the amount of precious metal in the catalyst and the total weight of the catalyst in operation within a FTS unit, i.e. projection of 25,000 t for a FTS plants producing 1,000,000 br/day, represents a price between 500 Mill. US\$ and 1,500 Mill. US\$ (60).

Silicon carbide is a highly chemical inert material which can withstand a prolonged contact with aggressive media without any structural integrity modification (Table 3) (16). According to the results presented in Table 3 the SiC material shows an extremely high resistance towards aggressive media which is not the case for traditional materials such as alumina or silica where dissolution slowly proceed leading to the final loss of the carriers. According to this high chemical inertness, one should expect that an acid treatment could be efficient to remove the active phase leaving behind the undamaged support for a subsequent use.

Table 3. Chemical resistance evaluation of porous beta SiC extrudates in various corrosive media; neither the crushing strength nor the specific surface area were altered.

SiC extrudates (\varnothing 2 mm)	Fresh	HF (40 %)	HCl (37 %)	HNO ₃	NaOH
		(3 weeks)	(2 weeks)	(68 %)	(20 %)
				(2 weeks)	(2 weeks)
Δ weight (%)	-	- 1.8	- 0.4	0.0	- 0.5
Crushing strength (N. mm ⁻¹)	20	18	21	21	21
Specific surface area (m ² . g ⁻¹)	30	29	30	29	30

The spent catalysts were submitted to an acid treatment (HNO₃, 65 %, Fluka) at room-temperature and the results are presented in Fig. 10A. The acid concentration was two times higher than that needed for the complete dissolution of the cobalt phase present on the catalyst. The cobalt active phase was totally recovered on the SiC-based catalyst due to the weak metal-support interaction and the high chemical inertness of the support. The SiC support after acid treatment was washed several times with de-ionized water until a neutral pH was reached. XRD pattern (not shown) recorded on the recovered support only shows diffraction lines corresponding to the β -SiC and confirms the complete removal of the cobalt phase during the acid treatment. In order to evaluate the possibility of re-use, the support was further impregnated with a new solution of cobalt and re-tested for the FTS reaction. The results obtained are compared with those obtained on the fresh catalyst (Fig. 10B). Both the activity and selectivity were retained which indicated the possibility to re-use the support. It is worth noting that such result regarding the support and active phase recovery has not been reported so far in the literature and can contribute to a cost reduction of the catalyst investment for this high demanding reaction.

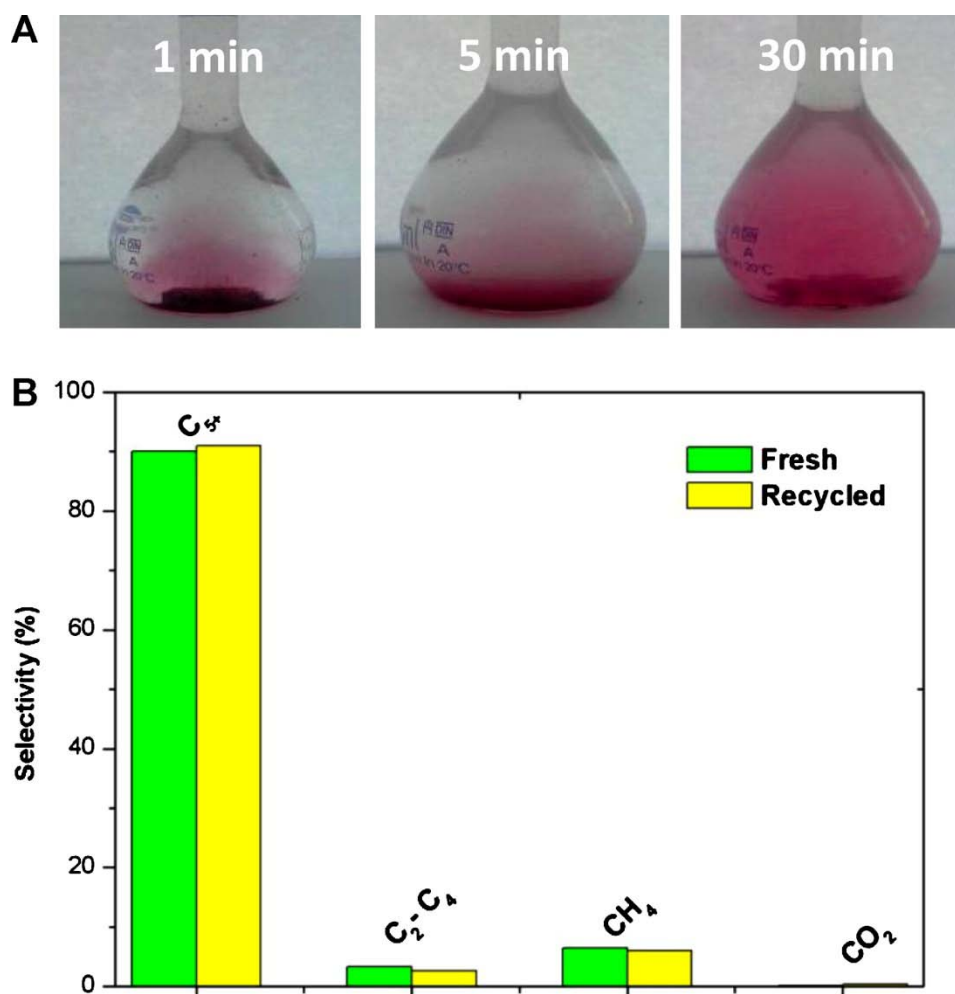


Figure 10. (A) Active phase recovery from the spent Co/SiC catalyst by acid treatment (HNO₃, 65 wt. %) at room temperature. The cobalt-based catalyst, after the FTS test, was thermally treated under helium at 400°C to remove the residual condensed hydrocarbons and was further reduced in flowing H₂ at 300°C for 6 h before removing the active phase. (B) FTS activity and selectivity between the fresh SiC support and the same after acid treatment followed by cobalt re-deposition. FTS data: T_{reaction} = 222 °C, CO conversion = 34 %, GHSV = 670 h⁻¹.

4. Conclusion

Fischer-Tropsch synthesis with high activity and C₅₊ selectivity can be achieved on a Co-based catalyst supported on SiC carrier. On an insulator support, Al₂O₃, the FTS activity and intrinsic C₅₊ selectivity, at medium CO conversion, are similar to those obtained on the

SiC support with higher thermal conductivity. However, at higher reaction temperature a large difference in terms of the C_{5+} selectivity is observed between the tested catalysts, i.e. 80% for the SiC-based catalyst and only 54% for the Al_2O_3 -based catalyst. Such low C_{5+} selectivity on the Al_2O_3 -based catalyst is attributed to the presence of local hot spots, which are likely to be generated under these severe reaction conditions, on the catalyst surface which induce secondary cracking reactions leading to the formation of light products. These results indicate that the catalyst surface temperature control can be achieved in an easy way on the SiC-based, due to its high intrinsic thermal conductivity, compared to the insulator support based on alumina.

The FTS activity can be further improved by supporting the cobalt phase on a hybrid support, i.e. Al_2O_3 coated SiC carrier, which provides higher cobalt dispersion. It is striking to point out the fact that on such hybrid support the C_{5+} selectivity is completely different compared to that which was observed on the Al_2O_3 -based catalyst, i.e. 80% for the Al_2O_3 -SiC compared to 54 % on the Al_2O_3 . These results are attributed to the presence of an underlying conductive SiC matrix which acts as a heat dissipating structure allowing a better homogeneization of the catalyst surface temperature and prevents local hot spots formation leading to the selectivity degradation. It is the first time that this support effect is reported. The results obtained are of an extreme importance in the quest of high active and selective FTS catalysts regarding their future development. Experiments are underway to measure the radial and axial heat dispersion within the SiC foam structure, under conditions as close as possible to those encountered under the FTS test, in order to get more insight about the possible thermal conductivity effect of the SiC foam support for the FTS performance. The influence of the foam window size on the CO conversion and C_{5+} selectivity is also underway. Work is also on going to evaluate the FTS performance on this SiC-based catalyst in a more conventional shape, i.e. grains size with granulometry ranged between 0.125 to 0.250 mm, in a high aspect ratio tubular fixed-bed reactor, i.e. inner diameter x length, 6 mm x 200 mm, with a higher space velocity, i.e. 3800 h^{-1} STP, and will be presented soon.

The chemical inertness of the SiC support also allows one to perform an efficient active phase and support recovery by a simple acid treatment at room temperature. Elemental analysis carried out on the recovered support confirms the complete removal of the metal active phase after the acid treatment. The recovered support can also be fully re-used without any loss in term of catalytic activity and selectivity. This result is of great economical interest as it allows the recovery of the expensive and toxic metal active phase and the disposal of

solid supports which is environmentally unacceptable. Additional work is underway to investigate in detail this recovery process by using a more accurate characterization technique such as the nil field ^{59}Co NMR.

References

- [1] A. Y. Khodakov, W. Chu, P. Fongarland, *Chem. Rev.* 107 (2007) 1692-1744.
- [2] M. E. Dry, *Catal. Today* 71 (2002) 227-241.
- [3] A. Y. Khodakov, *Catal. Today* 144 (2009) 251-257.
- [4] R. Rostrup-Nielsen, *Science* 308 (2005) 1421-1422.
- [5] C. Perego, R. Bortolo, R. Zennaro, *Catal. Today* 142 (2009) 9-16.
- [6] J. I. Yang, J. H. Yang, H. J. Kim, H. Jung, D. H. Chun, H. T. Lee, *Fuel* 89 (2010) 237-243.
- [7] A. Martinez, G. Prieto, J. Rollan, *J. Catal.* 263 (2009) 292-305.
- [8] Z. Yan, Z. Wang, D. B. Bukur, D. W. Goodman, *J. Catal.* 268 (2009) 196-200.
- [9] N. Tsubaki, S. Sun, K. Fujimoto, *J. Catal.* 199 (2001) 236-246.
- [10] D. Xu, W. Li H. Duan, Q. Ge, H. Xu, *Catal. Lett.* 102 (2005) 229-235.
- [11] F. Diehl, A. Y. Khodakov, *Oil & Gas Sci. Technol.* 64 (2009) 11-24.
- [12] S. Hiuchiranan, Y. Zhang, S. Nagamori, T. Vitidsant, N. Tsubaki, *Fuel Proc. Technol.* 89 (2008) 455-459.
- [13] M. J. Ledoux, S. Hantzer, C. Pham-Huu, J. L. Guille, M. P. Desaneaux, *J. Catal.* 114 (1988) 176-185.
- [14] M. J. Ledoux, C. Pham-Huu, J. L. Guille, H. M. Dunlop, S. Hantzer, S. Marin, M. Weibel, *Catal. Today* 15 (1992) 263-284.
- [15] Website : www.sicatcatalyst.com
- [16] P. Nguyen, Ch. Pham, *Appl. Catal. A*, doi: 10.16/j.apcata.2010.07.054 (2010).
- [17] S. Savin-Poncet, M. J. Ledoux, C. Pham-Huu, J. Bousquet, B. Madani, *Int. Pat. Appl. WO 2005/073345 A1*, assigned to TOTAL France (2005).

- [18] C. Pham-Huu, B. Madani, M. Lacroix, L. Dreibine, M. J. Ledoux, S. Savin-Poncet, J. Bousquet, D. Schweich, *Int. Pat. Appl. WO 2007/000506 A1*, assigned to TOTAL SA (2007).
- [19] M. Lacroix, PhD dissertation, University of Strasbourg (2008).
- [20] R. Philippe, M. Lacroix, L. Dreibine, C. Pham-Huu, D. Edouard, S. Savin, Fr. Luck, D. Schweich, *Catal. Today* 147S (2009) S305-S312.
- [21] M. J. Ledoux, C. Crouzet, C. Pham-Huu, V. Turines, K. D. Kourtakis, P. L. Mills, J. J. Lerou, *J. Catal.* 203 (2001) 495-508.
- [22] P. Nguyen, D. Edouard, J. M. Nhut, M. J. Ledoux, C. Pham-Huu, *Appl. Catal. B* 76 (2007) 300-310.
- [23] C. Reuel, C. H. Bartholomew, *J. Catal.* 85 (1984) 78-88.
- [24] M. A. Vannice, *J. Catal.* 37 (1975) 449-461.
- [25] M. J. Ledoux, C. Pham-Huu, *CaTTech* 5 (2001) 226-246.
- [26] R. Pampuch, W. Ptak, S. Jonas, J. Stoch, *Mater. Sci. Monographs* 6 (1980) 435-448.
- [27] R. Moene, M. Makee, J. A. Moulijn, *Appl. Catal. A* 167 (1998) 321-330.
- [28] N. Keller, F. Di Gregorio, C. Pham-Huu, V. Keller, *Dia. Rel. Mater.* 17 (2008) 1867-1870.
- [29] C. H. Bartholomew, in "History of Cobalt Catalyst Design for Fischer-Tropsch Synthesis", presentation at AIChE 2003, New Orleans, LA (www.fischertropsch.org).
- [30] B. H. Davis, *Ind. Eng. Chem. Res.* 46 (2007) 8938-
- [31] R. Oukaci, A. H. Singleton, J. G. Goodwin Jr., *Appl. Catal. A* 186 (1999) 129-
- [32] P. J. van Berge, J. van de Loosdrecht, E. Caricato, S. Barradas, *United States Pat.* 6,638,889 (2004).
- [33] P. J. van Berge, J. van de Loosdrecht, S. Barradas, A. M. Van der Kraan, *Catal. Today* 58 (2000) 321.

- [34]. P. J. van Berge, J. van de Loosdrecht, J. L. Visagie, T. J. van der Walt, H. Veltman, C. Solie, European Pat. 1 444 040 B1 (2003), Sasol.
- [35]. C. H. Bartholomew, *Catal. Lett.* 7 (1990) 27-52.
- [36]. A. M. Saib, A. Borgna, J. van de Loosdrecht, P. J. van Berge, J. W. Niemantsverdriet, *Appl. Catal. A* 312 (2006) 12.
- [37]. H. Oosterbeek, *Phys. Chem. Chem. Phys.* 9 (2007) 3570.
- [38]. E. van Steen, G. S. Sewell, R. A. Makhothe, C. Micklethwaite, H. Manstein, M. de Lange, C. T. O'Connor, *J. Catal.* 162 (1996) 220-229.
- [39]. P. Arnoldy, J. A. Mouljin, *J. Catal.* 93 (1985) 38-54.
- [40]. R. Bechara, D. Balloy, J. Y. Dauphin, J. Grimblot, *Chem. Mater.* 11 (1999) 1703-1711.
- [41]. G. Jacobs, P. M. Patterson, Y. Zhang, T. Das, J. Li, B. H. Davis, *Appl. Catal. A* 233 (2002) 215-226.
- [42]. S. Storsater, O. Borg, E. A. Blekkan, A. Holmen, *J. Catal.* 231 (2005) 405-419.
- [43]. M. Hilmen, D. Schanke, K. F. Hanssen, A. Holmen, *Appl. Catal. A* 123 (1999) 169-188.
- [44]. H. Ming, B. G. Baker, *Appl. Catal. A* 123 (1995) 23-26.
- [45]. F. Dumond, E. Marceau, M. Che, *J. Phys. Chem. C* 111 (2007) 4780-4789.
- [46]. S. Rane, O. Borg, J. Yang, E. Rytter, A. Holmen, *Appl. Catal. A*, doi: 10.1016/j.apcata.2010.08.038.
- [47]. E. Iglesia, *Appl. Catal. A* 161 (1997) 59-78.
- [48]. D. Edouard, T. Truong Huu, C. Pham-Huu, F. Luck, D. Schweich, *Int. J. Heat Mass Transfer* 53 (2010) 3807-3816.
- [49]. I. T. Ghampson, C. Newman, L. Kong, E. Pier, K. D. Hurley, R. A. Pollock, B. R. Walsh, B. Goundie, J. Wright, M. C. Wheeler, R. W. Meulenberg, W. J. DeSisto, B. G. Frederick, R. N. Austin, *Appl. Catal. A* 388 (2010) 57-67.
- [50]. J. Hong, P. A. Chernavskii, A. Y. Khodakov, W. Chu, *Catal. Today* 140 (2009) 135-141.

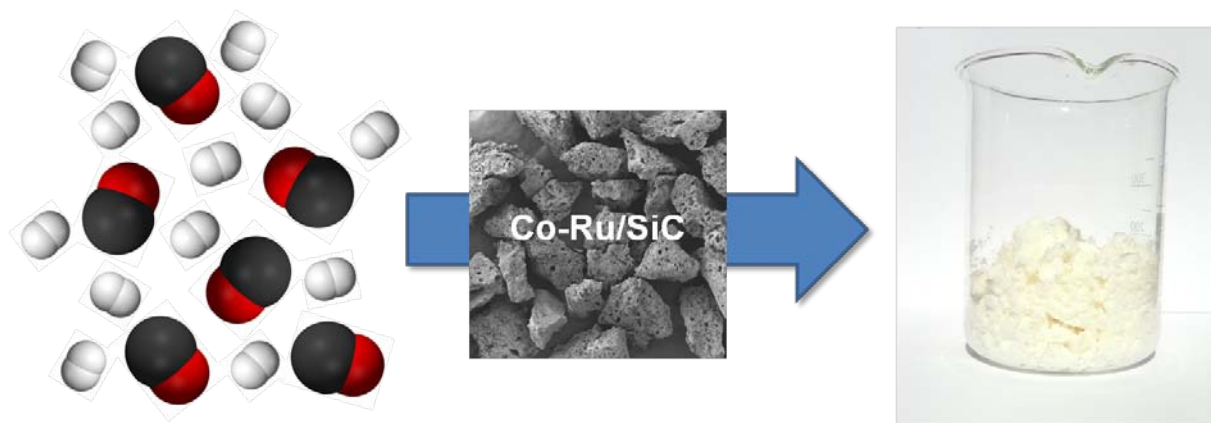
- [51] D. Song, J. Li, *J. Mol. Catal. A: Chem.* 247 (2006) 206-212.
- [52].X. Zhu, X. Lu, X. Liu, D. Hildebrandt, D. Glasser, *Ind. Eng. Chem. Res.*, in press (2010)
- [53]. D. Edouard, M. Lacroix, Ch. Pham, M. Mbodji, C. Pham-Huu, *AIChE J.* 54 (2008) 2823-2832.
- [54]. O. Borg, P. D. C. Dietzrael, A. I. Spjelkavik, E. Z. Tveten, J. C. Walmsley, S. Diplas, S. Eri, A. Holmen, E. Rytter, *J. Catal.* 259 (2008) 161-164.
- [55]. O. Borg, S. Eri, E. A. Blekkan, S. Storsaeter, H. Wigum, E. Rytter, A. Holmen, *J. Catal.* 248 (2007) 89-100.
- [56].G. L. Bezemer, J. H. Bitter, H. P. C. E. Kuipers, H. Oosterbeck, J. E. Holewijn, X. Xu, F. Kapteijn, A. J. Van Dillen, K. P. de Jong, *J. Am. Chem. Soc.* 128 (2006) 3956-3964.
- [57]. Y. Wang, D. P. Vanderwiel, A. L. Y. Tonkovich, Y. Gao, E. G. Baker, US Patent 7,045,486, Battelle Memorial Institute (2006).
- [58]. N. E. Tsakoumis, M. Ronning, O. Borg, E. Rytter, A. Holmen, *Catal. Today*, 154 (2010) 162-182.
- [59]. A. M. Saib, D. J. Moodley, J. M. Ciobica, M. M. Hauman, B. H. Sigwebela, C. J. Weststrate, J. W. Niemantsverdriet, J. Van de Loosdrecht, *Catal. Today* 154 (2010) 271-282.
- [60]. A. Brumby, M. Verhelst, D. Cheret, *Catal. Today* 106 (2005) 166-169.

CHAPTER III

C_o-Ru/SiC IMPREGNATED WITH ETHANOL AS AN EFFECTIVE CATALYST FOR THE FISCHER-TROPSCH SYNTHESIS

Benoit de Tymowski, Yuefeng Liu, Christian Meny, Christophe Lefèvre, Dominique Begin, Patrick Nguyen, Charlotte Pham, David Edouard, Francis Luck, Cuong Pham-Huu

Graphical abstract



Abstract

Silicon carbide containing cobalt (30 wt. %) doped with 0.1 wt. % of ruthenium catalysts prepared by incipient wetness impregnation of cobalt nitrate with either ethanol or water were tested in the Fischer-Tropsch synthesis (FTS) in a fixed-bed configuration. The catalyst prepared with ethanol exhibits a higher FTS performance compared to the one prepared with water and especially at high reaction temperature, i.e. 230 °C. The FTS performances of the cobalt-based catalyst impregnated with ethanol further increases, under high temperature and high space velocity, to reach a steady state reaction rate of 0.54 g_{CH₂}/g_{cat}/h along with a relatively high C₅₊ selectivity, i.e. 90 %. In addition, the catalyst also exhibits a relatively high stability as a function of time on stream. ⁵⁹Co zero field NMR analysis has indicated that the proportion of cobalt atoms engaged in the small hcp cobalt particles (< 8 nm) was higher for the ethanol impregnated catalyst and also an increased homogeneity of dispersion ruthenium atoms within the cobalt network forming an alloy.

Keywords:

Silicon carbide – Cobalt – Ruthenium - Fischer-Tropsch synthesis – Ethanol – ⁵⁹Co NMR – Stacking faults

1. Introduction

Due to the stagnation of proven reserves of crude oil it is expected that the utilization of natural gas will probably become of prime importance in the energy field in the near future. In the Gas-To-Liquid (GTL), Coal-To-Liquid (CTL) and Biomass-To-Liquid (BTL) processes, Fischer-Tropsch synthesis (FTS) is a key technology, which allows the transformation of synthesis gas issued from different sources into very long chain hydrocarbons followed by hydrocracking of the heavy fraction into useful compounds such as naphtha, diesel, lubricants and others. Among these processes which have received increasing scientific and industrial interest in the last decades [1, 2, 3, 4, 5, 6]. The GTL is the most developed one. Recent advances in catalyst development and reactor technology have significantly contributed to the fast growth of the GTL process during the last decade for supplying ultra-clean fuels (sulfur- and nitrogen-free and no aromatics) for transportation. Cobalt is one of the most active metals for the FTS reaction and is mostly employed as supported catalyst due to its reasonable price, high stability, high activity, high selectivity to higher hydrocarbons and low water-gas shift activity [1]. Typically, the cobalt metal loading ranges from 10 to 30 g per 100 g support. In order to increase the active site density per volume it is generally supported on a high specific surface area carriers such as alumina, silica or titanium dioxide [7, 8, 9]. Since FTS is a highly exothermic reaction, the removal of reaction heat at high CO conversion is a major concern. However, the above-mentioned supports are insulating materials which are not able to prevent hot spot formation within the catalyst bed, leading to low liquid hydrocarbon selectivity. Indeed, on insulating supports such as alumina or silica the heat transfer within the catalyst bed could induce temperature gradients in different parts of the bed. In areas where high conversion of CO occur the catalyst temperature could be high whereas in other parts of the bed the temperature could be significantly lower. Depending to the pore size distribution of the support, a temperature gradient could also occur within the catalyst body, i.e. between the catalyst outer surface and the catalyst matrix, which could modify the liquid hydrocarbon selectivity of the reaction. New developments dealing with the use of conductive supports such as metallic foams or monoliths have recently been reported for improving the heat transfer for the FTS reaction [10, 11, 12, 13,14].

Recently, silicon carbide (SiC) has been reported to be an efficient support for the FTS reaction allowing working at high CO conversion along with a high C₅₊ selectivity [15, 16]. Silicon carbide possesses all the physical properties required for being used as catalyst support, namely: high mechanical strength, high thermal conductivity, high oxidative

resistance and chemically inertness. It is also worth mentioning that the SiC contains high pore volume in the meso- and macro-pores range which significantly enhances mass transfer for the FTS reaction. Such influence has been reported by Borg et al. [17] on the Co-Re/Al₂O₃ catalyst with different pore sizes. Indeed, during the FTS reaction the catalyst pores were mostly filled with liquid waxes and thus, both the gaseous reactants and the products had to diffuse through a liquid layer. Such gas-liquid diffusion layer causes more severe concentration gradients for CO than for H₂ due to the higher diffusivity of the later. The difference in term of reactants diffusivity leads to the formation of high local concentration of H₂ versus CO and as a consequence, a higher selectivity towards light products formation.

Recent results have shown that SiC containing cobalt catalysts are active and highly selective, especially under severe FTS conditions, compared to Co/Al₂O₃ catalysts [18]. It is also worthwhile to note that for the SiC-based catalyst both the active phase, i.e. Co, and the support can be effectively recovered after complete deactivation [18] which is economically advantageous compared to other FTS catalysts where recovery of the active phase and the support is difficult and costly.

Ho et al. [19] and Tsubaki et al. [20, 21] have reported that the nature of the impregnation solvent, i.e. ethanol versus water, induces a strong modification of the active phase and the support interaction leading to a significant improvement of the FTS activity, while keeping a similar liquid hydrocarbon selectivity, in a slurry reactor configuration. However, such influence is not documented for the same catalyst operated in a fixed-bed configuration where heat and mass transfer could be a critical issue for the FTS performance and stability.

The aim of the present article is to report on the influence of ethanol as impregnation solvent on the FTS catalytic performance of the cobalt-based catalysts, doped with a trace amount of ruthenium, operated in a fixed-bed configuration under a total pressure close to that operated in the industrial FTS plants. The FTS activity and C₅₊ selectivity evolution are investigated at different gas space velocities (1900, 2850 and 3800 h⁻¹) and temperatures (215 to 235 °C) and compared with those obtained on conventional catalysts supported on Al₂O₃ and SiO₂. The possible influence of the different cobalt species, i.e. face centered cubic (fcc) or hexagonal packed (hcp), on the FTS performance was also investigated using a ⁵⁹Co zero field NMR technique. It is worthwhile mentioning that it is the first time that such technique is applied for studying the cobalt species involved in the FTS reaction. The long-term stability

of the catalyst under the reaction conditions is a matter of concern as well and thus, the stability of the catalyst as a function of time on stream was also evaluated.

2. Experimental section

2.1 Support

Silicon carbide (β -SiC) was synthesized via a gas-solid reaction between the SiO vapour and dispersed solid carbon. The detailed synthesis of the SiC-based materials is summarized in a recent review [22]. The pure SiC exhibits a specific surface area ranged from 20 to about 40 m². g⁻¹ which is lower than those of alumina or silica supports. Some examples of SiC material with different shapes are presented in Figure 1A. The high-resolution TEM micrograph of the topmost surface of the SiC is presented in Figure 1B which clearly shows the presence of a thin amorphous layer on the SiC surface. Such amorphous layer consists of a mixture of SiO_xC_y and SiO₂ according to the reports in the literature [23, 24]. The amount of these SiO_x species present on the SiC surface, after synthesis and after calcination at 800°C to remove the un-reacted carbon, was determined by submitting the sample to a soda (20 wt. %) treatment at 80°C which removed the SiO₂ and SiO_xC_y phases, is about 3.5±0.5 wt. % [25]. Such silicon containing oxygen phases were expected to play a role of a natural wash-coat for anchoring the active phase onto the SiC surface. Indeed, on the SiC sample treated with aqueous NaOH (20 wt. %) solution at 80°C, the cobalt active phase is poorly dispersed resulting in the formation of aggregates with size of a few micrometers due to the low interaction between the hydrophobic SiC surface and the salt precursor.

2.2 Catalyst preparation

Silicon carbide-supported cobalt catalysts were prepared by pore volume impregnation of the support with cobalt nitrate (Acros) solution. The solvent used was either deionized water or ethanol (99.95 % purity, Acros). The cobalt loading was kept at 30 wt. % of the silicon carbide support which is the upper range of cobalt loading according to the literature and patent survey [26, 27]. The cobalt phase was loaded onto the support via a successive impregnation method following patented recipes [28, 29]. The catalyst was calcinated at 350 °C in air between each impregnation step. After impregnation the solid was allowed to dry at room temperature for 2 hrs and then oven-dried at 110°C for 2 hrs and calcined at 350 °C for additional 2 hrs in order to decompose the cobalt salt into its corresponding cobalt

oxide. The catalyst was further impregnated a second time followed by a same thermal treatment. The oxide form was further reduced in flowing hydrogen ($300 \text{ mL} \cdot \text{min}^{-1}$) at 300°C for 6 hrs. The catalyst prepared using water as impregnated solvent is noted Co-Ru/SiC-W whereas the one prepared with ethanol is noted Co-Ru/SiC-E.

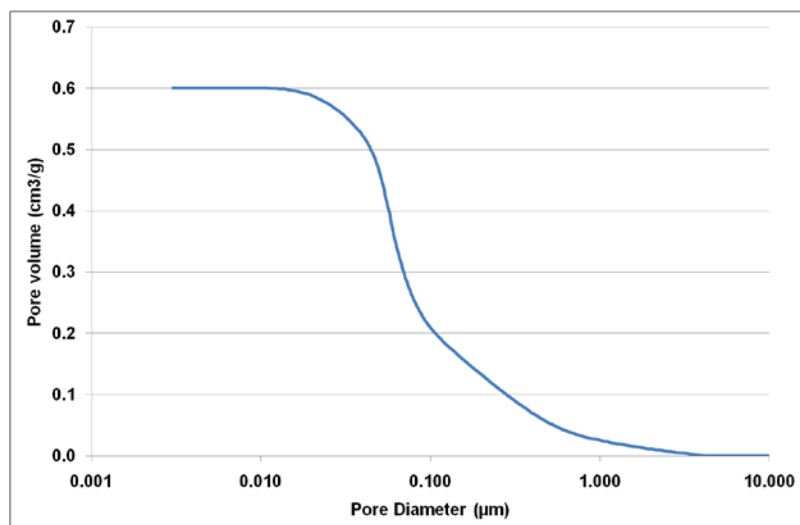
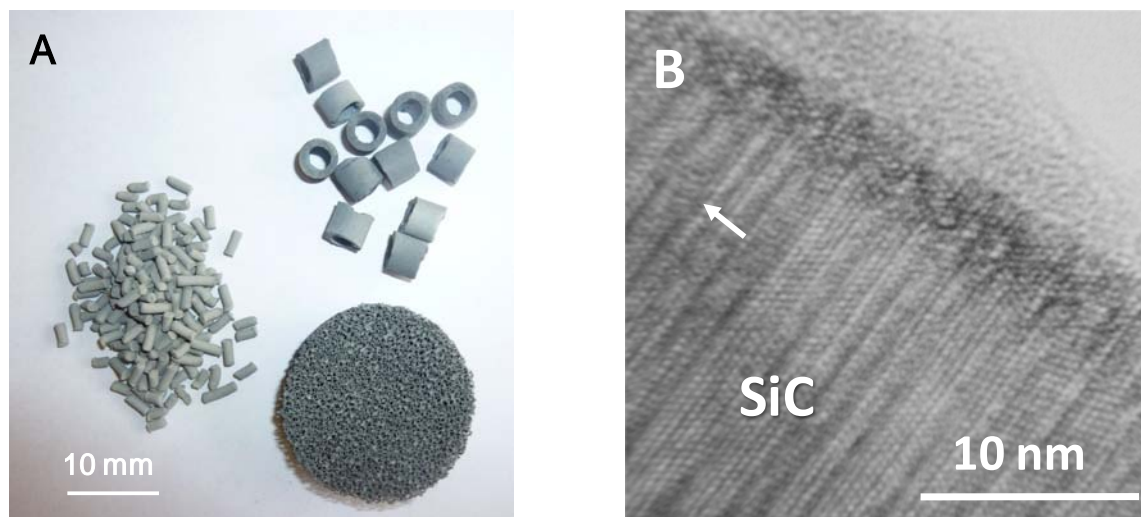


Figure 1. (A) Silicon carbide (SiC) with different macroscopic shapes synthesized according to the gas-solid reaction. (B) HR-TEM micrograph showing the presence of an amorphous layer constituted by a mixture of SiO_2 and SiO_xC_y on the SiC surface and a high number of stacking faults along the [111] growth axis. (C) Representative pore size distribution of the SiC support measured by mercury intrusion.

2.3 Characterization techniques

X-ray diffraction (XRD) measurements were carried out in a Bruker D-8 Advance diffractometer equipped with a Vantec detector. The powdered sample was packed onto a glass slide. ASTM powder diffraction files were used to identify the phase present in the sample. Crystallite sizes were calculated from line broadening using the Scherrer equation.

The specific surface area of the support and the catalyst, after reduction, were determined in a Micromeritics sorptometer. The sample was outgassed at 250 °C under vacuum for 14 hrs in order to desorb moisture and adsorbed species on its surface. The measurements were carried out using N₂ as adsorbent at liquid N₂ temperature.

Temperature-Programmed Reduction (TPR) was carried out in a Micromeritics ASAP-2100 setup under diluted hydrogen flow (10 vol. % in helium) with a heating rate of 15°C·min⁻¹. The hydrogen consumption was continuously monitored with a thermal conductivity detector (TCD). The steam formed during the reduction was trapped at -88 °C.

Scanning electron microscopy (SEM) analyses were carried out on a JEOL 6700F microscope working at 10 kV accelerated voltage. The solid was fixed on the sample holder by a graphite paste for examination. Before analysis the sample was covered by a thin layer of gold in order to avoid charging effect. The SEM analysis allows one to get access to the morphology of the cobalt aggregate after reduction in order to correlate with the metal particle size determined by the XRD line broadening.

⁵⁹Co NMR experiments were performed in a home-made zero magnetic field at a temperature of 4.2 K. The integrated spin-echo intensity was recorded every 1 MHz using a coherent pulsed NMR spectrometer with phase-sensitive detection and automated frequency scanning. The NMR spectra were taken at five different values of the excitation RF field, covering a range over more than one order of magnitude. Such a procedure allowed us to determine the optimum excitation field at each frequency and to correct for the variation of the local electronic susceptibility and thus of the NMR enhancement factor as a function of frequency. After this a further correction for the usual ω^2 frequency dependence of the NMR signal was applied. The NMR amplitudes obtained in such a way represent the true distribution of nuclei with a given HF. Detailed description of the technique can be found in the literature [30, 31]. The analysis was performed on the tested catalyst covered with a

homogeneous solid waxes layer in order to prevent any surface oxidation of the cobalt phase during air exposure.

2.4 Fischer-Tropsch synthesis reaction

The Fischer-Tropsch synthesis reaction was carried out in a tubular fixed-bed stainless steel reactor (*I.D.* = 6 mm) with circulating silicon oil as heating source. The reduced catalyst (5 g of catalyst, in a grain form with an average size between 150 to 400 μm , containing 30 wt. % of cobalt and 0.1 wt. % of ruthenium) was deposited between quartz wool plugs in the middle of the reactor. The reactor pressure was slowly increased from 0.1 to 4 MPa (ramping rate of $1 \text{ MPa}\cdot\text{h}^{-1}$) under argon. The total pressure was controlled by a back pressure regulator (MFI Ltd.). At 4 MPa the reactor temperature was raised from room temperature to the desired reaction temperature (heating rate of $2^\circ\text{C}\cdot\text{min}^{-1}$). Then, the argon flow was replaced by a 50:50 v:v mixture of synthesis gas ($\text{CO}:\text{H}_2 = 1:2$) and argon. The catalyst was activated under a synthesis gas-argon mixture with different synthesis gas concentrations during three days before evaluation under pure synthesis gas condition. The catalyst bed temperature was monitored with a thermocouple (\varnothing 0.3 mm) inserted inside a stainless steel finger (\varnothing 1 mm) passing through the catalyst bed. The products of the reaction were condensed in two high pressure traps maintained at 85°C and 15°C respectively. The exit gas was analyzed on-line, both by Thermal Conductivity Detector (TCD) and Flame Ionization Detector (FID), with a gas chromatography (GC Varian 3800 equipped with a DP-1 and Carbobond capillary columns).

3. Results and discussion

3.1 Catalyst characteristics

The final specific surface areas of the catalysts after reduction were $23 \text{ m}^2/\text{g}$ (Co-Ru/SiC-E) and $22 \text{ m}^2/\text{g}$ (Co-Ru/SiC-W). Compared to the SiC support ($29 \text{ m}^2/\text{g}$) the BET surface areas only slightly decreased at high cobalt loading. This result was attributed to the presence of macrospore in SiC support. The XRD patterns of the catalysts after reduction under H_2 at 300°C for 6 hrs are presented in Figure 2. The XRD patterns only display

diffraction lines corresponding to the SiC support and metallic cobalt phase whereas no diffraction lines corresponding to the cobalt oxide phases are observed, results were confirmed by TPR Figure 3. The complete cobalt phase reduction observed was directly attributed to the low interaction between the cobalt phase and the SiC support which avoid the formation of a hardly reducible cobalt phase as usually observed for alumina or silica supports [18, 32, 33]. The average cobalt particle size determined by the Scherrer formula is reported in Table 1. The particle size calculated by Scherer equation indicates that there are two particle populations, small hcp particles and bigger fcc particles.

Table 1. Average cobalt particle size determined by the Scherrer formula.		
	<i>fcc</i> diffraction plane (111)	<i>hcp</i> diffraction plane (101)
Co-Ru/SiC-W	54 nm	17 nm
Co-Ru/SiC-E	70 nm	17nm

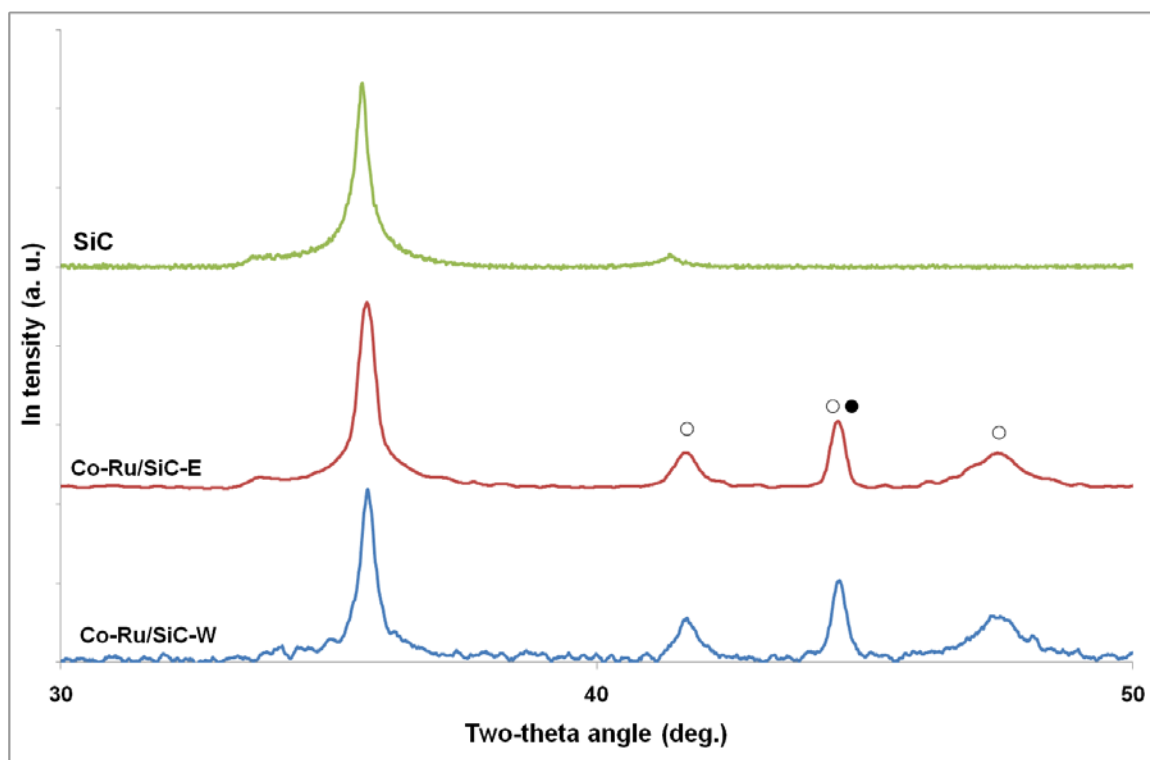


Figure 2. XRD patterns of the SiC, Co-Ru/SiC-W (H₂O) and Co-Ru/SiC-E (CH₃OH) catalysts. The catalysts were calcined at 350°C for 2 hrs followed by a reduction under H₂ at 300°C for 6 hrs. The different cobalt phases were denoted as: (○) cobalt hcp, (●) cobalt fcc.

The TPR spectra of the Co-Ru/SiC-W, after calcinations and after in situ reduction at 300 °C for 6 hrs, are presented in Figure 3. The reduction of cobalt oxide supported on the SiC started at a lower temperature due to the low metal support interaction (blue curve). The sequential TPR analysis was also performed, i.e. isotherm reduction at 300 °C for 6 hrs followed by a second in situ TPR, in order to ensure the complete reduction of the catalyst under the applied reduction conditions and the results are presented in the same figure (Figure 3, red curve). According to the results one can see that after the reduction at 300 °C for 6 hrs all the cobalt oxide was reduced and no additional reduction peaks were observed in the TPR spectrum of the reduced catalyst. During the transfer part of the metallic cobalt was re-oxidized. According to the TPR results (not shown), the cobalt oxide formed on the catalyst surface is amounted to about 10 wt. % of the total cobalt phase (3 wt. % in absolute) and is mostly consisted by CoO phase. Such superficial CoO phase is expected to be further reduced under the FTS conditions which are well known to be a strong reductive medium [34].

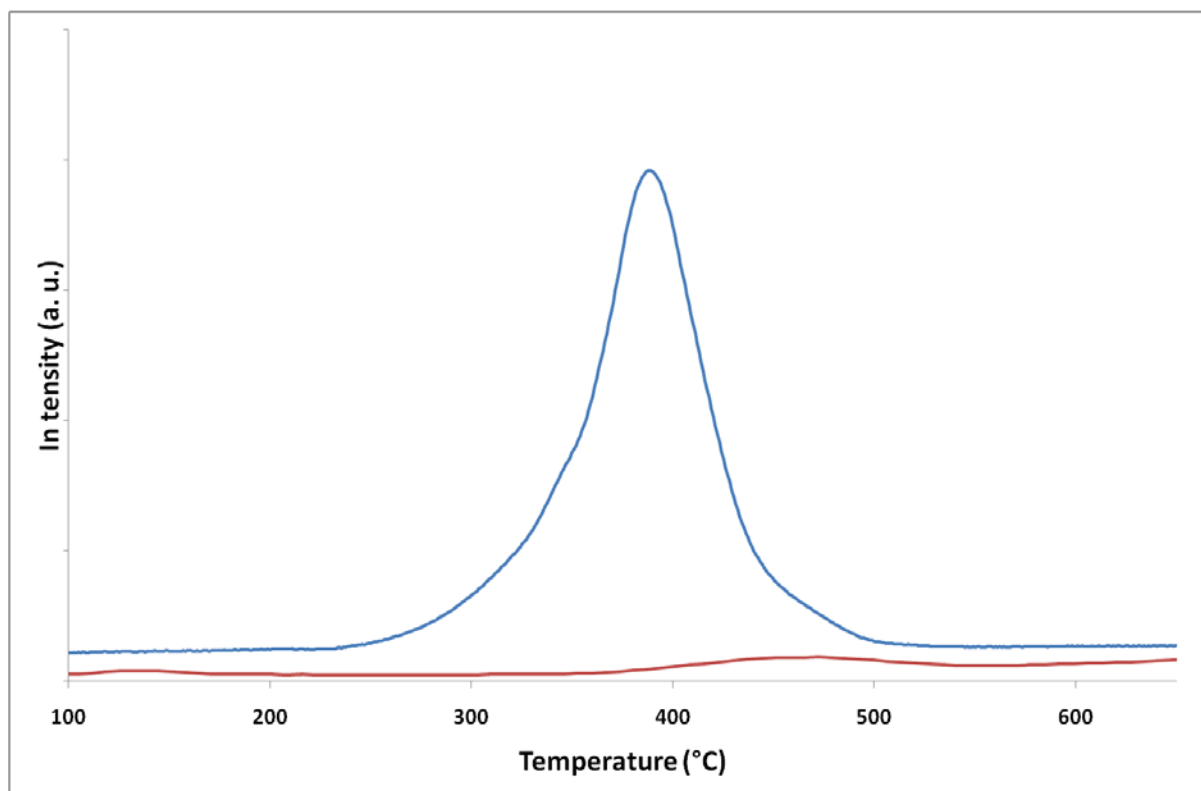


Figure 3. TPR profiles of the Co-Ru/SiC-W (H₂O) catalysts: after calcinations at 350°C for 2 hrs (blue curve) and after reductions at 300°C for 6 hrs (red curve).

The corresponding SEM micrographs of the two catalysts after reduction are presented in Figure 4A and B. The particle size observed on Co-Ru/SiC-E seems to be larger than those on Co-Ru/SiC-W.

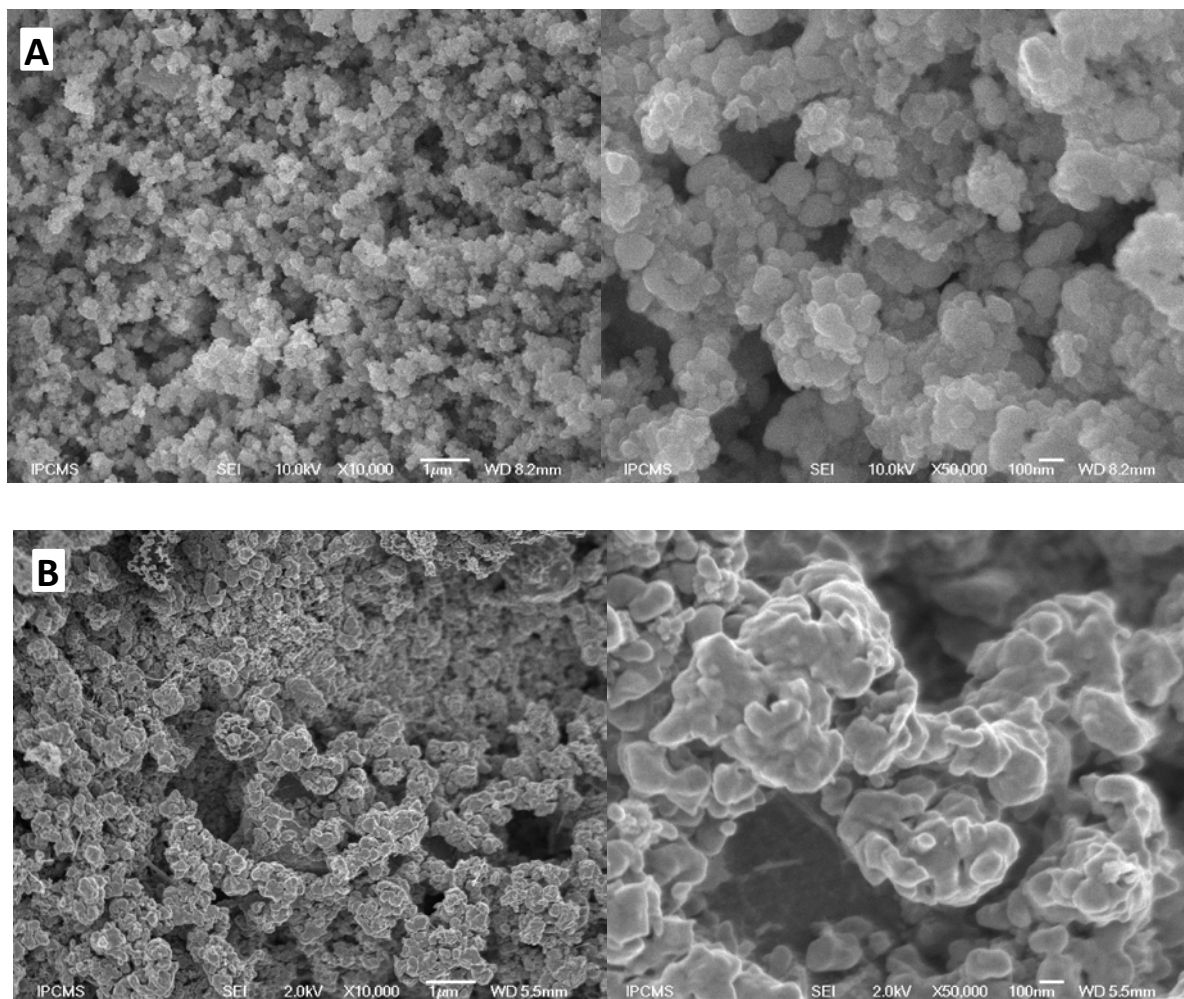


Figure 4. (A) SEM micrographs of the Co-Ru/SiC-W after reduction under H₂ at 300 °C for 6 hrs. (B) SEM micrographs of the Co-Ru/SiC-E after reduction under H₂ at 300 °C for 6 hrs.

3.2 FTS performance as a function the GHSV and temperature

The FTS activity and C₅₊ selectivity obtained on the Co-Ru/SiC-E and the Co-Ru/SiC-W catalysts as a function of the reaction temperature and under a relatively high GHSV, 2850 h⁻¹, are presented in Figure 5. The FTS activity steadily increases on both catalysts with increasing reaction temperatures, whereas S_{C₅₊} selectivity remains relatively high at around 91 %. It is worthy to note that the FTS activity on the Co-Ru/SiC-E remains higher than the one obtained on the Co-Ru/SiC-W catalyst and increases with increasing the reaction temperature. The FTS activity also remains stable for the whole test, i.e. > 200 hrs, indicating that deactivation is relatively low on such catalysts after stabilization. The most remarkable

fact is that the $S_{C_{5+}}$ selectivity remains extremely high whatever the reaction temperature up to 230 °C. The high $S_{C_{5+}}$ selectivity obtained in the present work could be attributed to several facts: (i) firstly, to the homogeneous catalyst bed temperature thanks to the good thermal conductivity of the support and the liquid hydrocarbon film formed on the catalyst surface [35], the internal temperature of the reaction was measured by a thermocouple placed inside a stainless steel finger inserted through the catalyst bed. The internal reaction temperature measured during the course of the reaction is about one to two degrees higher than the silicon oil temperature and remains unchanged all along the catalyst bed, (ii) secondly, to the increased partial pressure of steam within the catalyst bed due to the relatively low space velocity [36, 37]. The promoting effect of steam on the $S_{C_{5+}}$ has been proposed to be due to its inhibition of hydrogenation reactions leading to a lower methane selectivity [38], and (iii) the meso- and macro-porosity of the support which favors the evacuation of the products and better accessibility of the reactant.

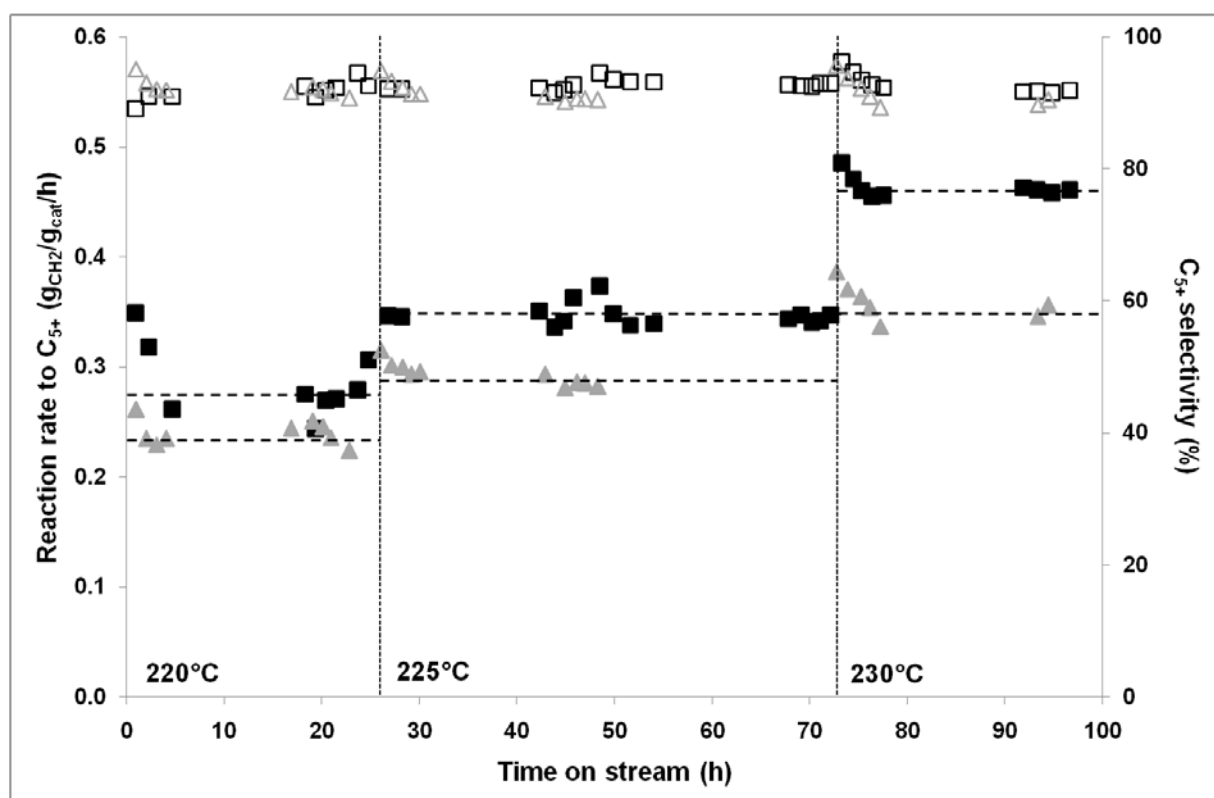


Figure 5. FTS performance and stability of the Co-Ru/SiC-W and Co-Ru/SiC-E catalysts as a function of the reaction temperature. Reaction conditions: total pressure: 4 MPa, GHSV: 2850 h⁻¹, catalyst weight: 5 g. The catalyst tested has already been evaluated in the FTS reaction at 215 °C and under a GHSV of 1900 h⁻¹ during about 200 hrs on stream (not reported).

The product distribution obtained at the steady-state condition, at different reaction temperatures, and with a GHSV (STP) of 2850 h⁻¹ on the Co-Ru/SiC-E catalyst is presented in Table 2. The S_{C₅₊} selectivity remains high, i.e. 93 %. Such high S_{C₅₊} selectivity has also recently been reported by de la Osa et al. [39] on the cobalt phase supported on similar SiC carrier. According to these results, Co/SiC displays S_{C₅₊} selectivity higher than 90 % at reaction temperature as high as 240 °C and under a space velocity of 6000 h⁻¹. The SiC-based catalyst also exhibits an improved FTS activity at reaction temperature higher than 235 °C compared to other catalysts: Co/SiC > Co/bentonite > Co/Al₂O₃ > Co/TiO₂.

Table 2. Product selectivity at steady-state (100 hrs of test) on the Co-Ru/SiC-E catalyst as a function of the reaction temperature. Reaction conditions: Co loading = 30 wt. %, H ₂ :CO = 2, total pressure = 4 MPa, GHSV (STP) = 2850 h ⁻¹ .						
Temperature (°C)	C _{CO} (%)	CH ₄ (%)	CO ₂ (%)	C ₂ -C ₄ (%)	C ₅₊ (%)	ASM
220	39	5.1	0.0	2.6	92 ± 1	0.27
225	50	6.0	0.0	2.0	92 ± 1	0.34
230	67	6.0	0.3	2.7	91 ± 1	0.42

The high C₅₊ selectivity could be attributed to the relatively high thermal conductivity of the SiC support which contributes to the homogenization of the catalyst temperature. Such heat transfer is also favored by the formation of liquid film within the catalyst bed with better

thermal conductivity [35]. The continuous liquid hydrocarbon film present on the catalyst is evidenced by the SEM micrographs of the catalyst after reaction showing the presence of a solid waxes film homogeneously covering the catalyst surface (Figure 6). The hydrocarbon film can be effectively removed by treating the catalyst in helium flow at 400 °C for 2 hrs. The SEM analysis carried out on the helium treated catalyst indicates the complete morphological integrity of the cobalt active phase (Figure 6).

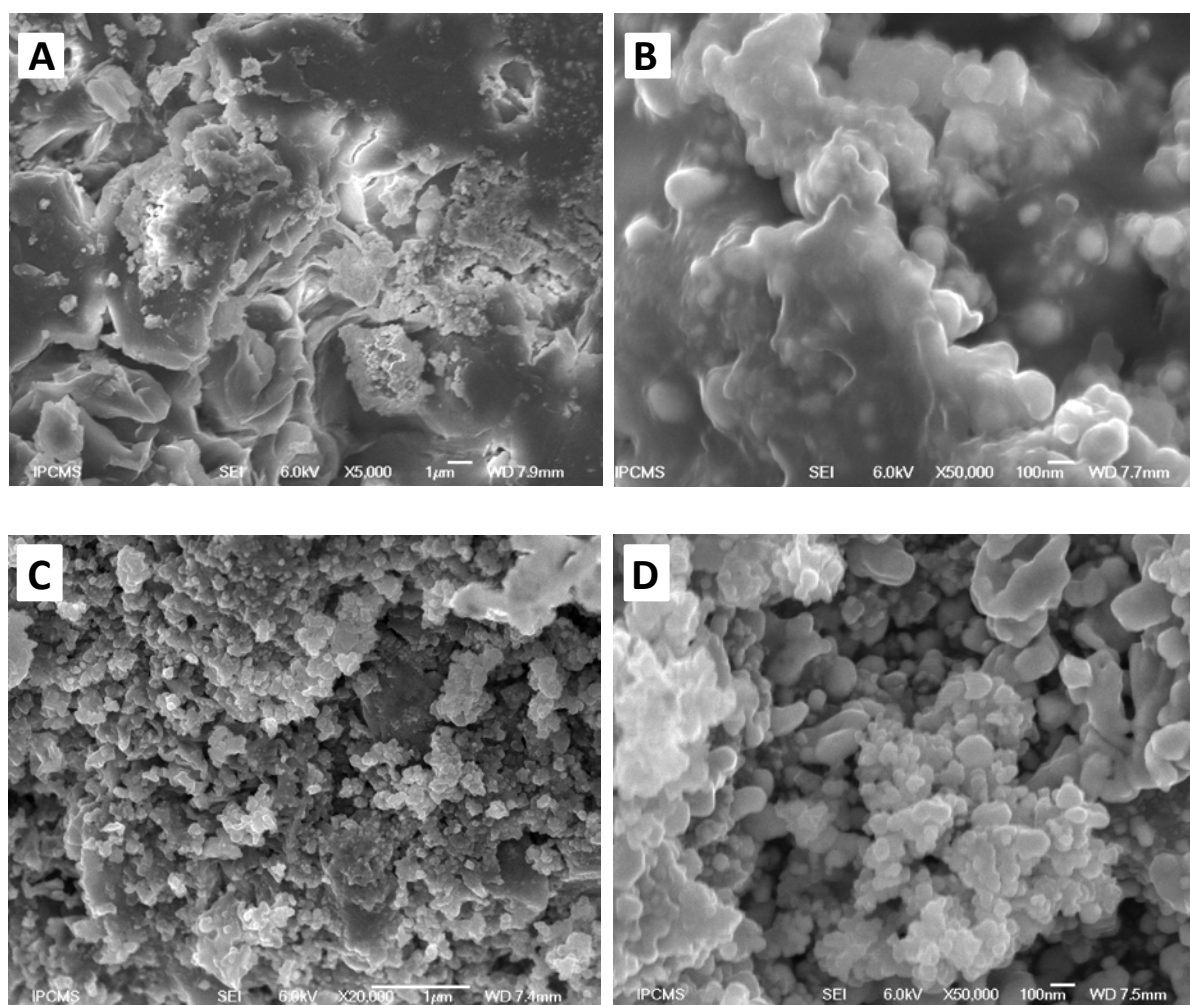


Figure 6. (A, B) SEM micrographs of the Co-Ru/SiC-E catalyst after FTS reaction showing the complete coverage of the catalyst surface by a relatively thick solid hydrocarbons film. (C, D) SEM micrographs of the Co-Ru/SiC-E catalyst after FTS reaction and wax removal at 400°C under He.

The FTS performance on the Co-Ru/SiC-E catalyst under more severe reaction conditions, i.e. high temperature and high space velocity, is also evaluated and the results are presented in Figure 7. At a reaction temperature of 235 °C and a space velocity of 3800 h⁻¹ the FTS activity reached 0.54 g_{CH₂}·g_{catalyst}⁻¹·h⁻¹ while the S_{C₅₊} selectivity remains high at around 91 %. Oukaci et al. [26] have reported the FTS activity on several patented catalysts which were between 0.087 and 0.254 g_{CH₂}·g_{catalyst}⁻¹·h⁻¹. According to such results the FTS activity obtained on our catalyst is relatively high compared to those reported for the patented catalysts by Oukaci et al. [26]. The FTS reaction rate obtained on the Co-Ru/SiC-E catalyst is also relatively high and more stable compared to those obtained on the Co-Re/Al₂O₃, Co-Re/SiO₂ and Co-Re/TiO₂ catalysts as reported by Tsakoumis et al. [40]. The most active catalyst reported in the work of Tsakoumis et al. [40] is the Co-Re/Al₂O₃ with an initial reaction rate of about 0.56 g_{CH₂}·g_{catalyst}⁻¹·h⁻¹ followed by a rapid deactivation down to 0.45 g_{CH₂}·g_{catalyst}⁻¹·h⁻¹ after about 22 hrs on stream. In the present work, the Co-Ru/SiC-E catalyst exhibits a reaction rate of about 0.56 g_{CH₂}·g_{catalyst}⁻¹·h⁻¹ at a GHSV of 3800 h⁻¹ and 235 °C and no deactivation was observed for the test. It is also worth mentioning that the Co-Ru/SiC-E catalyst has been run for more than 400 hrs under different reaction conditions.

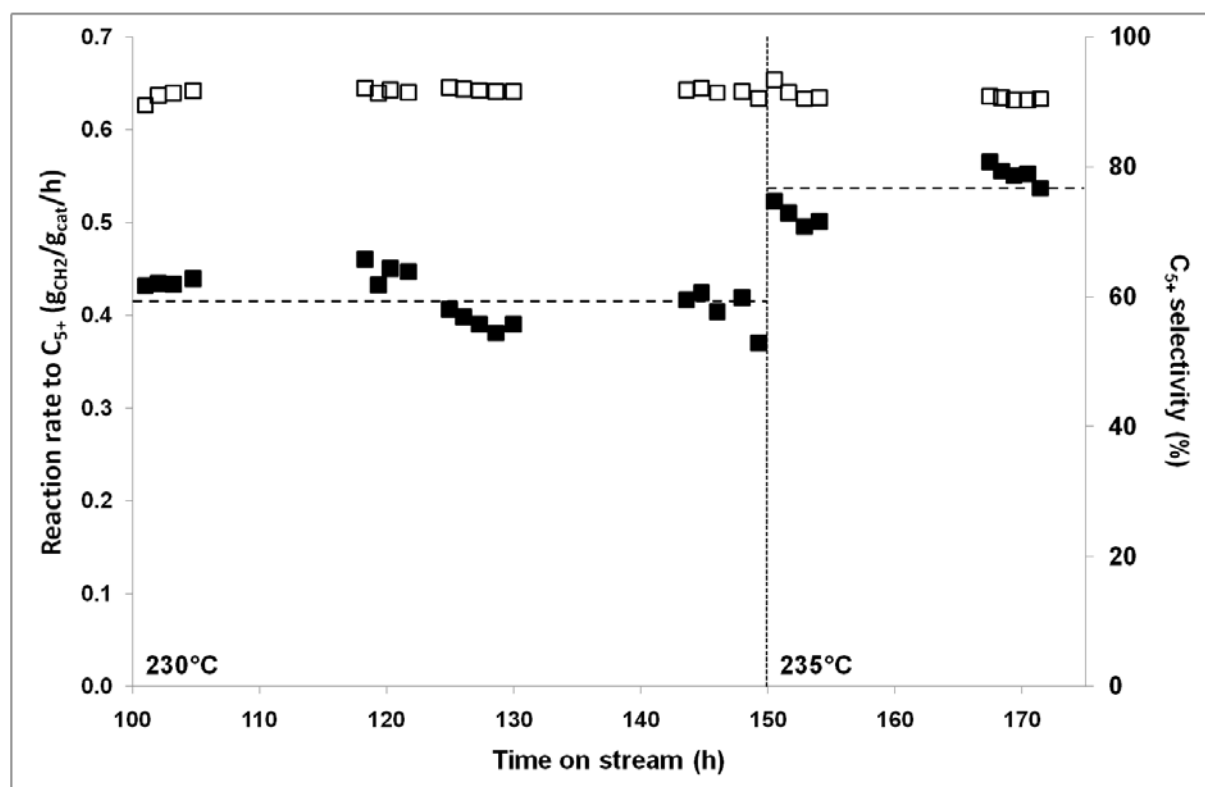


Figure 7. FTS activity ($\text{g}_{\text{CH}_2} \cdot \text{g}_{\text{catalyst}}^{-1} \cdot \text{h}^{-1}$) and C_{5+} selectivity of the Co-Ru/SiC-E catalyst as a function of the GHSV and reaction temperature. Reaction conditions: total pressure: 4 MPa, GHSV (STP): 3800 h^{-1} , catalyst weight: 5 g.

The product distribution is presented in Table 3 and indicates that high $\text{S}_{\text{C}_{5+}}$ selectivity can still be obtained, i.e. 91 % at 230 °C and 90 % at 235 °C, even at high reaction temperature, by increasing the total flow rate of the reactant mixture. However, it is worthwhile to note that at the reaction temperature of 235 °C the selectivity towards methane becomes significant, i.e. 4 %, on the SiC-based catalyst. The relatively high $\text{S}_{\text{C}_{5+}}$ selectivity at high reaction temperature can be explained by the concomitant increase of the steam partial pressure within the catalyst bed due to the higher CO conversion. It is reported that at high partial pressures steam competitively adsorbs on the methanation sites and thus, favor the formation of liquid hydrocarbons, leading to a higher $\text{S}_{\text{C}_{5+}}$ selectivity [9, 33]. The influence of water on different FTS catalysts has been reviewed by Dalai and Davis [41]. The data indicates that water appears to have significant positive effect on the FTS activity and C_{5+} selectivity for the silica-based FTS catalyst with a relatively well dispersed cobalt particle size by noble metal promoting. As the SiC support was covered with a thin layer of SiOx compounds it is expected that the same effect again operated. The positive influence of water on the C_{5+} selectivity has been reported by several groups in the literature [42,43,44]. The relatively high C_{5+} selectivity of the SiC-based catalysts could also be linked with the thermal conductivity of the SiC support which provides high heat dissipation throughout the catalyst body preventing hot spot formation. The total amount of the liquid hydrocarbons recovered after the FTS test was around $83 \text{ g} \pm 5 \text{ g}$. The solid wax retained on both the catalyst and the underneath quartz wool is around 5 g (determined by heating the sample in helium at 400 °C for 2 h). The carbon mass balance calculated was around $90 \pm 3 \text{ wt. \%}$ taken into account the amount of incomplete wax recovery in the traps (the lost was mostly due to the need to heat up the trap in order to melt the solid waxes which were trapped between the condenser lines of the high-temperature trap), and the error margin in the CO flow rate ($\pm 5 \%$) at the entrance of the reactor and at the exit of the gas-chromatograph. The error margin is added to the total C_{5+} selectivity.

Table 3. Product selectivity at steady-state (100 hrs of test) on the Co-Ru/SiC-E catalyst as a function of the reaction temperature. Reaction conditions: Co loading = 30 wt. %, H₂:CO = 2, total pressure = 4 MPa, GHSV (STP) = 3800 h⁻¹.

Temperature	C _{CO} (%)	CH ₄ (%)	CO ₂ (%)	C ₂ -C ₄ (%)	C ₅₊ (%)	ASM
230	47	5.5	0.0	3.0	91.5 ± 1.5	0.43
235	59	6.8	0.3	3.1	89.8 ± 1.5	0.54

At high reaction temperatures, i.e. > 230 °C, where the contribution of hydrogenation reactions becomes important, the S_{C₅₊} selectivity on the SiC-based catalyst only slowly decreases and still remains high, i.e. 90 %, compared to other catalysts supported on insulating supports (Al₂O₃, SiO₂, TiO₂) tested at lower reaction temperature [45]. The same behavior was also observed with the water-impregnated catalyst but with a lower activity.

The chain growth factor (α) determined on both catalysts are presented in Figure 8. According to the results one can state that the chain growth factor (α) is relatively high on both catalysts, i.e. 0.92 for ethanol impregnated catalyst and 0.93 for water impregnated catalyst, which is in good agreement with the relatively high C₅₊ selectivity obtained on both catalysts. Davis and co-workers [46] have reported that the usual α -value of the cobalt, 0.87, is significantly improved in the presence of trace amount of ruthenium (high α -value active phase). The high α -value observed in the present work could be thus attributed to the formation of Co-Ru alloy (see NMR results below) which behaves more like Ru than Co.

According to previous works by Shi and Davis [47] and Borg et al. [48], cobalt dispersion has no direct influence on the S_{C₅₊} selectivity. Holmen and co-workers [49] have stated that the S_{C₅₊} selectivity increases when the BET surface area of the support decreases for the alumina-based catalyst, i.e. α -Al₂O₃ > γ -Al₂O₃. The high S_{C₅₊} selectivity observed on the SiC catalyst could be attributed to the medium thermal conductivity of the support which prevents local hot spot formation on the catalyst surface leading to the formation of CH₄, C₂-C₄ and CO₂ products.

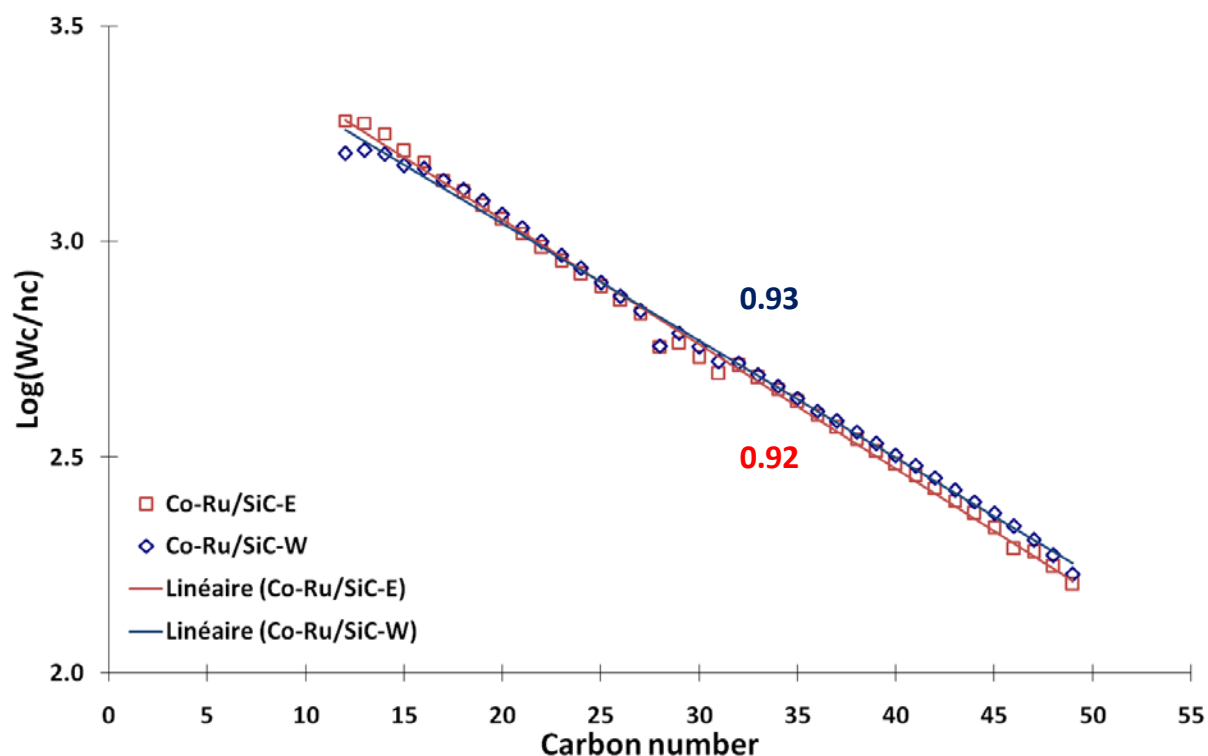


Figure 8. Calculated chain growth factor (α) from the linear portion of the hydrocarbons.

The high C_{5+} selectivity obtained on the SiC-based catalysts, either impregnated with ethanol or water, could also be tentatively attributed to the pore size distribution of the support that facilitates access to the reactants and evacuation of the products [50, 51]. Rane et al. [52] have recently reported that the C_{5+} selectivity obtained on the cobalt supported alumina catalysts strongly depended on the support pore size with a highest C_{5+} selectivity recorded on the α - Al_2O_3 with larger pore. Ghampson et al. [53] have also reported similar results on mesoporous silica-based catalysts. The SiC support pore size, i.e. 40-120 nm, is in a similar range with those of the α - Al_2O_3 support reported by Rane et al. [52] having a similar specific surface area, i.e. $23 \text{ m}^2 \cdot \text{g}^{-1}$ for SiC and $22 \text{ m}^2 \cdot \text{g}^{-1}$ for α - Al_2O_3 . The higher selectivity obtained on the SiC-based catalyst compared to that of the α - Al_2O_3 could be attributed to the pore morphology between the two supports, i.e. ink-bottled pore for the α - Al_2O_3 and connected pore for the SiC according to our recent TEM tomography investigation [54].

The Co-Ru/SiC-E catalyst also exhibits a relatively high stability as a function of the FTS test duration according to the results presented in Figure 5 and Figure 7. Almost no

deactivation is observed on the catalyst up to 170 hrs on stream which indicates that deactivation linked with cobalt surface oxidation or sintering is unlikely to occur under the reaction conditions used in the present work.

3.3 ^{59}Co zero field NMR

In order to get more insight into the FTS activity of the Co-Ru/SiC-E catalysts zero field ^{59}Co NMR was carried out. The ^{59}Co NMR spectrum of the Co-Ru/SiC-E catalyst recorded at 4.2 K (Figure) indicates the presence of several cobalt species within the catalyst: hexagonal close packed (fcc), face centered cubic (hcp) and stacking faults either from the fcc or the hcp phases [55, 56]. For pure metallic cobalt, the base NMR frequencies are 217 MHz for the high-temperature fcc phase, 219-228 MHz (depending on the magnetization orientation) for the anisotropic hcp phase and 200 MHz in the bcc metastable phase [57]. For comparison, the NMR spectrum of the Co-Ru/SiC-W is presented in the same figure. The main observation is that both spectra are dominated by contributions arising from Co atoms in stacking faults (mid frequency range contributions). It is expected that stacking faults are more prone to be generated on small metal particles than the bigger ones. The stacking faults could be present in a single fault or as consecutive double faults, i.e. ABABABCABAB (hhchh) or ABABABCABAB (hhcchh). Since the NMR technique probes the short range order around the Co atoms, stacking faults up to two can be quantitatively detected whereas the higher faults, i.e. three or more, are already assigned to bulk fcc or hcp Co.

Table 4 summarizes the FTS activity and product selectivity obtained on the Co-Ru/SiC-E and Co-Ru/SiC-W catalysts. According to the results the catalyst impregnated with ethanol shows a FTS activity about 40 % higher than the one impregnated with water under the same reaction conditions.

Table 4. Product selectivity at steady-state on the Co-Ru/SiC-E and Co-Ru/SiC-W catalysts. Reaction conditions: Co loading = 30 wt. %, H₂:CO = 2, total pressure = 4 MPa, temperature = 215 °C, GHSV (STP) = 1,900 h⁻¹.

Catalyst	C _{CO} (%)	CH ₄ (%)	CO ₂ (%)	C ₂ -C ₄ (%)	C ₅₊ (%)	ASM
Co-Ru/SiC-E	57	3.5	1.2	2.3	93 ± 1	0.26
Co-Ru/SiC-W	42	4.7	1.2	2.1	92 ± 1	0.20

Recent reports have deal with the possibility of difference FTS activity depending to the cobalt phases, i.e. fcc, hcp or defects surface linked with stacking faults [55,56]. It is expected that in cobalt nanoparticles several cobalt species, i.e. fcc, hcp and stacking faults, may coexist which induce a possible influence on the final catalytic activity [58, 59]. Kala et al. [60] have reported that the presence of stacking faults in nanoparticles gives rise to a large amounts of hydrogen incorporation. Previous studies [55,56] seem to indicate that the FTS activity was enhanced in the presence of the cobalt hcp phase. However, the role of stacking faults, either from the fcc or hcp phases, is not well clarified yet due to the inability to get access to their relative concentrations inside the sample based on the diffraction technique.

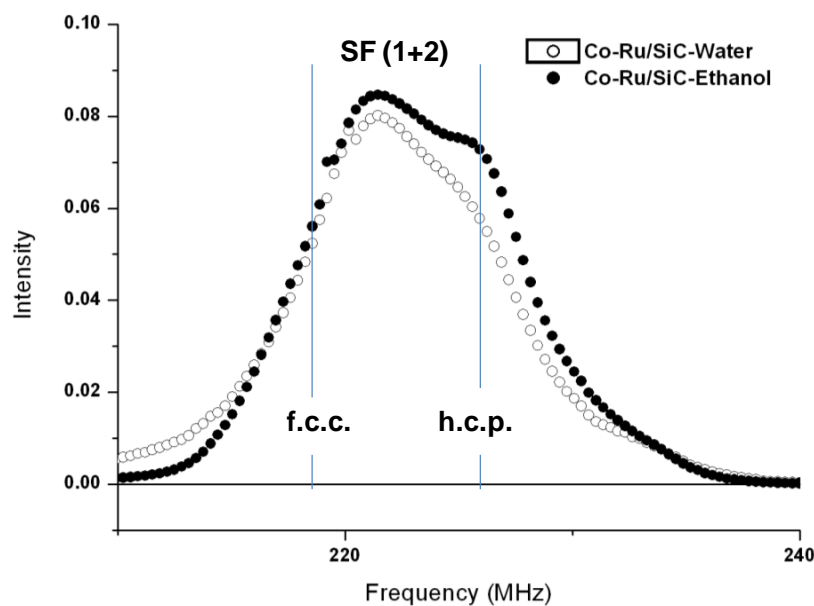


Figure 9. ^{59}Co NMR spectra of the Co-Ru/SiC-E and Co-Ru/SiC-W catalysts, recorded at 4.2 K, showing the presence of several cobalt species in the sample: Co (fcc), Co (hcp) and stacking faults (SF (1+2)). The total stacking faults (single and double faults) $56 \pm 1\%$ for the Co-Ru/SiC-E and $52 \pm 1\%$ for the Co-Ru/SiC-W respectively and is relatively high compared to the pure phases.

The contribution of the different cobalt phases present in the catalysts is presented in Table 5 along with the hcp Co fraction determined from the Rietveld refining of the X-ray data. In addition Co NMR has also been performed at 77K. This allows getting some hint of the Co particle size distribution. Indeed in zero-field NMR the particles that become super paramagnetic vanish from NMR spectra. Therefore, by comparing the NMR spectra, obtained at 4.2 and 77 K, one can determine the amount of Co atoms contained in the small (< 8 nm) Co particles. The fraction of Co atoms in Co particles smaller than 8 nm is therefore also reported in table 5. It can be noticed in table 5 that the amount of pure hcp observed by NMR seems significantly larger than the one observed by X-ray. Indeed, if we consider only the fraction of pure fcc and hcp Co (discarding the stacking faults and small particles contributions) the fraction of hcp Co vs. the total amount of hcp and fcc Co, determined by NMR is 51 and 58 % for the Co-Ru/SiC-E and Co-Ru/SiC-W respectively which is much larger than the values reported by X-ray technique, i.e. 45 and 43 % respectively. However if we consider that the stacking faults NMR contributions arise mainly from single stacking faults and we attribute SF1 to fcc Co and SF2 to hcp, the hcp fractions become respectively 46 and 51%

which are much closer to the fractions obtained by X-ray. The remaining discrepancy might be due to the detailed distribution of single and double stacking faults within the fcc and fcc Co phases. In any case both techniques do not show an hcp fraction difference large enough to account for the difference in the activities of the two samples. Actually, the main difference observed in those samples can be found in the fraction of Co involved in the small hcp Co particles. Since these Co particles have a large surface to volume ratio they are likely to play a major role in the FTS activity. Indeed in the Co-Ru/SiC-E the amount of Co atoms engaged in the small Co particle (< 8 nm) is about 40 % higher than in the same catalyst impregnated with water which could be directly correlated to the FTS activity improvement of ca. 36 % when using ethanol as an impregnation solvent (Table 5).

Table 5. Distribution of the cobalt atoms in the different phases according to the deconvolution of the ^{59}Co NMR envelop. Notation: fcc: face centered cubic, SF1: hcp stacking faults in the fcc phase (and double fcc stacking faults in the hcp phase), SF2: fcc stacking faults in the hcp phase (and double hcp stacking faults in the fcc phase), hcp: hexagonal close-packed structure, small hcp: cobalt atoms engaged in the cobalt particles with diameter equal or smaller than 8 nm, X-ray hcp: the amount of Co atoms in hcp determined by Rietveld refining of the XRD patterns.

	Co at. %					
	Fcc	SF1	SF2	hcp	Small hcp*	X-Ray hcp
Co-Ru/SiC-E	19	27	19	20	15	45
Co-Ru/SiC-W	16	28	23	22	11	43

*The small hcp particle diameter is around 8 nm which is determined according to the following formula:

$$K * V = \ln\left(\frac{\tau}{\tau_0}\right) * k_B * T$$

K: anisotropy constant of Co = $5 * 10^6$ Erg/cm³

V: volume of the particle

τ : characteristic time of measurement = 20 to 100 micro seconds in NMR

τ_0 : Test time for a particle to turn back: between 10^9 to 10^{10} second

k_B : Boltzmann constant = $1.38 * 10^{-16}$ Erg / Kelvin

T: blocking temperature in Kelvin

Ducieux et al. [56] and Sadeqzadeh et al. [61] have reported that the FTS activity is correlated with the concentration of the hcp phase in the catalyst based on the XRD results. Taking into account the results reported by Ducieux et al. [56] and the relatively large contribution of the hcp phase in the catalyst, determined by the NMR technique, one should expect that high density stacking faults, i.e. $> SF(2)$, are mostly linked with fcc faults inside the hcp phase. Enache et al. [62] using *in situ* XRD technique have reported that a zirconia support promotes the formation of a poorly crystalline hexagonal metallic cobalt. The authors have proposed that amorphous cobalt or hexagonal cobalt with crystallographic defects (stacking faults) constituted to the active phases in the FTS reaction whereas the cubic phase is hardly active.

Additional work based on the ^{59}Co NMR is ongoing to get more insight into the direct influence of these different cobalt species containing stacking faults on the FTS performance. Indeed, the advantage of the ^{59}Co NMR versus the diffraction techniques used nowadays relies on the fact that the NMR technique could allow to get access to the relative concentration of each cobalt species in the sample which could be helpful for determining the structure-catalytic relationship in the FTS reaction.

The high FTS activity observed on the Co-Ru/SiC-E could also be attributed to the alloy formation between the two metallic phases according to the ^{59}Co zero field NMR spectra (Figure 10). A large shoulder was observed at low frequency (195 MHz) in the ^{59}Co NMR spectrum of the Co-Ru/SiC-E and can be attributed to the resonance peak of cobalt having a ruthenium atom as a nearest neighbour [63, 64]. This peak is very small in the sample impregnated with water, indicating that with water as impregnation solvent the ruthenium is not well mixed with the cobalt phase. Quantitative analysis of the resonance peak indicates that about 0.4 ± 0.2 % of the cobalt atoms had ruthenium as the first neighbour. The theoretical atomic fraction of Ru/Co in the catalyst is about 0.2 ± 0.1 % (this ratio was calculated by taken into account the nominal loading of cobalt of 30 wt. % and ruthenium of 0.1 wt. %) in the catalyst which is close to the experimental value determined above. It is worth mentioning that it is the first time that we have access to the quantitative amount of direct bonding between the cobalt and ruthenium phases. The existence of Co-Ru alloy at nanoscale range has also been reported by Davis and co-workers [46] by using EXAFS and HR-TEM techniques.

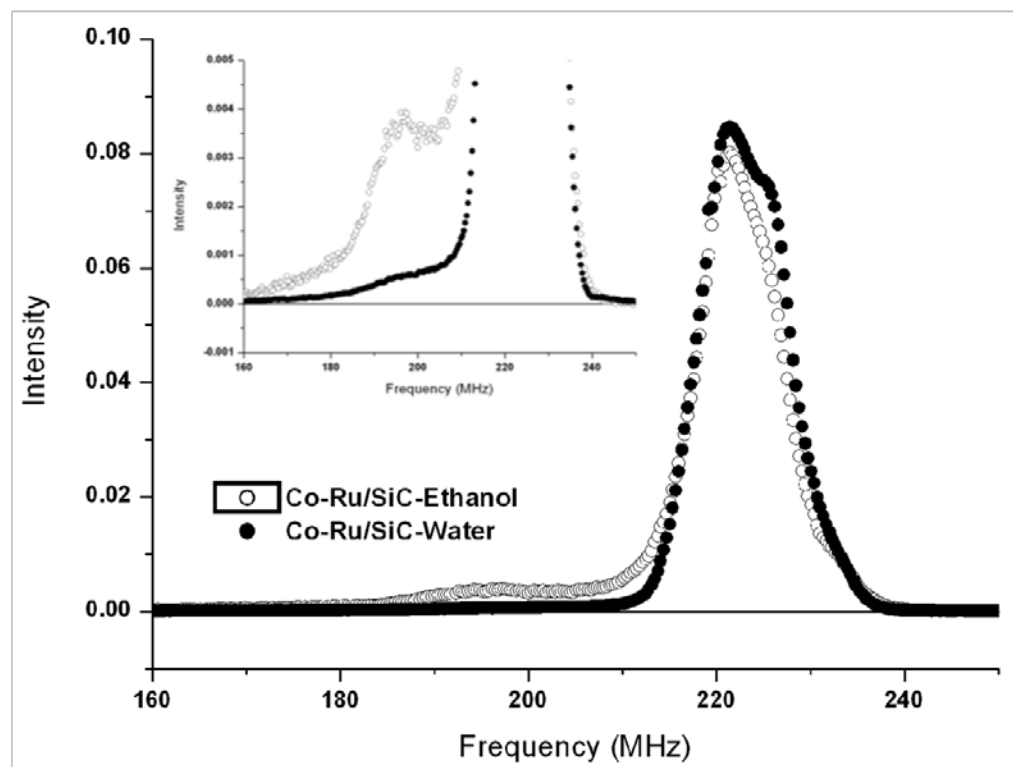


Figure 10. ^{59}Co NMR spectra recorded on the Co-Ru/SiC-W and Co-Ru/SiC-E catalysts at 4.2 K showing the presence of a broad peak at low frequency linked to the Co-Ru alloy. **Inset:** Enlargement of the ^{59}Co NMR peak originated from a Co linked with Ru allows one to confirm the complete integration of the ruthenium into the cobalt matrix.

3.4 SiC surface wetting

Recent results obtained from TEM tomography have shown that the porosity of the SiC support presented two pore networks, i.e. channel pores with an average diameter larger than 50 nm, and ink-bottled pores with an average diameter varying from 4 to 50 nm [54]. Additional energy-filtered TEM (EF-TEM) tomography study [65] indicates that both pore surfaces exhibit difference reactivity towards oxidation: the channel pore is more prone to oxidize, leading to a thicker oxide layer, i.e. hydrophilic character, compared to the ink-bottled pore surface, i.e. hydrophobic-like character. During the impregnation step the wetting of each type of pore is different depending on the nature of the impregnated solvent. Using water it has been observed that only the channel pore was wetted whereas with ethanol both pores were wetted leading to a higher efficiently use of the support surface for metal

dispersion. According to these previous results one should expect that with ethanol as solvent a higher dispersion of cobalt is reached throughout the support porosity, leading to better cobalt accessibility. When using water the problem of pore plugging could occur, and probably exacerbated by the relatively high loading of the metal active phase, i.e. 30 wt. %. Additional work is ongoing using TEM tomography technique to extract the location of the metal active phase versus the support porosity and also the final porosity of the catalyst.

4. Conclusion

Cobalt supported on silicon carbide catalyst prepared via an incipient wetness impregnation using ethanol as solvent exhibits an extremely high FTS activity along with a high $S_{C_{5+}}$ selectivity under severe FTS conditions, i.e. high temperature (235 °C) and high gaseous space velocity (ca. 3800 h⁻¹). The high FTS activity was linked to the large pore size of the catalyst which provides a high escape rate for the product, reducing by such a way the pore plugging by heavy liquid hydrocarbons, and facilitating high access of the reactant to the active sites located within the pore. The relatively high $S_{C_{5+}}$ selectivity could be attributed to the thermal conductivity of the support which prevents hot spot formation or gradient temperature inside the catalyst bed which could promote the formation of light products. The Co-Ru/SiC-E catalyst also exhibits an extremely high FTS stability over more than 400 hrs.

⁵⁹Co zero field NMR analysis carried out on the catalysts indicates that while the overall fcc Co to hcp Co ratio does not change significantly upon the solvent that is used, the ethanol solvent seems to promote a much larger amount of small size (< 8 nm) Co particles. These small particles have a large surface-to-volume ratio and could be responsible for the enhanced FTS activity. The NMR analysis also evidences for the first time the quantitative determination of the formation of an alloy between Co and Ru when using ethanol as the impregnation solvent. Work is on going to determine quantitatively the relative concentration of the different cobalt species present in the sample, by varying the acquisition temperature from 4 to 77 K and to correlate these values with the FTS activity.

References

- [1] A. Y. Khodakov, Z. Wei, P. Fongarland, *Chem. Rev.* 107 (2007) 1692-1744.
- [2] D. Leckel, *Ener. Fuels* 23 (2009) 2342-2358.
- [3] B. H. Davis, *Catal. Today* 71 (2002) 249-300.
- [4] H. Schulz, *Top. Catal.* 26 (2003) 73-85.
- [5] Y. Traa, *Chem. Commun.* 46 (2010) 2175-2187.
- [6] J. L. Casci, C. M. Lok, M. D. Shannon, *Catal. Today* 145 (2009) 38-44.
- [7] W. J. Wang, Y. W. Chen, *Appl. Catal.* 77 (1991) 223-233.
- [8] B. Ernst, S. Libs, P. Chaumette, A. Kiennemann, *Appl. Catal. A* 186 (1999) 145-168.
- [9] S. Storsæter, Ø. Borg, E.A. Blekkan, B. Tøtdal, A. Holmen, *Catal. Today* 1000 (2005) 343-347
- [10] J. I. Yang, J. H. Yang, H. J. Kim, H. Jung, D. H. Chun, H. T. Lee, *Fuel* 89 (2010) 237-243.
- [11] C. G. Visconti, E. Tronconi, L. Lietti, G. Groppi, P. Forzatti, C. Cristiani, R. Zennaro, S. Rossini, *Appl. Catal. A* 370 (2009) 93-101.
- [12] A. M. Hilmen, E. Bergene, A. Lindvag, D. Schanke, S. Eri, A. Holmen, *Catal. Today* 105 (2005) 357-361.
- [13] D. Schanke, E. Bergene, A. Holmen, Fischer-Tropsch synthesis, WO98-38147 A1.
- [14] C. G. Visconti, E. Tronconi, G. Groppi, L. Lietti, M. Iovane, S. Rossini, R. Zennaro, *Chemical Engineering Journal* 71 (2011) 1294-1307
- [15] S. Savin-Poncet, M. J. Ledoux, C. Pham-Huu, J. Bousquet, B. Madani, WO 2005/073345 A1 (2005).
- [16] C. Pham-Huu, B. Madani, M. Lacroix, L. Dreibine, M. J. Ledoux, S. Savin-Poncet, J. Bousquet, D. Schweich, *Int. Pat. Appl. WO* 2007/000506 A1 (2007).
- [17] Ø. Borg, N. Hammer, S. Eri, O. A. Lindvag, R. Myrstad, E. A. Blekkan, M. Ronning, E. Rytter, A. Holmen, *Catal. Today* 142 (2009) 70-77
- [18] M. Lacroix, L. Dreibine, B. de Tymowski, F. Vigneron, D. Edouard, D. Begin, P. Nguyen, Ch. Pham, S. Savin-Poncet, *Fr. Luck, M. J. Ledoux, C. Pham-Huu, Appl. Catal. A*, 397 (2011) 62-72.
- [19] S. W. Ho, Y. S. Su, *J. Catal.* 168 (1997) 51-59.
- [20] Y. Zhang, Y. Liu, G. Yang, S. Sun, N. Tsubaki, *Appl. Catal. A* 321 (2007) 79-85.
- [21] Y. Zhang, Y. Liu, G. Yang, Y. Endo, N. Tsubaki, *Catal. Today* 142 (2009) 85-89.
- [22] P. Nguyen, Ch. Pham, *Appl. Catal. A* 391 (2011) 443-454.

-
- [23] R. Pampuch, W. Ptak, S. Jonas, J. Stoch, *Mater. Sci. Mon.* 6 (1980) 435-448.
- [24] R. Moene, M. Makee, J. A. Moulijn, *Appl. Catal. A* 167 (1998) 321-330.
- [25] N. Keller, F. Di Grégorio, C. Pham-Huu, V. Keller, *Dia. Rel. Mater.* 17 (2008) 1867-1870.
- [26] R. Oukaci, A. H. Singleton, J. G. Goodwin Jr., *Appl. Catal. A* 186 (1999) 129-144
- [27] F. Diehl, A. Y. Khodakov, *Oil & Gas Sci. Technol.* 64 (2009) 11-24.
- [28] P. J. van Berge, J. van de Loosdrecht, E. Caricato, S. Barradas, *US Pat.* 6,638,889 (2004).
- [29] P. J. van Berge, J. van de Loosdrecht, J. L. Visagie, T. J. van der Walt, H. Veltman, C. Solie, *Eur. Pat.* 1.444.040 B1 (2003).
- [30] C. Meny, P. Panissod, *Modern Magnetic Resonance*. G. Webb, Ed., Springer, Heidelberg, Germany (2006).
- [31] P. Panissod, C. Meny, *Appl. Magn. Reson.* 19 (2000) 447-660.
- [32] G. Jacobs, P. M. Patterson, Y. Zhang, T. Das, J. Li, B. H. Davis, *Appl. Catal. A* 233 (2002) 215-226.
- [33] S. Storsæker, Ø. Borg, E. A. Blekkan, A. Holmen, *J. Catal.* 231 (2005) 405-419.
- [34] A. M. Saib, A. Borgna, J. van de Loosdrecht, P. J. van Berge, J. W. Niemantsverdriet, *Appl. Catal. A* 312 (2006) 12.
- [35] X. Zhu, X. Lu, X. Liu, D. Hildebrandt and D. Glasser, *Ind. Eng. Chem. Res.* 21 (2010), 10682–10688
- [36] E. Rytter, S. Eri, T. H. Skagseth, D. Schanke, E. Bergene, R. Myrstad, A. Lindvag, *Ind. Eng. Chem. Res.* 46 (2007) 9032-9036
- [37] S. Krishnamoorthy, M. Tu, M. P. Ojeda, D. Pinna, E. Iglesia, *J. Catal.* 211 (2002) 422-433
- [38] E. Iglesia, *Appl. Catal. A* 161 (1997) 59-78
- [39] A. R. de la Osa, A De Lucas, A. Romero, J. L. Valverde, P. Sanchez, *Catal. Today*, in press (2011) DOI: 10.1016/j.cattod.2010.12.010.
- [40] N. E. Tsakoumis, M. Ronning, Ø. Borg, E. Rytter, A. Holmen, *Catal. Today* 154 (2010) 162-182.
- [41] A. K. Dalai, B. H. Davis, *Appl. Catal. A* 348 (2008) 1-15.
- [42] A. K. Dalai, T. K. Das, K. V. Chaudhari, G. Jacobs, B. H. Davis, *Appl. Catal. A* 289 (2005) 135-142.
- [43] M. Claeys, E. van Steen, *Catal. Today* 71(2002) 419-427.

-
- [44] S. Krishnamoorthy, M. Tu, M. P. Ojeda, D. Pinna, E. Iglesia, *J. Catal.* 211 (2002) 422-433.
- [45] C. Li, QW. Sun, FH. Cao, WY. Ying, DY. Fang, *J. Natur. Gas Chem.* 16 (2007) 308-315.
- [46] G. Jacobs, A. Sarkar, Y. Ji, M. Luo, A. Dozier, B. H. Davis, *Ind. Eng. Chem. Res.* 47 (2008) 672-680.
- [47] B. Shi, B. H. Davis, *Catal. Today* 106 (2005) 129-131.
- [48] Ø. Borg, P. D. C. Dietzrael, A. I. Spjelkavik, E. Z. Tveten, J. C. Walmsley, S. Diplas, S. Eri, A. Holmen, E. Rytter, *J. Catal.* 259 (2008) 161-164.
- [49] C. Aaserud, A. M. Hilmen, E. Bergene, S. Eri, D. Schanke, A. Holmen, *Catal. Lett.* 94 (2004) 171-176.
- [50] A. M. Saib, M. Claeys, E. van Steen, *Catal. Today* 71 (2002) 395-402
- [51] E. van Steen, M. Claeys, *Chem. Eng. Technol.* 31 (2008) 655-666
- [52] S. Rane, Ø. Borg, J. Yang, E. Rytter, A. Holmen, *Appl. Catal. A* 388(2010) 160-167.
- [53] I. T. Ghampson, C. Newman, L. Kong, E. Pier, K. D. Hurley, R. A. Pollock, B. R. Walsh, B. Goundie, J. Wright, M. C. Wheeler, R. W. Meulenberg, W. J. DeSisto, B. G. Frederick, R. N. Austin, *Appl. Catal. A* 388 (2010) 57-67.
- [54] I. Florea, M. Houllé, O. Ersen, L. Roiban, A. Deneuve, I. Janowska, P. Nguyen, C. Pham and C. Pham-Huu, *J. Phys. Chem. C*, 113 (2009) 17711–17719
- [55] H. Karaca, J. Hong, P. Fongarland, P. Roussel, A. Griboval-Constant, M. Lacroix, K. Hortmann, O. V. Safonova, A. Y. Khodakov, *Chem. Commun.* 46 (2010) 788-790.
- [56] O. Ducreux, B. Rebours, J. Lynch, M. Roy-Auberger, D. Bazin, *Oil & Gas Sci. Technol.* 64 (2009) 49-62.
- [57] J. P. Wójcik, J. P. Jay, E. Jedryka, P. Panissod, J. Dekoster, G. Langouche, *Z. Phys. B* 103 (1997) 5-12.
- [58] R. Srinivasan, R. J. De Angelis, P. J. Reucroft, A. G. Dhere, J. Bentley, *J. Catal.* 116 (1989) 144-163.
- [59] G. L. Bezemer, P. B. Radstake, V. Koot, A. J. van Dillen, J. W. Geus, K. P. de Jong, *J. Catal.* 237 (2006) 291-302.
- [60] S. Kala, B. R. Mehta, *J. Alloy Compd.* 431 (2007) 10-15.
- [61] M. Sadeqzadeh, H. Karaca, O. V. Safonova, P. Fongarland, S. Chambrey, P. Roussel, A. Griboval-Constant, M. Lacroix, D. Curulla-Ferré, F. Luck, A. Y. Khodakov, *Catal. Today*, 164 (2011) 62-67.

- [62] D. Enache, B. Rebours, M. Roy-Auberger, R. Revel, *J. Catal.* 205 (2002) 346-353.
- [63] C. Meny, E. Jedryka, P. Panissod, *J. Phys.: Cond. Matt.* 5 (1993) 1547-1556.
- [64] M. Malinowska, C. Mény, E. Jedryka, P. Panissod, *J. Phys.: Cond. Matt.* 10 (1998) 4919-4928.
- [65] I. Florea, O. Ersen, Ch. Hirlimann, L. Roiban, A. Deneuve, M. Houllé, I. Janowska, P. Nguyen, Ch. Pham, C. Pham-Huu, *Nanoscale* 2 (2010) 2668-2678.

CHAPTER IV

FISCHER–TROPSCH SYNTHESIS WITH IMPROVED ACTIVE–SITE AVAILABILITY ON A LARGE PORE SILICON CARBIDE MICROSPHERES CONTAINING COBALT CATALYST

**Benoit de Tymowski, Yuefeng Liu, Patrick Nguyen, Charlotte Pham, Francis Luck,
Cuong Pham-Huu**

Abstract

The influence of the support pore size on the Fischer-Tropsch synthesis (FTS) performance was investigated on the silicon carbide (SiC) containing cobalt catalyst with different loading, i.e. 10 and 30 wt. %. At low cobalt loading the pore size distribution hardly influence the overall FTS activity and selectivity. On the other hand, the large pore size support exhibits a significant positive influence at high cobalt loading. Such results could be attributed to the fact that at low cobalt loading the pore accessibility, regardless the pore size, is similar whereas at high cobalt loading, catalyst with small pore is more sensitive to the problem of pore plugging leading to a low accessibility of the metal active phase. In the catalyst with a large pore size the problem linked with the pore plugging is less critical and thus, a large part of the cobalt active phase was still accessible to the reactants and thus, leads to a higher FTS performance. The selectivity towards liquid hydrocarbons remains similar on both catalysts which could be attributed to the presence of meso- and macropores in the SiC support and also to the thermal conductivity of the support which could prevent local hot spot formation, especially at high carbon monoxide conversion.

1. Introduction

Diminishing petroleum reserves and oil price increase necessitate the development of synthetic fuel route based on other fossil resources such as natural gas and charcoal. Synthesis gas mixture ($n\text{H}_2 + \text{CO}$) generated by reforming of natural gas will have a leading role in the generating of such synthetic fuel via the Fischer-Tropsch synthesis [1, 2]. Fischer-Tropsch synthesis (FTS) which allows the conversion of synthesis gas, a mixture of H_2 and CO , into valuable liquid hydrocarbons has received an over increasing scientific and industrial interest since the last decade [3, 4]. The FTS is nowadays in close competition with different technologies dealing with the transportation of gas to the market over a long distance: high pressure pipelines, liquefaction of natural gas (LNG), and wire transportation (Gas-To-Wire). However, one should distinguish the final market of each technology: LNG and wire transportation mostly end-up with traditional power generation, industries and domestic heating while the final market of the GTL is mostly concerning the transportation domain and more especially, to provide kerosene for aviation transportation. On the other hand, the FTS process also allows the reduction of natural gas flaring which is environmental prohibited due to the formation of CO_2 which is a green house gas. In addition, the synthetic fuels derived from the FTS process are sulphur-free which could be further blended with others to meet the forwards environmental requirements about the sulphur content in the diesel fuel and also for aviation fuel needs [5]. The two most frequently employed active phase for the FTS process are iron and cobalt, generally promoted with a foreign element [4, 6]. Cobalt supported catalysts are the most preferred, despite the difference price between Fe and Co, 1 and 1000, respectively, because of their high FTS activity and selectivity for linear hydrocarbons and low activity for water-gas shift reaction (WGS). The cobalt phase is deposited on the support which allows the dispersion of the final metallic phase in order to increase the reactant-to-active phase surface and also to prevent excessive sintering of the active phase during reaction. The popular supports include Al_2O_3 , SiO_2 and to a less extent, TiO_2 [4,7].

FTS reaction is an exothermic reaction with a $\Delta H = -165 \text{ kJ/mol}$ and thus, the catalyst surface temperature control during the operation is a crucial factor since local high temperatures could lead to excessive methane yields along with catalyst body disintegration due to carbon formation [8]. Despite a great effort of research, liquid hydrocarbons selectivity in the current FTS reaction on oxide supported catalysts is still severely limited, especially at high conversion per pass. Indeed, both alumina and silica supports have poor thermal

conductivity and thus, at high CO conversion a local hot spot formation could occur leading to a catalyst surface temperature runaway on area close to the reactive site, which lower the liquid hydrocarbons selectivity and increase the methane formation. It is of interest to find support with better thermal conductivity in order to reduce as much as possible the problem of hot spot formation and to enhance the selectivity towards liquid hydrocarbons without losing the FTS performance. The support should also possess an adequate porosity, i.e. meso- and macro-pores, in order to reduce as much as possible the problem of liquid plugging which conducts to the CO concentration enrichment next to the active site leading to the production of light molecules, i.e. CH₄ and C₂-C₄. The chemical inertness of the support is also another factor that should be taken into account regarding the possibility of the support and the active phase recovery which represents interesting perspectives for environmental concerns and cost investment of the process taken into account a high amount of catalyst employed in the FTS units.

Silicon carbide (SiC) exhibits a relatively high thermal conductivity, a high resistance towards oxidation, a high mechanical strength, a low specific weight, and chemical inertness which render it interesting for use as catalyst support material, especially in the exothermic reactions. However, to be useful as a catalyst support, SiC must be prepared with a sufficiently high specific surface area, i.e. $\geq 200 \text{ m}^2 \cdot \text{g}^{-1}$ in order to ensure the dispersion of the metal active phase for subsequent catalytic reaction. A simple synthesis method based on a gas-solid reaction [9, 10] has been developed in the laboratory at the beginning of 80's to make silicon carbide (β -SiC) with medium specific surface area for use as catalyst support in the heterogeneous catalysis field [11, 12, 13]. The high thermal conductivity of the SiC allows the significant improvement in the selectivity in several exothermic reactions, i.e. *n*-butane and H₂S partial oxidation, where traditional alumina or silica supports reach their limit [14, 15]. Here we report on the use of a high thermal conductive and medium surface area β -SiC with different pore size aperture as a catalyst support for Co-based FTS catalyst with a high improvement on the FT activity along with a high selectivity towards liquid hydrocarbons [16, 17]. The catalysts also exhibit a high resistance towards deactivation during the long-term test.

2. Experimental section

2.1 SiC support characteristics

The SiC support have been supplied by SICAT. The detailed synthesis of the SiC is summarized in a recent review [18]. Pore size can be tuned by changing the physical properties of precursor materials (particle size, specific surface area) or by the use of additives or pore formers. The synthesis method also allows the preparation of the silicon carbide with different shape depending to the downstream application.

2.2 Co/SiC catalysts

The cobalt phase was deposited onto the supports via an incipient wetness impregnation method using an aqueous solution containing cobalt nitrate (Acros). After impregnation the solid was allowed to dry at room temperature for 2 h and then oven-dried at 110°C for 2 h. The solid was calcined at 350°C for 2 h in order to decompose the nitrate into its corresponding oxide. The oxide form was further reduced in flowing hydrogen (30 mL·g_{cat}⁻¹·min⁻¹) at 300 °C for 6 h. The catalyst was passivated under a stream containing O₂-1 vol. % diluted in argon at room temperature before unloading.

2.3 Characterization techniques

The nature and crystallinity of the cobalt phase, after calcination and after reduction, were characterized by means of the powder X-ray diffraction (XRD) technique. The analysis was carried out on a Bruker D-8 Advance diffractometer with a Cu K α radiation equipped with a Vantec detector. The sample was crushed into powder and deposited on a glass plate for analysis. ASTM powder diffraction files were used to identify the phase present in the sample. Crystallite sizes were calculated from line broadening using the Scherrer equation.

The microstructure of the support was examined by transmission electron microscopy (TEM) on a JEOL 2100F microscope working with an accelerated voltage of 200 kV and a point-to-point resolution of 0.17 nm. The sample was dispersed by ultrasounds in an ethanol solution during 5 minutes and a drop of the solution was deposited onto the copper grid covered with holey carbon membrane for observation.

The pore size distribution was carried out by mercury intrusion using Micromeritics Autopore III by assuming an Hg contact angle of 130° and a surface tension of 0.485 N/mm. Before analysis, the sample was outgassed under 6.67 Pa for 2 min.

The specific surface area of the support and the catalyst, after reduction, were determined in a Micromeritics sorptometer. The sample was outgassed at 250 °C under vacuum for 6 hrs in order to desorb moisture and adsorbed species on its surface. The measurements were carried out using N₂ as adsorbent at liquid N₂ temperature.

The morphology of the solid was examined by scanning electron microscopy (SEM) on a JEOL 6700-FEG microscope. The solid was fixed on the sample holder by a graphite paste for examination. Before analysis the sample was covered by a thin layer of gold in order to avoid charging effect. The SEM analysis allows one to get access to the morphology of the cobalt aggregate after reduction in order to correlate with the metal particle size determined by the XRD line broadening.

Temperature-Programmed Reduction (TPR) was carried out in a Micromeritics ASAP-2100 setup under diluted hydrogen flow (10 vol. % in helium) with a heating rate of 15 °C·min⁻¹. The hydrogen consumption was continuously monitored with a thermal conductivity detector (TCD). The steam formed during the reduction was trapped at -88 °C.

2.4 Fischer-Tropsch synthesis

The Fischer-Tropsch synthesis reaction was carried out in a tubular fixed-bed stainless steel reactor (*i.d.* = 6 mm) with circulating silicon oil as heating source. The reduced catalyst (5 g of catalyst, in a grain form average size between 150 to 400 μm) was deposited between quartz wool plugs in the middle of the reactor. The reactor pressure was slowly increased from 0.1 to 4 MPa (ramping rate of 1 MPa·h⁻¹) under argon. At 4 MPa the reactor temperature was raised from room temperature to the desired reaction temperature, 215°C (heating rate of 2°C·min⁻¹). Then, the argon flow was replaced by a 50:50 v:v mixture of syngas and argon (CO:H₂ = 1:2). The catalyst was activated under a syngas-argon mixture with different syngas concentrations during three days before evaluated under pure syngas condition. The catalyst bed temperature was monitored with a thermocouple (Ø 0.3 mm) inserted inside a stainless steel finger (Ø 1 mm) passing through the catalyst bed. The products were condensed in two high pressure traps maintained at 85°C and 15°C, respectively. The exit gas was analyzed on-line, both by Thermal Conductivity Detector (TCD) and Flame Ionization Detector (FID), with a gas chromatography (GC Varian 3800 equipped with a Carbobond capillary column).

The liquid phase and water were condensed in the traps and were analyzed off-line at the end of the test. A known amount (100 mg) of the organic phase, liquid hydrocarbons and waxy products, was dissolved in 3 ml of dichloro-methane under sonication during 30 minutes. Then 20 ml of CS₂ were further added to the solution in order to ensure the complete

dissolution of the organic phase. For analysis 1 μL of the solution was injected in a GC apparatus equipped with a Simdist column operated at 400 $^{\circ}\text{C}$ and allows the detection of hydrocarbons from C_9 to C_{70} .

3. Results and discussion

3.1 Support characteristics

The XRD pattern indicates that all the silicon was reacted during the synthesis process as no diffraction lines corresponding to silicon phase were observed. Representative TEM micrographs with different magnifications indicate that the SiC material is covered by a thin amorphous layer which is constituted by a mixture of SiO_2 and SiO_xC_y (Figure 1A and B). Such oxygen contained surface is expected to play a role of anchoring site for the deposition of the cobalt salt onto the SiC surface.

The porosity of the different SiC support, measured by means of the mercury intrusion, is presented in Figure 1C. The pore size distribution of the SiC is mostly constituted by a meso- and macropores with a pore size diameter ranged between 0.01 and 10 μm . The pore size diameter of the high porosity support was more important in a range of pore size between 0.1 to 10 μm . The specific surface area measured by means of the N_2 adsorption is respectively 30 $\text{m}^2 \cdot \text{g}^{-1}$ and 40 $\text{m}^2 \cdot \text{g}^{-1}$.

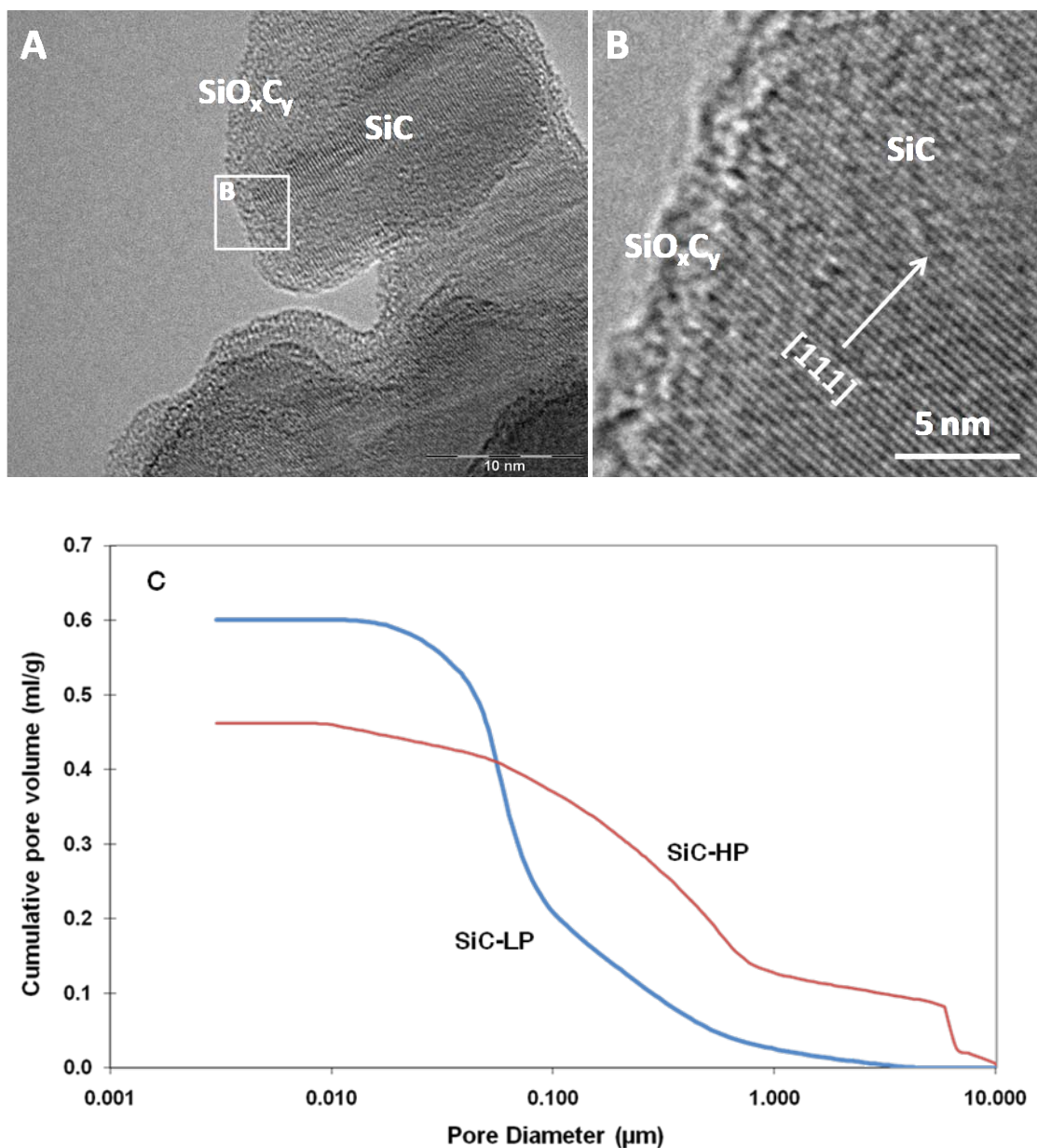


Figure 1. (A, B) Representative TEM micrographs of the SiC material showing the presence of SiC and a thin amorphous layer of SiO₂ and SiO_xC_y (noted SiO_xC_y in the image). (C) Pore size distribution of the different SiC microspheres by mercury intrusion: mesoporous (SiC-LP) and high porous (SiC-HP).

3.2 Co/SiC catalyst characteristics

In this study, SiC-based catalysts with different cobalt loading, i.e. 10 and 30 wt.%, were prepared and tested in the FTS reaction in order to evaluate the influence of the support pore size as a function of the cobalt loading on the FTS performance. The aim is to prepare a

catalyst with an activity per pass as high as possible for subsequent industrial development. The crystallinity of the cobalt phase on the high porosity support was characterized by XRD and the results are presented in Figure 2. Only diffraction lines corresponding to the Co and SiC are observed which indicate the complete reduction of the active phase. Indeed, on the traditional supports such as alumina and silica the strong interaction between the metal oxide and the support generally leads to the formation of a hardly reducible phase [19,20,21]. The relatively low interaction between the thin $\text{SiO}_x\text{C}_y/\text{SiO}_2$ passivated layer on the SiC surface favours the complete reduction of the metal oxide precursor with the formation of a slightly larger metal particles. The XRD pattern of the low porosity catalyst shows also a similar reducibility (not shown).

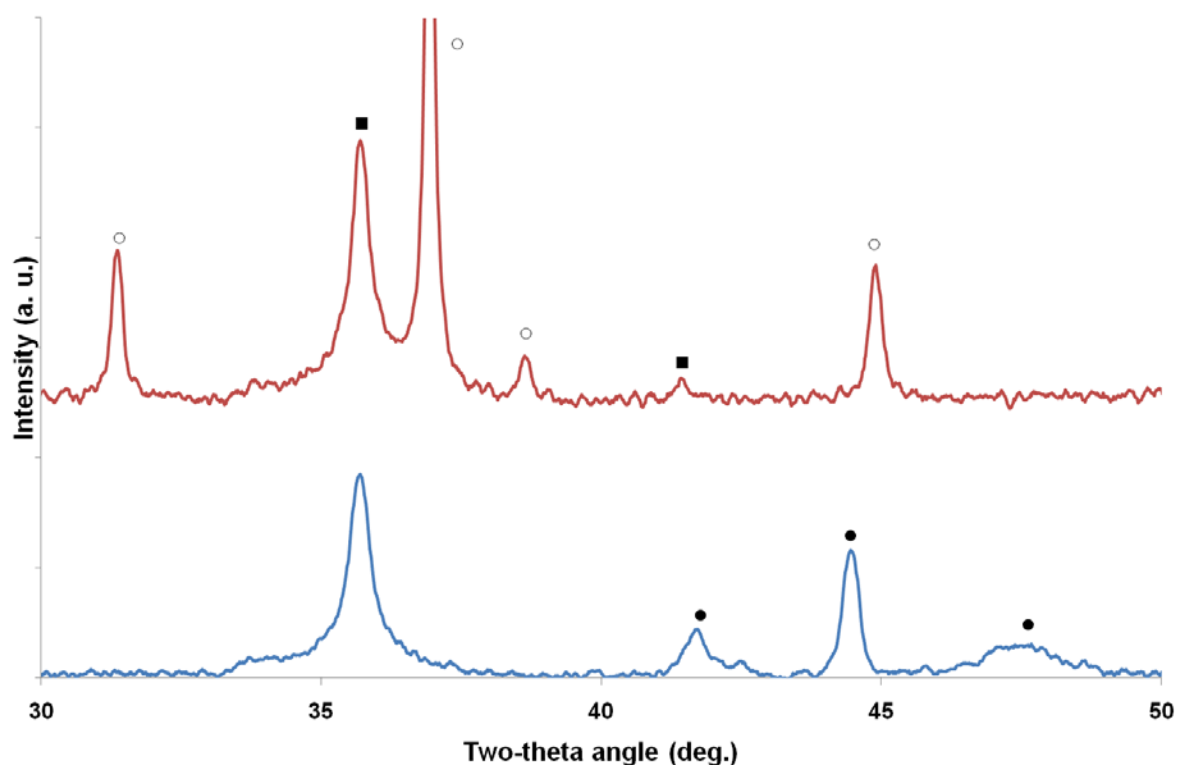


Figure 2. XRD patterns of the 30Co/SiC-HP before and after reduction under H_2 flow at 300 °C for 6 h confirming the complete reduction of the cobalt oxide phase. (■) SiC, (○) Co_3O_4 , (●) Co^0 .

The representative SEM micrographs of the Co/SiC-HP are presented in Figure 3 with different magnifications. The cobalt particles seem to be relatively well dispersed on the support surface and within the support porosity. The SEM analysis indicates that the cobalt phase is present as agglomerates constituted by several cobalt particles with an average

particle size ranged between 30 and 80 nm. Such cobalt dispersion is in good agreement with the low metal-support interaction between the deposited active phase and the ceramic support as explained above.

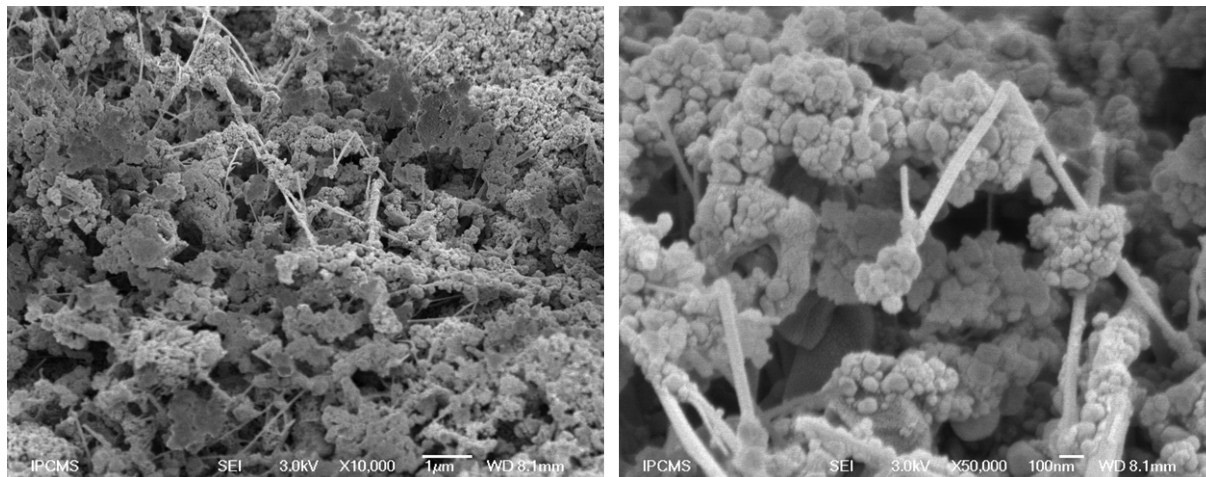


Figure 3. Representative SEM micrographs of the 30Co/SiC-HP after reduction under hydrogen at 300 °C showing the homogeneous size of the cobalt particles.

In the case of low cobalt loading the specific surface area of the catalysts only slightly decreased compared to that of the pristine support. When the cobalt loading was increased from 10 to 30 wt. % the effect of pore size to maintain the final catalyst surface area is more pronounced as shown in Table 1. According to the results one can state that for the high porosity support the pore plugging seems to be much less significant while for the support with low porosity the specific surface area loss is more pronounced due to extensive pore plugging. Indeed, it is expected that in the case of the catalyst with low porosity the high metal loading leads to the pore aperture plugging which render inaccessible the metal particles localized deep inside the pore.

Table 1 BET surface area and pore volume of the various porosity SiC carriers and the same after cobalt deposition. The corresponding cobalt particle size, before and after reduction, under H₂ at 300 °C for 6 h, determined by the Scherrer formula is also presented.

Sample	Surface area (m ² /g)	Total pore volume (cm ³ /g)	BJH pore diameter (nm)
SiC-LP	29.0	0.11	16.4
SiC-HP	40.4	0.12	12.8
10Co/SiC-LP	25.4	0.10	17.2
10Co/SiC-HP	32.7	0.14	17.1
30Co/SiC-LP	21.3	0.08	16.7
30Co/SiC-HP	32.0	0.09	12.1

Temperature-programmed reduction (TPR) was also carried out to analyze the reduction behaviour of the cobalt oxide phase supported on different types of SiC, i.e. foam, extrudates and grains with large pores (Figure 4). The reduction of the cobalt oxide supported on the SiC-based catalyst is achieved at relatively low temperature, i.e. 380°C which indicates the low metal-support interaction and the absence of the formation of a hardly reducible cobalt-phase as usually observed in the case of alumina-based catalyst [22, 23]. The reduction profile seems to be independent of the support pore size according to the TPR results.

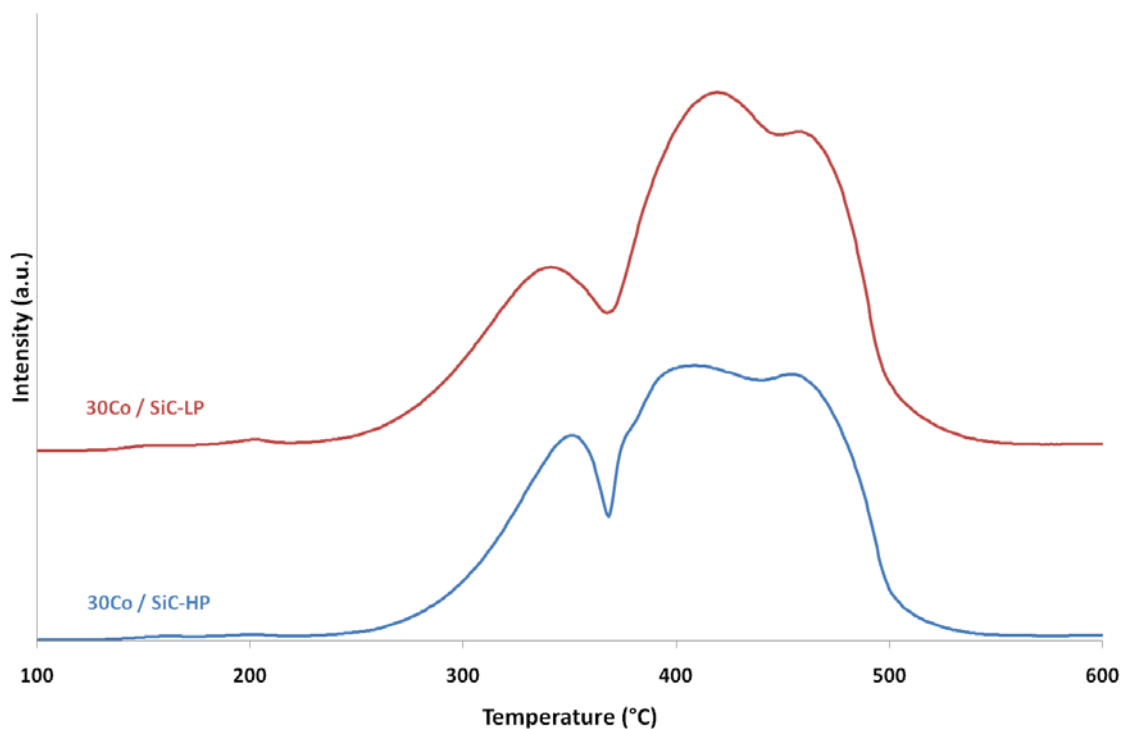


Figure 4. TPR spectra of the cobalt-based catalyst deposited on SiC supports with different porosities. TPR conditions: catalyst weight: 100 mg, reduction mixture: H₂-10 vol. % in helium, ramping rate: 15 °C·min⁻¹.

3.3 Fischer-Tropsch synthesis (FTS)

The FTS results, conversion and C₅₊ selectivity, obtained on the Co/SiC catalysts with different pore size distribution are presented in Figure 5. The FTS activity change during the first five hours on stream is due to the dead volume of the setup and not to a deactivation. The FTS activity remains stable for the duration of the test, i.e. 100 h, indicating that no apparent deactivation linked with the active phase particle size sintering or oxidation were occurred under the reaction conditions.

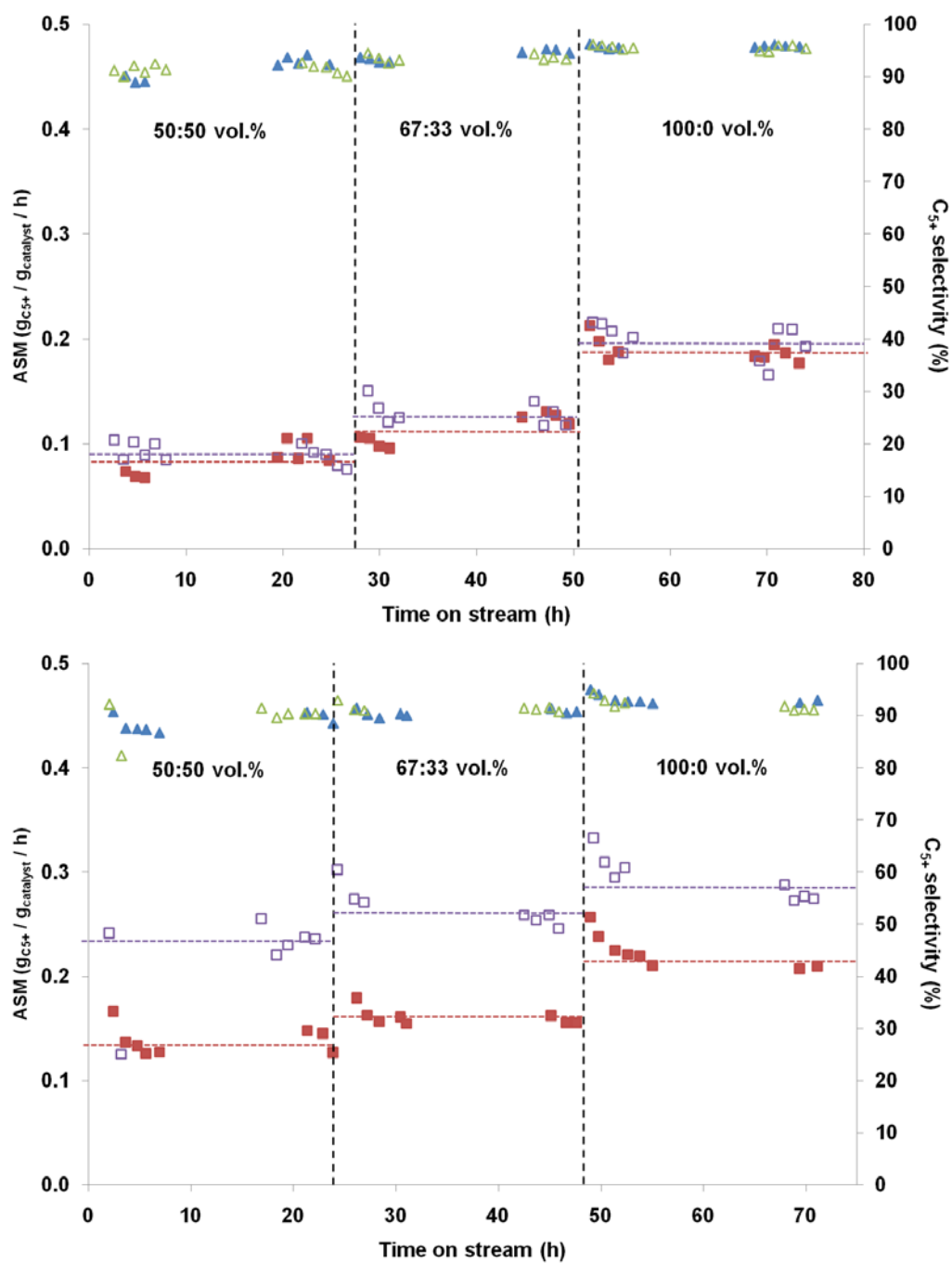


Figure 5. FTS performance on the different cobalt-based SiC catalysts with cobalt loading of (A) 10 wt.% and (B) 30 wt.% as a function of the $H_2:CO$ concentrations. (■) ASM of SiC-LP supported catalyst, (□) ASM of SiC-HP supported catalyst, (▲) C_{5+} selectivity of SiC-LP supported catalyst, (△) C_{5+} selectivity of SiC-HP supported catalyst.

At low cobalt loading, i.e. 10 wt. %, the FT activity is almost similar regardless the porosity while at high cobalt loading, i.e. 30 wt. %, a significant FT activity increases was observed (Table 2). It is expected that for low cobalt loading the pore aperture of the support

was high enough to avoid plugging by the cobalt particle size localized at the pore entrance and thus, a large part of the active phase remains accessible to the reactant regardless the pore size diameter (Scheme 1A). At high cobalt loading, i.e. 30 wt. %, it is expected that part of the pore aperture of the low porosity support was blocked by the cobalt particles and thus a large fraction of the deposited cobalt was not accessible leading to a low improvement of the FT activity (Scheme 1B). In the case of a large pore support the pore plugging is less dramatic and thus, a substantial part of the cobalt particle remains accessible leading to a higher FT activity improvement under similar reaction conditions compared to that was obtained on the low porosity catalyst (Scheme 1B). FTS performance enhancement has been reported in the literature by replacing the powdered catalyst by a wash-coated metallic structured support with a more open porosity [24, 25, 26, 27].



Schematic illustrations highlighting the pore size accessibility as a function of the cobalt loading on the two types of SiC carriers. (A) Low cobalt loading (10 wt. %) and (B) High cobalt loading (30 wt. %).

The C_{5+} selectivity is relatively high, i.e. $> 90\%$, on both catalysts which indicate that the dimension of the pores has a little effect on the overall selectivity of the reaction. Such effect could be explained by the fact that even the small pore size of the SiC support is large

enough for allowing the easy access of the gaseous reactants and escaping of the product and thus, inhibits the problem of CO shortage at the catalytic sites which contribute to the decrease of the selectivity to long-chain hydrocarbons. The high C₅₊ selectivity could also be attributed to the thermal conductivity of the SiC support which prevents local hot spot formation leading to secondary reactions yielding lower hydrocarbons, i.e. C₁-C₄. The hot spot formation is more pronounced when the CO conversion was high. It is worth noting that SiC is usually employed as heat disperser for the FTS catalysts supported on an insulator supports such as Al₂O₃ or SiO₂ [28, 29].

The detailed selectivity of the different products formed is presented in Table 2. According to the results the modification of the support porosity has no direct effect on the product distribution which confirms that the nature of the active phase and its interaction with the support are remain unchanged and only the overall FTS activity is modified as a function of the support porosity due to the higher active sites accessibility when using a large pore SiC support.

Table 2. Product distribution at the steady-state on the Co/SiC-LP and Co/SiC-HP catalysts. Reaction conditions: Co loading = 10-30 wt.%, H₂:CO = 2, temperature = 215°C, total pressure = 40 atm., GHSV = 1900 h⁻¹.

Catalyst	CH ₄ (%)	CO ₂ (%)	C ₂ -C ₄ (%)	C ₅₊ (%)	ASM
10 Co/SiC-LP	2.5	0	1.8	95.7	0.14
10 Co/SiC-HP	2.9	0	1.6	95.5	0.15
30 Co/SiC-LP	4.2	0.09	3.1	92.6	0.17
30 Co/SiC-HP	5.1	0.05	3.55	91.3	0.20

The influence of the reaction temperature was also investigated on the large pore high cobalt loading catalyst keeping the other reaction conditions similar. The FTS activity on the Co/SiC-HP is significantly improved by increasing the reaction temperature from 215 °C to 220 °C and finally, 225 °C, without a significant change of the C₅₊ selectivity (Table 3 and Figure 6). It is worth noting that the FT activity remains stable within the reaction duration indicating that almost no appreciable deactivation due to the particle size sintering was

occurred on the catalyst. Such results have already been reported in our previous articles [30, 31] and also in those of De la Osa et al. [32, 33, 34].

Table 3. Product distribution at the steady-state on the Co/SiC-HP catalysts as a function of the reaction temperature. Reaction conditions: Co loading = 30 wt. %, H₂:CO = 2, temperature = 215°C, total pressure = 40 atm., GHSV = 1900 h⁻¹.

Temperature	CH ₄ (%)	CO ₂ (%)	C ₂ -C ₄ (%)	C ₅₊ (%)	STY (h ⁻¹)	ASM
215°C	5.4	0.06	3.4	91.2	3.0	0.20
220°C	5.9	0.1	4.2	89.8	4.0	0.26
225°C	6.7	0.16	4.4	88.8	4.9	0.31

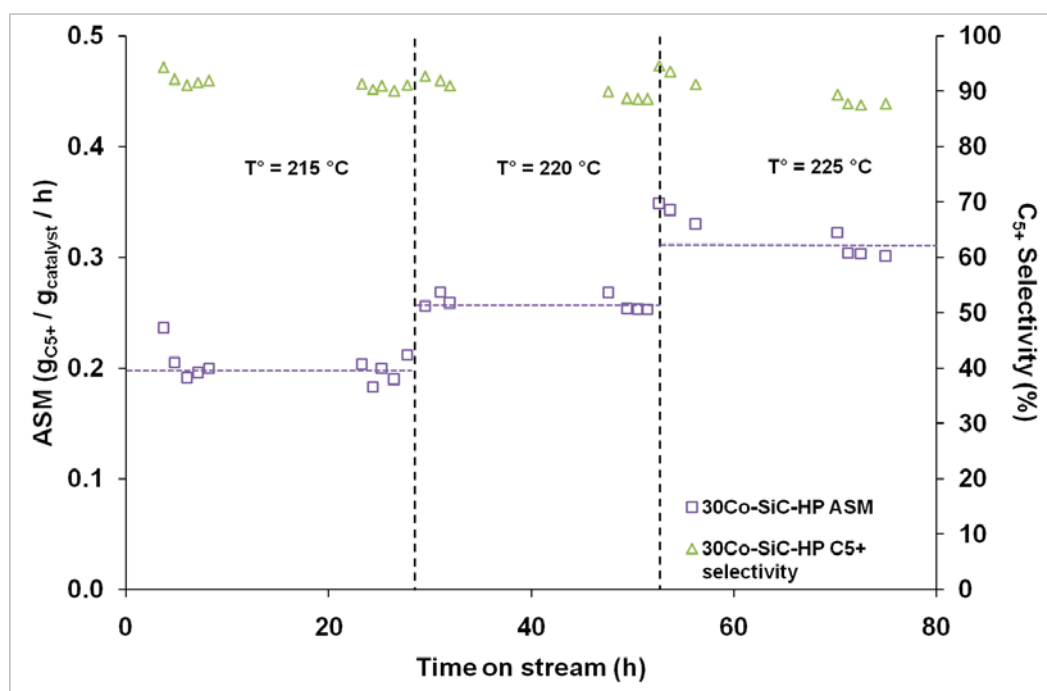


Figure 6. FTS performances on the 30Co/SiC-HP as a function of the reaction temperature. Reaction conditions: catalyst weight = 5 g, Co weight = 1.5 g, H₂/CO = 2, total pressure = 4 MPa, space velocity = 1900 h⁻¹.

4. Conclusion

Fischer-Tropsch synthesis with high activity and C₅₊ selectivity can be achieved on a Co-based catalyst supported on SiC carriers. An effect of the pore size diameter has been

observed on a silicon carbide support with a highly loaded cobalt catalyst. At low cobalt loading the FTS activity was hardly change regardless the support pore size diameter whereas at high cobalt loading there is a significant improvement in the FTS activity for the large pore carrier. It is expected that the high porosity of the support significantly limits the problem of pore plugging at high metal loading and thus allows a better accessibility of the cobalt phase localized within the pore which yield a high FTS activity. The FTS activity obtained on the high porosity cobalt-based catalyst at high space velocity and high reaction temperature was in the upper range of the most active FTS catalysts, without noble metal doping, reported nowadays in the literature. The catalyst also exhibits an high stability as a function of time on stream which indicates that deactivation, either to the active phase sintering or carbonaceous residue, was slow on such catalyst. Work is on going to evaluate the combination effect of the high porosity and the doping on the cobalt dispersion and accessibility and will be presented soon. The liquid hydrocarbon selectivity is high, i.e. 90 %, on both catalysts regardless the support pore size diameter. Such high liquid hydrocarbon selectivity was attributed to the presence of meso- and macropores and also to the thermal conductivity of the supports which significantly reduce the enrichment of the CO and the hot spot formation on/or next to the active site.

References

- [1] J. R. Rostrup-Nielsen, *Science* 308 (2005) 1421- 1422.
- [2] G. M. Whitesides, G. W. Crabtree, *Science* 315 (2007) 796- 798.
- [3] C. Perego, R. Bortolo, R. Zennaro, *Catal. Today* 42 (2009) 9-16.
- [4] A. Khodakov, W. Chu, P. Fongarland, *Chem. Rev.* 107 (2007) 1692-1744.
- [5] Low sulfur fuel has been tested extensively by the US Department of Energy (DoE) and most recently, by the US Air Force. On December 15, 2006, a B-52H flight demonstration with a blend of FT fuel has been achieved with success. The B-52H demonstration flight with FT fuel was followed on October 22, 2007 by a C-17 Globemaster fuelled with FT fuel blend.
- [6] M. E. Dry, *Catal. Today* 71 (2002) 227-241.
- [7] R. Oukaci, A. H. Singleton, J. G. Goodwin Jr. *Appl. Catal. A* 281 (1999) 129-144.
- [8] C.M. Chun, J.D. Mumford, T.A. Ramanarayanan, *Journal of the Electrochemical Society* 150 (2003) B76-B82.
- [9] M. J. Ledoux, S. Hantzer, C. Pham-Huu, J. L. Guille, M. P. Desaneaux, *J. Catal.* 114 (1998) 176-185.
- [10] M. J. Ledoux, C. Pham-Huu, J. L. Guille, H. M. Dunlop, S. Hantzer, S. Marin, M. Weibel, *Catal. Today* 15 (1992) 263-24.
- [11] P. Leroi, B. Madani, C. Pham-Huu, M.-J. Ledoux, S. Savin-Poncet, J.L. Bousquet, *Catalysis Today* 91-92 (2004) 53-58.
- [12] L. Pesant, J. Matta, F. Garin, M.-J. Ledoux, P. Bernhardt, C. Pham, C. Pham-Huu, *Applied Catalysis A: General* 266 (2004) 21-27.
- [13] P. Nguyen, J.-M. Nhut, D. Edouard, C. Pham, M.-J. Ledoux, C. Pham-Huu, *Catalysis Today* 141 (2009) 397-402.
- [14] M. J. Ledoux, C. Crouzet, C. Pham-Huu, V. Turines, K. D. Kourtakis, P. L. Mills, J. J. Lerou, *J. Catal.* 203 (2001) 495- 508.

-
- [15] M. J. Ledoux, C. Pham-Huu, N. Keller, S. Savin-Poncet, J. B. Nougayrède, J. Bousquet, W. Boll, R. Morgenroth, *Catalysis Today* 61 (2000) 157-163.
- [16] C. Pham-Huu, B. Madani, M. Lacroix, L. Dreibine, M. J. Ledoux, S. Savin-Poncet, J. Bousquet, D. Schweich, *Int. Pat. Appl. WO 2007/000506 A1*, assigned to Total SA (2007).
- [17] S. Savin-Poncet, M. J. Ledoux, C. Pham-Huu, J. Bousquet, B. Madani, *Int. Pat. Appl. WO 2005/073345 A1*, assigned to Total France and Total SA (2005).
- [18] P. Nguyen, Ch. Pham, *Appl. Catal. A* 391 (2011) 443-454.
- [19] S. Storsæter, Ø. Borg, E.A. Blekkan, A. Holmen. *Journal of Catalysis* 231 (2005) 405-419
- [20] W. Chu, P. A. Chernavskii, L. Gengembre, G. A. Pankina, P. Fongarland, A. Y. Khodakov. *Journal of Catalysis* 252 (2007) 215-230.
- [21] R. Xie, D. Li, B. Hou, J. Wang, L. Jia, Y. Sun. *Catalysis Communications* 12 (2011) 380-383.
- [22] A.M. Hilmen, D. Schanke, A. Holmen, *Catalysis Letters* 38 (1996) 143-147
- [23] G. Jacobs, J.A. Chaney, P.M. Patterson, T.K. Das, B.H. Davis, *Applied Catalysis A: General* 264 (2004) 203-212.
- [24] C. G. Visconti, E. Tronconi, L. Lietti, G. Groppi, P. Forzatti, C. Cristiani, R. Zennaro, S. Rossini, *Appl. Catal. A* 370 (2009) 93-101.
- [25] A. M. Hilmen, E. Bergene, A. Lindvag, D. Schanke, S. Eri, A. Holmen, *Catal. Today* 105 (2005) 357-361.
- [26] F. Kapteijn, R. M. de Deugd, J. A. Moulijn, *Catal. Today* 105 (2005) 350-356.
- [27] B. H. Davis, *Top. Catal.* 32 (2005) 143-168.
- [28] G. Prieto, A. Martínez, P. Concepción, R. Moreno-Tost, *Journal of Catalysis* 266 (2009) 129-144.
- [29] J.P. den Breejen, J.R.A. Sietsma, H. Friedrich, J.H. Bitter, K.P. de Jong, *Journal of Catalysis* 270 (2010) 146-152.

[30] M. Lacroix, L. Dreibine, B. de Tymowski, F. Vigneron, D. Edouard, D. Bégin, P. Nguyen, C. Pham, S. Savin-Poncet, F. Luck, M. J. Ledoux, C. Pham-Huu, *Appl. Catal. A : Gen.* 397(2011) 62-72.

[31] B. de Tymowski, Y. Liu, C. Meny, C. Lefèvre, D. Begin, P. Nguyen, C. Pham, D. Edouard, F. Luck, C. Pham-Huu, *Appl. Catal. A: Gen.* 419-420 (2012) 31-40.

[32] A.R. de la Osa, A. De Lucas, A. Romero, J.L. Valverde, P. Sánchez, *Catal. Today* 176 (2011) 298- 302.

[33] A. R. De la Osa, A. De Lucas, A. Romero, J. L. Valverde, P. Sanchez, *Fuel* 90 (2011) 1935-1945.

[34] A. R. De la Osa, A. De Lucas, J. Diaz-Maroto, A. Romero, J. L. Valverde, P. Sanchez, *Catal. Today* 187 (2012) 173-182.

CHAPTER V

TITANIA-DOPED SILICON CARBIDE CONTAINING COBALT CATALYST FOR THE FISCHER-TROPSCH SYNTHESIS

**Yuefeng Liu, Benoit de Tymowski, Fabrice Vigneron, Ileana Florea, Ovidiu Ersen,
Patrick Nguyen, Charlotte Pham, Francis Luck, Cuong Pham-Huu**

Graphical abstract

Abstract

Keywords:

Silicon carbide – Cobalt – Titanium oxide - Fischer-Tropsch synthesis –EFTEM– Catalysis

1. Introduction

The Fischer-Tropsch synthesis (FTS) is a key technology in the more global Gas-To-Liquids (GTL) process which allows the transformation of synthesis gas ($2\text{H}_2 + \text{CO}$), issued from natural gas reforming into liquid hydrocarbons, followed by hydrocracking of the heavy fraction into useful compounds such as naphtha, diesel, lubricants and others [1,2,3,4,5]. The most employed active phase for the low-temperature FTS process is supported cobalt, either pure or doped with trace amounts of noble metal in order to enhance the reduction of the active phase and to improve the metal particles dispersion [6,7,8]. Cobalt presents several advantages such as: high stability, high activity for liquid hydrocarbons formation and low selectivity towards oxygenated products, resistance towards oxidation, low water-gas shift (WGS) tendency and acceptable price for industrial development. However, the high activity of the cobalt phase also leads to an extremely high sensitivity of the catalyst selectivity to the reaction temperature. Cobalt active phase is typically employed in a supported form for the FTS process. The support should display a relatively high specific surface area in order to achieve a high dispersion of the metal particles, good mechanical and hydrothermal resistance and a medium level of metal-support interaction in order to allow a complete reduction of the active phase and to prevent sintering of the later. The most employed supports for the FTS are alumina, silica, titania and carbon-based materials such as activated carbon, carbon nanotubes and nanofibers [9,10,11,12,13,14]. Among these supports, alumina is the most employed. However, on traditional supports such as alumina and silica, small particles of metal oxide precursor are difficult to be reduced due to the presence of high metal-support interactions which prevent the complete reduction at moderate temperatures [15,16,17]. In addition, the low thermal conductivity of alumina could lead to the formation of local hot spots during FTS which compromise the selectivity of the reaction and the plant safety, especially at high CO conversion. Wang et al. [18] have reported that the heat release by the FTS cannot be properly evacuated to the entire body of the alumina support and thus, leads to the formation of hot spots on the catalyst surface which favor formation of light products. It is therefore of interest to develop new supports with improved thermal conductivity in order to reduce as much as possible the temperature gradient within the catalyst bed. Supports with high chemical inertness show advantages for the recovery of the active phase at the end-life of the catalyst, taken into account the toxicity of cobalt and its relatively high amount in the FTS plant. Such new supports should also be inexpensive and readily available in various shapes in order to reduce the costs linked with reactor modifications.

Recently, silicon carbide (β -SiC) with medium specific surface area (20-40 m². g⁻¹), has been reported as an efficient support for FTS allowing working at high CO conversion along with a high C₅⁺ selectivity, as well as for the FTO (Syngas to Olefins) reaction with high selectivity towards light olefins [19,20,21,22,23,24]. Silicon carbide possesses all the physical properties required for being used as catalyst support, namely: high mechanical strength, high thermal conductivity (which allows a rapid homogenization of the temperature within the catalyst bed), high oxidative resistance, and chemically inertness (which facilitates the recovery of the active phase and the support for subsequent re-use [19]). It is also worthy to note that the pore network of SiC is mainly constituted by meso- and macro-pores which significantly enhance mass transfer during FTS and prevents the formation of concentration gradients between hydrogen and carbon monoxide. Indeed, during FTS the catalyst pores are mostly filled with liquid waxes and thus, both gaseous reactants and FTS products have to diffuse through a liquid layer. Such a gas-liquid diffusion layer causes more severe concentration gradients for CO than for H₂ due to the higher diffusivity of the latter. The difference in terms of reactants diffusivity leads to the formation of high local concentration of H₂ versus CO and as a consequence, a higher selectivity toward light products formation. It was suggested that a higher diffusion rate of hydrogen inside the pores filled up with liquid products compared to that of carbon monoxide entailed an increase in the local H₂/CO ratio in the catalyst pores, and thus, a shift toward the formation of lighter hydrocarbons and especially methane [25,26].

The β -SiC support also presents a low metal-support interaction which allows an easy reduction of the deposited metal particles at moderate reduction temperature [19,20]. However, the low metal-support interaction also prevents the high and homogeneous dispersion of the metal nanoparticles on the SiC-based support, leading to a relatively large metal particle size, i.e. 30-40 nm, which is higher than that desired for the optimum operation of the FTS process, i.e. 15-20 nm [27]. It is thus of interest to develop a new SiC-based support for such a highly demanding catalytic process, with a higher surface area and a stronger metal-support interaction in order to improve active phase dispersion and also to prevent excessive metal particle size growth by hydrothermal sintering.

The aim of the present study is to report on a new hybrid support consisted by a titanium doped silicon carbide with high specific surface area and improved metal-support interactions, and its use in the Fischer-Tropsch synthesis. The potential industrial development of this catalyst will be also evaluated with a long-term FTS test. Finally, the catalytic

performance of the Co/TiO₂-SiC catalyst will be benchmarked with those of different FTS catalysts reported in the literature.

2. Experimental section

2.1 Support

The SiC-based material have bee supplied by SICAT. The detailed synthesis of the SiC-based materials was summarized in a recent review [28]. The Ti-doped supports are prepared via mixed TiC-SiC composite that is selectively oxidised into a mixed TiO₂-SiC. The titanium-doped SiC was synthesized by mixing microsized silicon powder and TiO₂ nanoparticles with a carbon-containing resin. The paste was further processed into various shapes, such as extrudates, grains, beads, etc. Examples of SiC-based material with different size and shape are presented in Figure 1. The carbidization process was carried out under flowing argon at temperatures around 1350 °C during one hour. The TiC-to-TiO₂ transformation was carried out by treating the composite at 550 °C in air for 2 h. The details of the synthesis can be found in ref. [28].



Figure 1. Silicon carbide (β -SiC) with different size and shape synthesized via a gas-solid reaction (courtesy by www.sicatcatalyst.com).

2.2 Catalyst preparation

TiO₂-doped SiC and containing cobalt catalysts were prepared by pore volume impregnation of the support with cobalt nitrate (Acros) solution. The solvent used was either de-ionized water (99.95 % purity, Acros). The cobalt loading was kept at 10 and 30 wt. % of the catalyst which is the lower range of cobalt loading according to the literature and patent surveys [9, 29]. After impregnation the solid was allowed to dry at room temperature for 4 h and further oven-dried at 110 °C for 8 h and calcined at 350 °C (1 °C·min⁻¹) for 2 h in order to obtain the Co₃O₄/TiO₂-SiC catalyst precursor. The oxide form was then reduced in flowing hydrogen (30 mL·min⁻¹) at 300 °C for 6 h.

2.3 Characterization techniques

X-ray diffraction (XRD) measurements were carried out in a Bruker D-8 Advance diffractometer equipped with a Vantec detector. The powdered sample was packed onto a glass slide. ASTM powder diffraction files were used to identify the phase present in the sample. Crystallite sizes were calculated from line broadening using the Scherrer equation.

The specific surface area of the support and the catalyst, after reduction, were determined in a Micromeritics sorptometer. The sample was outgassed at 250 °C under vacuum for 14 h in order to desorb moisture and adsorbed species on its surface. The measurements were carried out using N₂ as adsorbent at liquid N₂ temperature at relative pressures between 0.05 and 0.25.

Temperature-Programmed Reduction (TPR) was carried out in a Micromeritics ASAP-2100 setup under diluted hydrogen flow (10 vol. % in helium) with a heating rate of 15°C·min⁻¹. The hydrogen consumption was continuously monitored with a thermal conductivity detector (TCD). The steam formed during the reduction was trapped at -88 °C.

Scanning electron microscopy (SEM) analyses were carried out on a JEOL 6700F microscope working at 10 kV accelerated voltage. The solid was fixed on the sample holder by a graphite paste for examination. Before analysis the sample was covered by a thin layer of gold in order to avoid charging effects. The SEM analysis allows access to the morphology of the cobalt aggregates after reduction in order to correlate with the metal particle size determined by the XRD line broadening.

TEM tomography was performed on a JEOL 2100 F (FEG) electron microscope operating at a beam voltage of 200 kV, using a 2048 × 2048 pixels Ultrascan cooled CCD array detector, and a high tilt sample holder. The process was controlled by the tomography plug-in of Digital Micrograph, which allows varying systematically the tilt angle step by step, to correct

for defocusing, to maintain the object under study within the field of view and to record and store the object projections. In our work the acquisition of the projection series was acquired by tilting the object between -60° and $+70^\circ$ with a tilt increment of 2° in saxton mode, resulting in a total of 85 projections. No apparent irradiation damage was observed on the specimen at the end of the acquisition process (about 40 min). The treatment of tilt series for image processing and reconstruction procedure was performed using the IMOD software from the University of Colorado which uses a weighted-back projection method to compute the volume of the specimen. With our acquisition parameters and the characteristics of the specimen, the spatial resolution of the final tomogram presented in this paper is about 0.7 nm in the directions perpendicular to the electron beam. In the parallel direction, the resolution is worsen by an elongation factor of 1.3 due to the limited maximum tilt angle, and consequently we consider that the information limit of the 3D-analysis, in our case is about 1 nm. To model the computed volume, we finally used a segmentation procedure based on the grey-level intensities of the voxels, followed by 3D-display using surface rendering methods. More details on the experimental set-up and volume reconstruction and analysis can be found elsewhere.

The sample preparation for classical and tomography TEM was done according to the following process: the solid was crushed in a mortar into a very fine powder. The powder was then dispersed in ethanol by sonication during 5 min. After ultrasonication a drop of the solution was deposited on a holey carbon copper grid and the solvent was evaporated at room temperature before introducing of the sample holder in the microscope.

2.4 Fischer-Tropsch synthesis reaction

Fischer-Tropsch synthesis was carried out in a tubular fixed-bed stainless steel reactor (*I.D.* = 6 mm) with circulating silicon oil as heating source. The reduced catalyst (5 g of catalyst, in form of grains (150-400 μm)) was deposited between quartz wool plugs in the middle of the reactor. The reactor pressure was slowly increased from 0.1 to 4 MPa (ramping rate of 1 MPa. h^{-1}) under argon. The total pressure was controlled by a back pressure regulator (MFI Ltd.). At 4 MPa the reactor temperature was raised from room temperature to the desired reaction temperature (heating rate of 2 $^\circ\text{C. min}^{-1}$). Then, the argon flow was replaced by a 50:50 v:v mixture of synthesis gas and argon ($\text{CO:H}_2 = 1:2$). The catalyst was activated under a synthesis gas-argon mixture with different synthesis gas concentrations during three days before evaluation under pure synthesis gas atmosphere. The catalyst bed temperature was monitored with a thermocouple (\varnothing 0.3 mm) inserted inside a stainless steel finger (\varnothing 1

mm) passing through the catalyst bed. The products were condensed in two high pressure traps maintained at 85°C and 15 °C respectively. The exit gas was analyzed on-line, both by Thermal Conductivity Detector (TCD) and Flame Ionization Detector (FID), with a gas chromatography (GC Varian 3800 equipped with a DP-1 and Carbobond capillary columns).

The liquid phase and water were condensed in the traps and analyzed off-line at the end of the test. The water was removed from the organic phase by decantation of the system. A known amount (100 mg) of the organic phase, liquid hydrocarbons and waxy products, was dissolved in 3 ml of dichloromethane under sonication during 30 minutes. Then, 20 ml of CS₂ were further added to the solution in order to ensure a complete dissolution of the organic phase. For analysis, 10 µL of the solution was injected in a GC apparatus equipped with a Simdist column operated at 400 °C which allowed the detection of hydrocarbons ranging from C₉ to C₇₀.

3. Results and discussion

3.1 Physicochemical properties of the supports and catalysts

The XRD patterns of the SiC, TiC-SiC and TiO₂-SiC supports are presented in Figure 2. The calcination step at 500 °C transforms TiC fully into TiO₂ as confirmed by the XRD pattern, since no other diffraction lines were observed in the pattern.

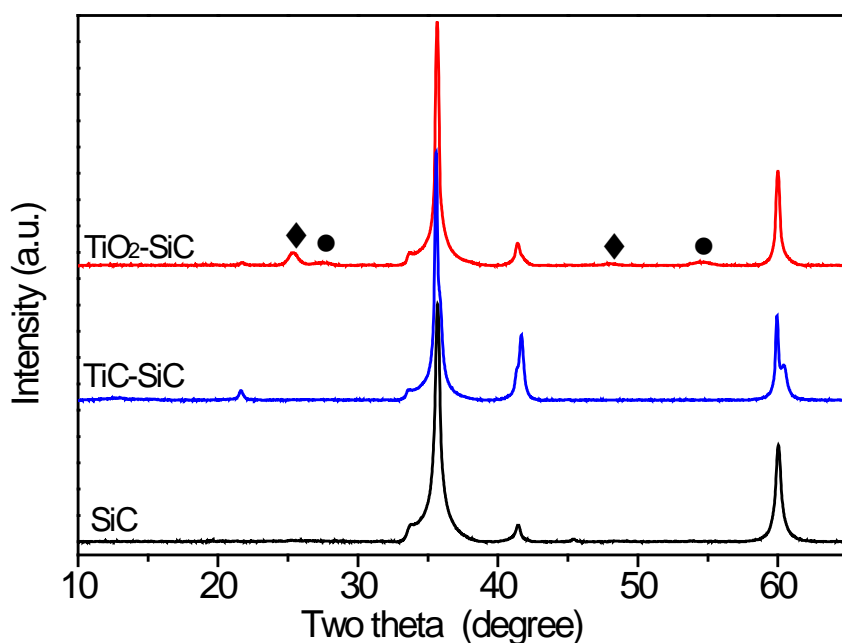


Figure 2. XRD patterns of SiC, TiC-SiC and TiO₂-SiC; The TiO₂-SiC were calcined by TiC-SiC at 500 °C for 2 h in air. Diamond (♦): anatase TiO₂; circles (●): TiO₂.

SEM micrographs representing the morphology of titanium carbide- and titanium dioxide-doped SiC are presented in Figure 3. The low magnification SEM micrographs (Figure 3A and B) clearly show the presence of macroporosity within the SiC-doped materials, before and after calcination. Medium and high-resolution SEM micrographs evidence fragmentation of TiC particles into smaller TiO₂ particles after the calcination step.

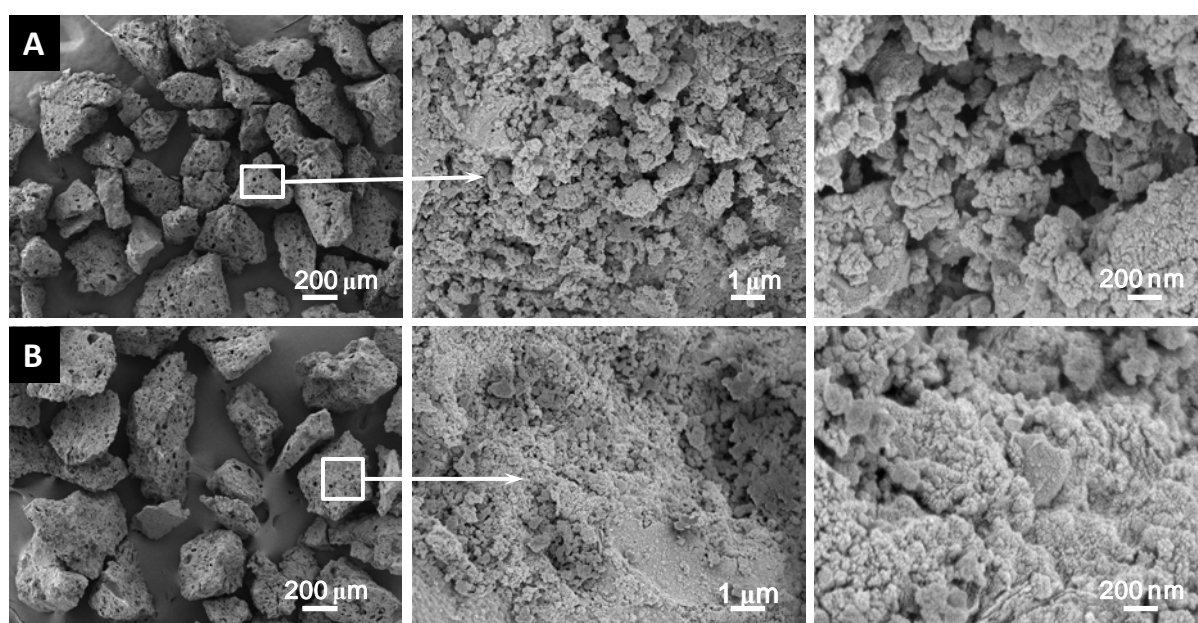


Figure 3. Representative SEM micrographs of (A) TiC-SiC and (B) TiO₂-SiC carriers. The TiC-to-TiO₂ transformation was carried out by calcination at 500 °C for 2 h in air.

The BET surface area, pore volume and average pore diameter of carriers and catalysts as prepared are shown in Table 1. The introduction of TiC into the SiC matrix leads to a strong improvement of the ceramic specific surface area compared to the undoped one, i.e. 77 m²·g⁻¹ instead of 40 m²·g⁻¹. Such a specific surface area increase could be attributed to the formation of TiC particles evenly dispersed throughout the SiC matrix which prevents the formation of large SiC particles with low specific surface area. According to the results the TiC-to-TiO₂ transformation leads to a significant increase of the specific surface area of the doped support, i.e. from 77 m²·g⁻¹ to 101 m²·g⁻¹. The TiO₂-SiC also contains a relatively large amount of micropores. The deposition of cobalt differently affects the surface area of the two

supports: the surface area of the undoped SiC slightly decreases from 40 to 33 $\text{m}^2\cdot\text{g}^{-1}$ after deposition of 10 wt. % of cobalt active phase while the surface area of the doped SiC significantly drops from 101 to 25 $\text{m}^2\cdot\text{g}^{-1}$ which is mostly due to the micropores plugging and a formation of a new mesoporous network.

XRD was used to characterize the crystalline structure of the catalysts. The XRD patterns of the catalysts after reduction under H_2 at 300 °C for 6 h are presented in Figure 4.

The 10Co/SiC catalyst only displays diffraction lines corresponding to the SiC support and metallic cobalt phase without diffraction lines corresponding to the cobalt oxide phases, confirming the complete reduction of the cobalt phase. A similar reduction pattern is also observed on the doped catalyst. The TPR results indicate that the presence of a dopant, i.e. TiO_2 with a loading of 17 wt. %, does not alter the reduction behavior of the cobalt oxide precursor.

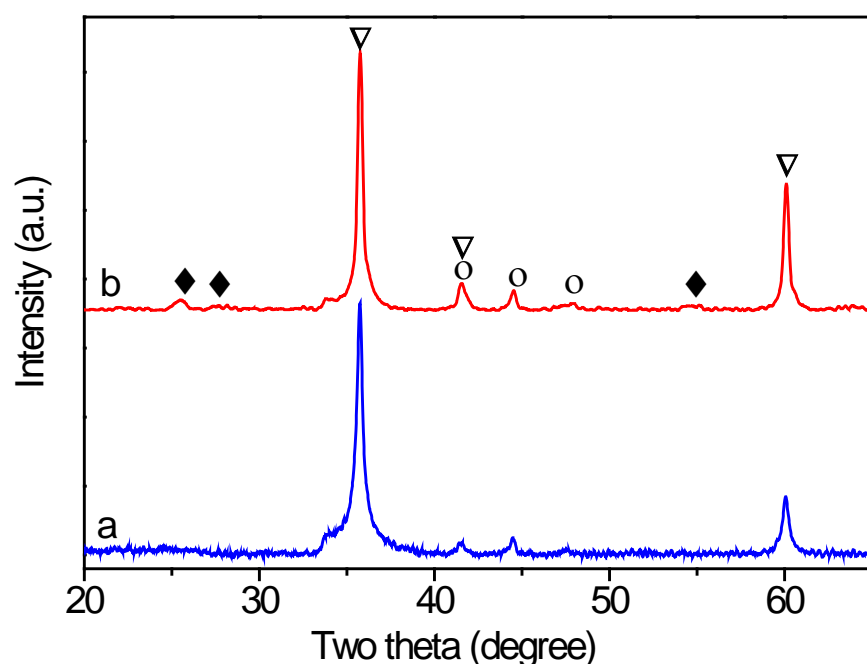


Figure 4. Ex-situ X-ray diffraction patterns of the catalysts: (a) 10Co/SiC; (b) 10Co/TiO₂-SiC. The catalysts were calcined at 350 °C for 2 h followed by reduction under H_2 at 300 °C for 6 h. Legends: Diamond (◆): TiO_2 ; circles (○): Co; triangle (▽): SiC.

The complete reduction of the cobalt phase was directly attributed to the low interaction between the cobalt oxide phase and the support, SiC and TiO_2 , which avoids the formation of a hardly reducible cobalt phase as usually observed with the alumina or silica

supports [30,31]. The average cobalt particle size determined by the Scherrer formula is reported in Table 1. Two methods are used to calculate the cobalt particle size. The average nanoparticle crystal size of 10Co/SiC is about 40-50 nm, and the size of 10Co/TiO₂-SiC is about 15-25 nm, being predicted to be the most active particle size for the FTS process [13]. The results indicate that the introduction of the TiO₂ phase into the SiC matrix significantly decreases the particle size of cobalt, probably by generating a higher chemical interaction with the metal precursor.

Table 1 BET surface area and pore volume of the undoped and doped SiC carriers and the same after cobalt deposition. The corresponding cobalt particle size, before and after reduction, under H₂ at 300 °C for 6 h, determined by the Scherrer formula is also presented.

Sample	Surface area (m ² /g)	Total pore volume (cm ³ /g)	BJH pore diameter (nm)	Co ⁰ particle size ^(a) (nm)	Average Co ⁰ particle size ^b (nm)	
					Co ⁰	Co ⁰
					fcc	hcp
SiC	40	0.120	12.8	-	-	-
TiO ₂ -SiC	101	0.123	4.4	-	-	-
10Co/SiC	33	0.139	17.1	42 ± 5	51 ± 5	29 ± 5
10Co/TiO ₂ -SiC	25	0.082	13.0	22 ± 5	44 ± 5	14 ± 5

$$(a) d(\text{Co}^0) = 0.75 \times d(\text{Co}_3\text{O}_4)$$

$$(b) d(\text{Co}^0) = k \cdot \lambda / (\tau \cdot \cos\theta), \text{The sample was reduced by H}_2 \text{ at 300 }^\circ\text{C for 6h}$$

3.2 Reduction behavior of catalysts

The TPR spectra of the 10Co/SiC and 10Co/TiO₂-SiC catalysts are presented in Figure 5. The first reduction peak for both catalysts located at around 200 °C can be attributed to the decomposition in the presence of hydrogen of residual cobalt nitrate [32,33]. In the paper by Borg et al. [33], calcinations temperatures above 450 °C are needed to completely decompose the supported cobalt nitrate. At lower calcinations temperatures some nitrate still remains in the calcined sample which further decomposed in the presence of hydrogen. The

reduction of cobalt species started at 260 °C and the first cobalt reduction peak is typically assigned to the reduction of Co_3O_4 to CoO , although a fraction of the peak likely comprises the reduction of the larger, bulk-like CoO species to Co . The second reduction step is composed of overlapping peaks which are due to the reduction of CoO to Co . These peaks also include the reduction of cobalt species that interact with the support [20, 34, 35]. The tailing was observed after 500 °C in the TPR profile of $10\text{Co}/\text{TiO}_2\text{-SiC}$ which is likely attributed to small cobalt in strong interaction with TiO_2 and the reduction of cobalt silicate-like species [36]. The reduction of cobalt silicate-like species was observed after 550 °C on $10\text{Co}/\text{SiC}$ catalyst. However, it is worthy to note that the amount of such cobalt species in strong interaction with the support remains relatively low.

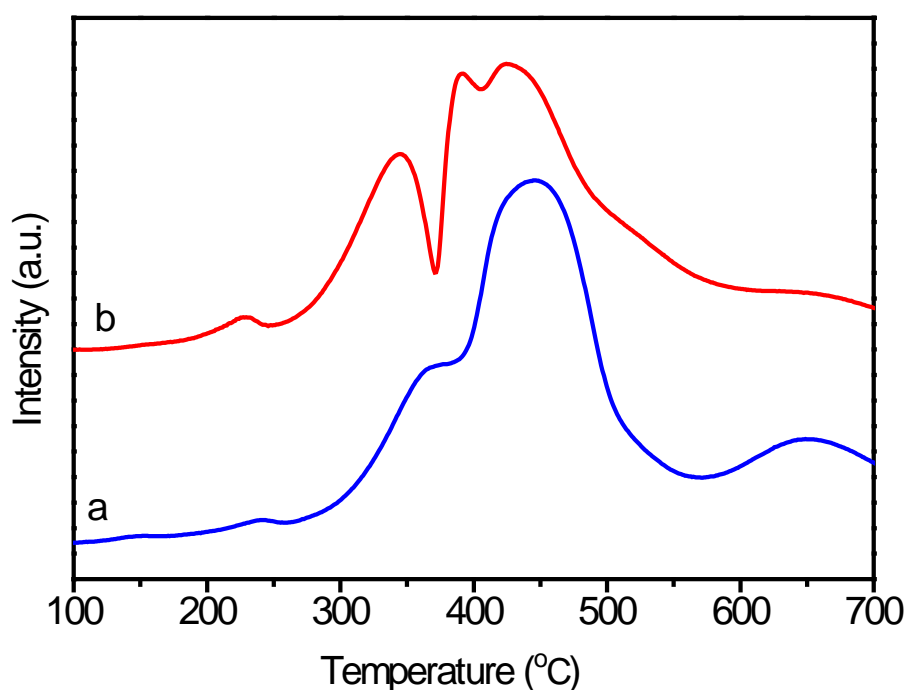


Figure 5. TPR profiles of the (a) $10\text{Co}/\text{SiC}$ and (b) $10\text{Co}/\text{TiO}_2\text{-SiC}$ catalysts after calcinations at 350 °C in air for 2 h.

The sequential TPR analysis of $10\text{Co}/\text{TiO}_2\text{-SiC}$ catalyst was also performed, i.e. isotherm reduction at 300 °C for 2, 3, 4 and 6 h followed by a second in situ TPR, in order to ensure the complete reduction of the catalyst under the applied reduction conditions (Figure 6). According to the results one can see that after the reduction at 300 °C for 6 h all the cobalt oxide was reduced and no additional reduction peaks were observed in the TPR spectrum of the reduced catalyst. Note that TPR experiments were conducted in 10 % H_2/Ar mixtures,

whereas the catalysts were reduced in pure hydrogen for catalytic measurements. Chernavskii [37] shown that the hydrogen partial pressure can significantly affect the extent of the cobalt reduction. Lower reduction temperature of cobalt is usually obtained in pure hydrogen. The TPR experiment was carried out under diluted hydrogen which could considerably underestimate of the extent of cobalt reduction. During the transfer one should expect that some superficial oxidation could occur, leading to the formation of a core-shell CoO-Co phase (see TEM analysis below). Such a superficial oxide layer will be rapidly reduced by the CO and H₂ mixture during the FTS process [34, 36, 37].

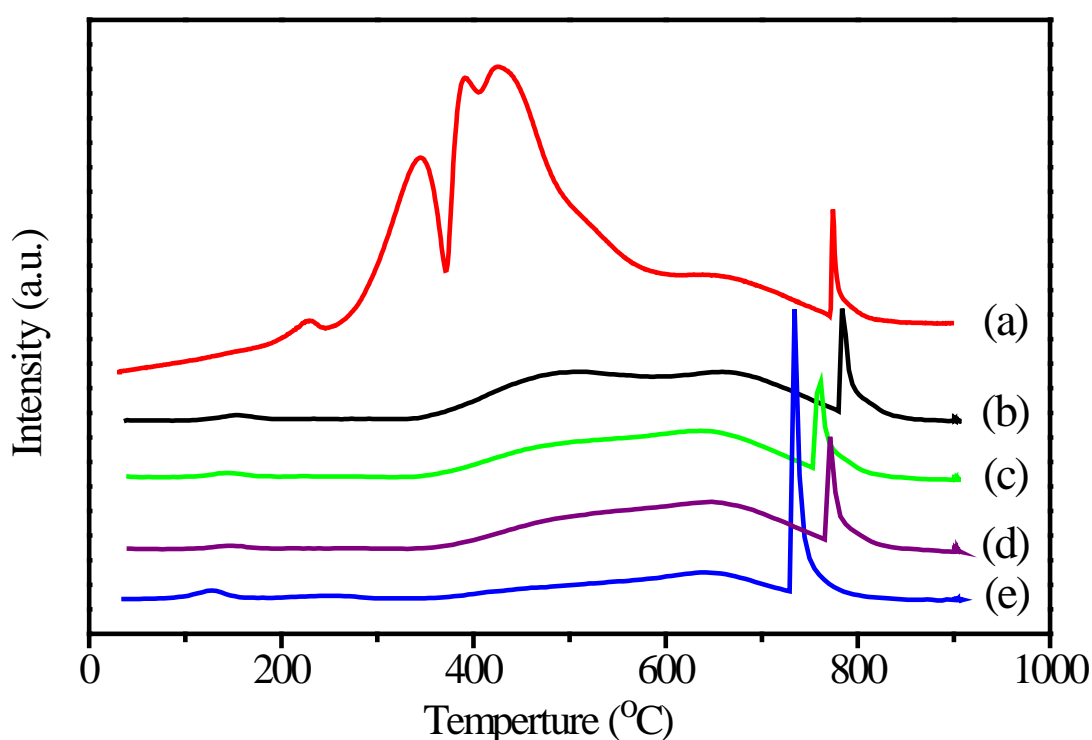


Figure 6. In-situ TPR profiles of Co₁₀/TiO₂-SiC. (a) The TPR was directly test under diluted H₂ with heating rate of 15 °C min⁻¹; The sample was in-situ reduced by diluted H₂ (10 vol. % in argon) at 300 °C for (b) 2 h; (c) 3 h; (d) 4 h ; (e) 6 h in TPR equipment, and then under the diluted H₂ with a heating rate of 15 °C. min⁻¹.

3.3 Morphological and microstructural characteristics of Co/SiC and Co/TiO₂-SiC catalysts

The corresponding SEM micrographs of the two catalysts after reduction are presented in Figure 7A and B: they clearly evidence the presence of a smaller cobalt particle size in the

doped catalyst. In addition, the cobalt particle size is more homogeneous on the TiO₂ doped SiC catalyst in comparison with the SiC catalyst.

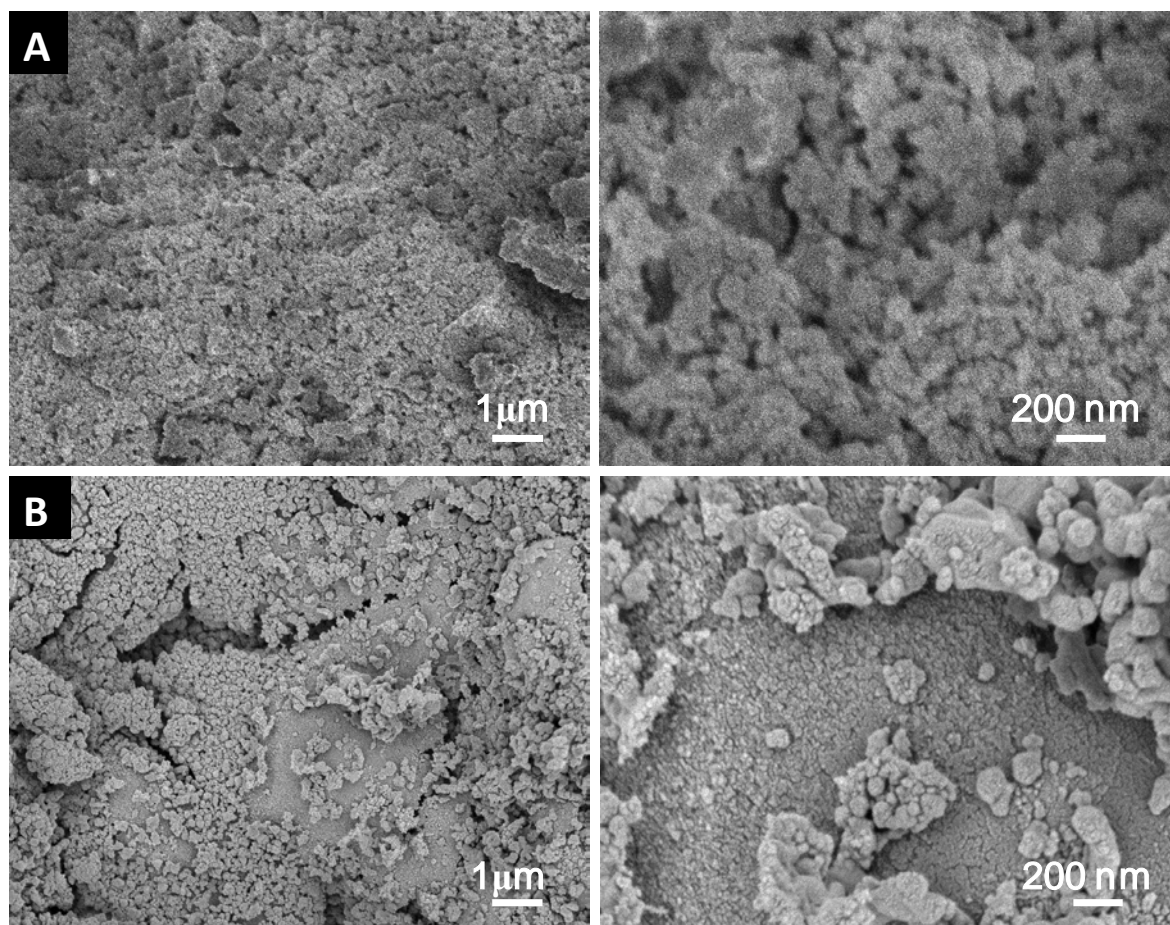


Figure 7. (A) SEM micrographs of the 10Co/SiC after reduction under H₂ at 300 °C for 6 h. (B) SEM micrographs of the 10Co/TiO₂-SiC after reduction under H₂ at 300 °C for 6 h.

The cobalt particle size on the pure and TiO₂-doped SiC catalysts was evaluated by TEM and EFTEM and the results are presented in Figure 8. The TEM micrographs of the Co/SiC catalyst indicate the presence of a relatively homogeneous cobalt particle size with an average size of around 40 nm (Figure 8A and B) dispersed throughout the support surface. In the case of the Co/TiO₂-SiC, in order to highlight the interaction between the cobalt particles and the different phases constituting the doped support, EFTEM analysis was used instead of traditional TEM analysis (Figure 8C and D). The volume reconstruction images indicate that the size of the cobalt particles was significantly changed depending on which surface they were in contact with, i.e. 5 to 15 nm for the Co particles in contact with TiO₂ and 30 to 50 nm for Co particles directly supported on the SiC surface. Such result is relatively close to those

obtained by the Scherrer formula (Table 1). According to the observed results one can state that the TiO_2 phase incorporated into the SiC composite support presents a stronger interaction with the active phase leading to the formation of cobalt particles with much smaller size compared to those obtained on the undoped SiC support. Similar results have also been reported previously on the SiC foam coated with a thin layer of alumina [19]. Indeed, the introduction of a thin alumina layer led to higher cobalt dispersion and an improvement in the FTS performance of the catalyst. However, it is worthy to note that the metal-support interaction between the cobalt oxide and the TiO_2 phase was not too strong to prevent the easy reduction of the cobalt phase according to the XRD and TPR experiments presented above.

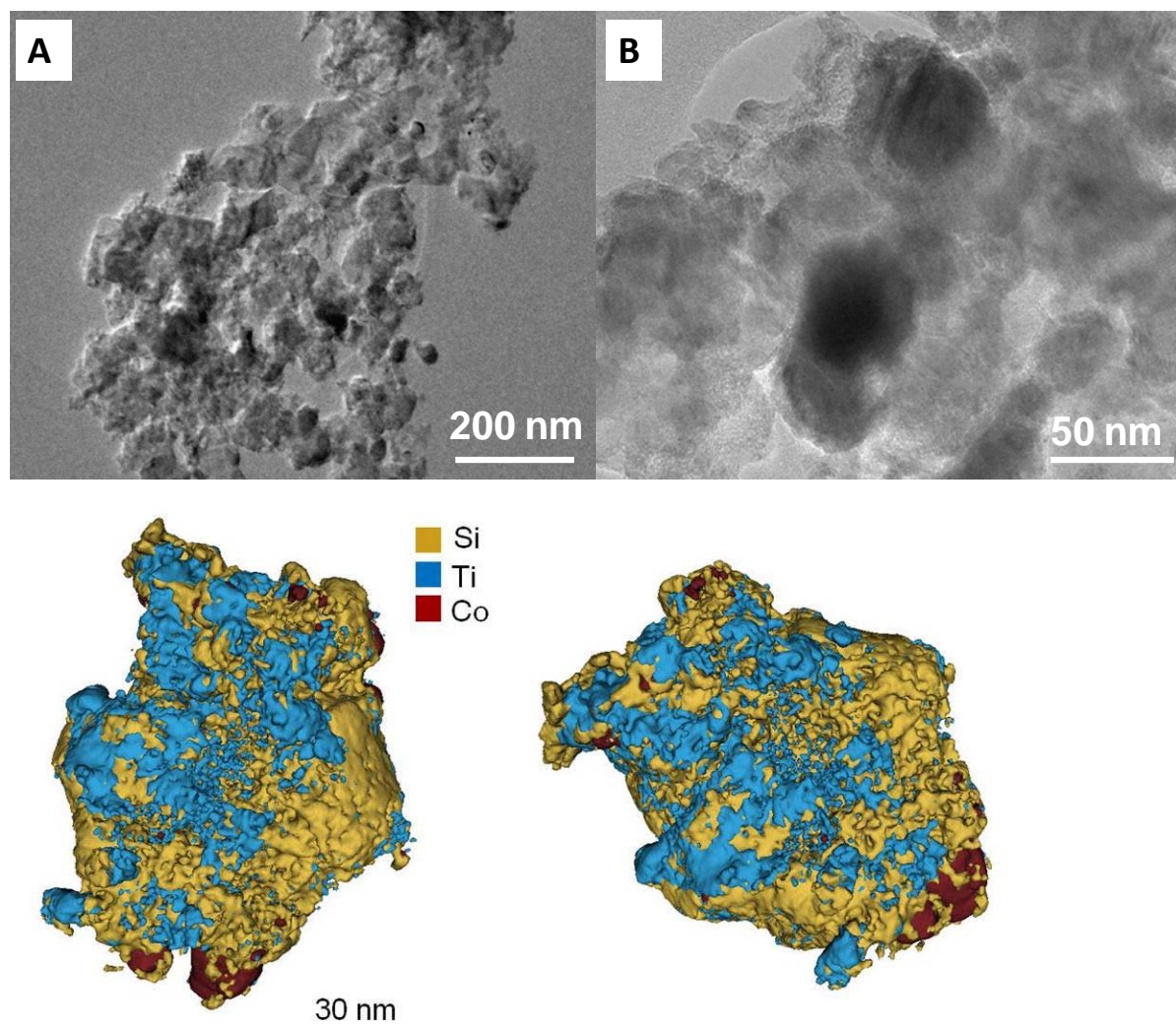


Figure 8. (A, B) TEM images of the 10Co/SiC. (C, D) EFTEM images of 10Co/TiO₂-SiC showing the interaction of the cobalt particles with the different compounds of the support: Ti (blue), Si (yellow), Co (red). The catalyst was calcined at 350 °C for 2 h followed by a

reduction under H₂ at 300 °C for 6 h.

3.4 Fischer-Tropsch synthesis (FTS) catalytic performance

The FTS activity (expressed in terms of specific rate, $\text{g}_{\text{HC}} \cdot \text{g}_{\text{catalyst}}^{-1} \cdot \text{h}^{-1}$) and C₅₊ selectivity obtained on the 10Co/SiC and 10Co/TiO₂-SiC catalysts as a function of the reaction temperature and under a relatively high GHSV, 2850 h⁻¹ (STP), are presented in Figure 9. The FTS activity steadily increases on both catalysts with increasing reaction temperatures, whereas S_{C₅₊} selectivity remains relatively high at around 91 % on both catalysts. It is worthy to note that the FTS activity on the 10Co/TiO₂-SiC remains higher than the one obtained on the 10Co/SiC catalyst and steadily increases with increasing reaction temperatures. The high FTS activity of the doped-SiC catalyst could be attributed to the better dispersion of the cobalt particles in the presence of TiO₂ phase according to the XRD and EFTEM analysis. The FTS activity is linked to the active phase dispersion and thus, the smaller the active phase particle size is (down to a certain level), the higher the FTS activity is. On the undoped SiC-based catalyst the relatively low cobalt dispersion, i.e. 40-50 nm, was linked to the lower FTS activity observed. In the doped catalyst the small cobalt particle size associated with the TiO₂ phase, i.e. 5-15 nm, seems to be responsible for the FTS activity enhancement.

The FTS activity also remains stable for the whole test, i.e. > 200 h, indicating that deactivation, i.e. carbonaceous deposition, sintering and/or superficial oxidation, is extremely low on such catalysts after stabilization. Similar results have already been reported by several research groups in the literature [26, 31].

The most remarkable fact is that the S_{C₅₊} selectivity remains extremely high whatever the reaction temperature up to 230 °C. The high S_{C₅₊} selectivity obtained in the present work could be attributed to several facts: (i) firstly, to the homogeneous catalyst bed temperature thanks to the good thermal conductivity of the support and the liquid hydrocarbon film formed on the catalyst surface [38], (ii) secondly, to the increased partial pressure of steam within the catalyst bed due to the relatively low space velocity [39,40]. The promoting effect of steam on the S_{C₅₊} has been proposed to be due to its inhibition of hydrogenation reactions leading to a lower methane selectivity [41], and (iii) the meso- porosity of the support which favor the evacuation of the products and a better accessibility to the reactants. A recent work published by Holmen and co-workers [11] on the low surface area α -Al₂O₃ catalyst has also pointed out the strong influence of the support porosity on the C₅₊ selectivity. Similar high C₅₊ selectivity was also reported recently by De la Osa et al. [21,22] on the large pore SiC-

based catalysts either undoped or doped with calcium. The strong influence of the support porosity on the $S_{C_{5+}}$ selectivity could be explained by the enhanced liquid hydrocarbons evacuation from the pores of the catalyst which significantly reduce the concentration gradients for CO versus H_2 , due to the higher diffusivity of the later, next to the active sites localized within the pore. Indeed, high local concentration of H_2 versus CO next to the active site leads to a higher selectivity toward light products formation by rapid hydrogenation of the intermediate olefins.

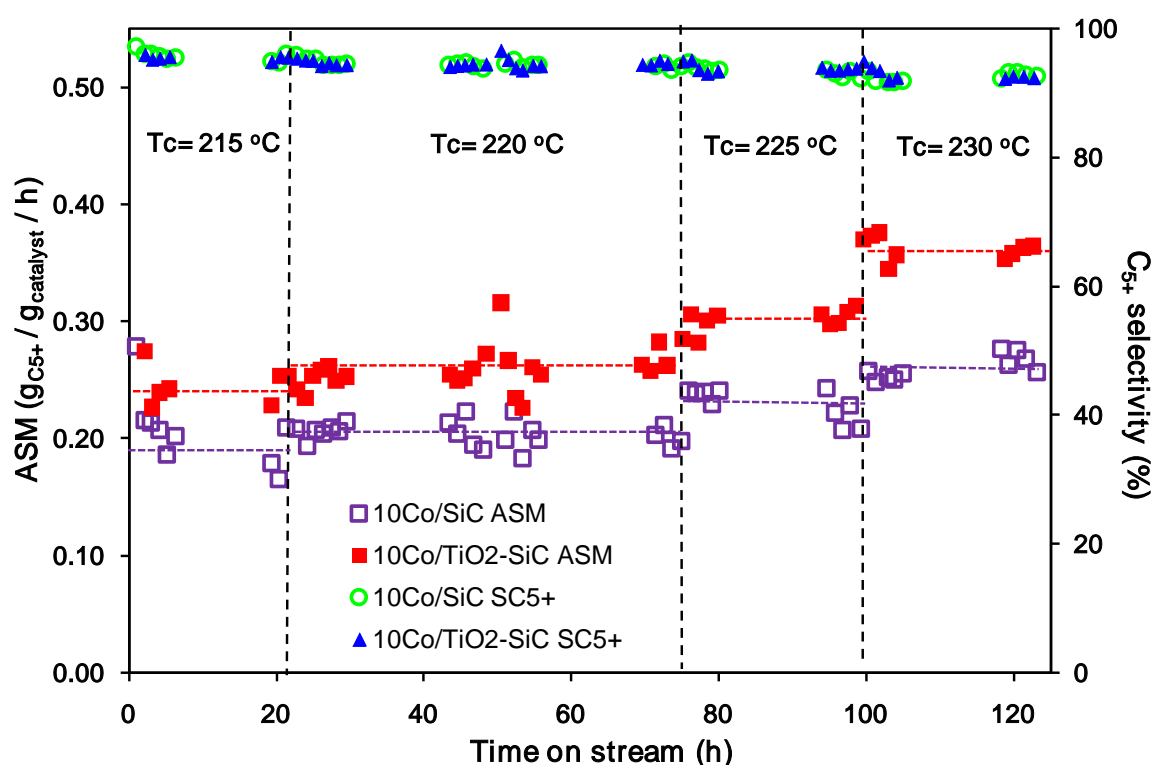


Figure 9. FTS performance and stability of the 10Co/SiC and 10Co/TiO₂-SiC catalyst as a function of the reaction temperature. Reaction conditions: H_2/CO molar ratio = 2, pure syngas, total pressure = 40 bar, GHSV = 2850 h⁻¹. The catalysts tested have already been evaluated in the FTS reaction at 215 °C and under a GHSV of 1900 h⁻¹ during about 100 h on stream (not reported).

The product distribution is presented in Table 2 and reveals that high $S_{C_{5+}}$ selectivity can still be obtained, i.e. 92 %, even at high reaction temperature. The relatively high $S_{C_{5+}}$ selectivity at high reaction temperature, i.e. 230 °C, can be explained by the concomitant increase of the steam partial pressure within the catalyst bed due to the higher CO conversion.

It is reported that at high partial pressures steam competitively adsorbs on the methanation sites and thus, favor the formation of liquid hydrocarbons, leading to a higher $S_{C_{5+}}$ selectivity [31]. At high reaction temperatures, i.e. 230 °C, where the contribution of hydrogenation reactions becomes important, the $S_{C_{5+}}$ selectivity on the SiC-based catalyst only slowly decreases and still remains high, i.e. 92 %, compared to other catalysts supported on insulating supports (Al_2O_3 , SiO_2 , TiO_2) tested at lower reaction temperature [42]. It is worthy to note that at the reaction temperature of 230 °C the selectivity towards methane becomes significant, i.e. 6 %, on the TiO_2 -SiC-based catalyst.

In Table 2, the FTS performance of undoped and doped SiC-based catalysts were compared with those reported on a similar catalyst supported on different supports. De la Osa et al. [22] have investigated the influence of the calcium as promoter on the cobalt supported SiC catalyst and have observed a relatively high C_{5+} selectivity with high CO conversion on the 12Co-2Ca/SiC catalyst at 250 °C. The high $S_{C_{5+}}$ could be explained by the relatively high space velocity used by De la Osa et al. [22] during the FTS reaction.

Holmen and co-workers [43] have stated that the $S_{C_{5+}}$ selectivity increases when the small porous network support was replaced by the one with larger pore size for the alumina-based catalyst, i.e. $\alpha-Al_2O_3 > \gamma-Al_2O_3$. The large pore $\alpha-Al_2O_3$ significantly reduces the problem of reactants diffusion allowing the maintaining of a balance between CO and H_2 which leads to a high selectivity towards liquid hydrocarbons.

Bezemer et al. [13] have studied the influence of the cobalt particles size on the FTS reaction using carbon nanofibers as support. The highest CTY ($19.2 \times 10^{-5} \text{ molCO/g}_{\text{Cat}}/\text{h}$) was observed with cobalt particle size centered at about 8 nm under severe reaction conditions, i.e. 35 bar and 250 °C. However, the high reaction temperature leads to the formation of a large amount of light products and thus, the C_{5+} selectivity was significantly decreased to 74 %. Jalama et al. [49] used synthesis gas to reduce the 10Co/ TiO_2 catalyst instead of pure H_2 during the FTS reaction. When the catalyst was activated under synthesis gas at 350 °C the FTS activity of $3.3 \times 10^{-5} \text{ molCO/g}_{\text{Cat}}/\text{h}$ was obtained compared to $1.5 \times 10^{-5} \text{ molCO/g}_{\text{Cat}}/\text{h}$ for the catalyst activated under pure hydrogen. The methane selectivity and C_{5+} selectivity were 17 % and 72 %, respectively. Breejen et al. [44] introduced MnO on Co/Pt/ SiO_2 catalyst followed by a calcinations step in a flow of 1vol% NO/He. For the Co/Mn/Pt/ SiO_2 catalyst with an optimum Mn/Co atomic ratio of 0.08, an increase in C_{5+} selectivity from 32 wt. % (unpromoted) to 54 wt% (promoted with Mn) was found, without a significant loss in cobalt time yield, i.e. $4.6 \times 10^{-5} \text{ molCO/g}_{\text{Cat}}/\text{h}$ compared to $4.9 \times 10^{-5} \text{ molCO/g}_{\text{Cat}}/\text{h}$.

The Ru-promoted plasma-assisted cobalt catalysts were tested for FTS exhibited enhanced activity thanks to the combination of high cobalt dispersion and good cobalt reducibility[45]. The plasma-assisted CoRu/SiO₂-P60 catalyst exhibited a cobalt-time yield of 2.5×10^{-5} mol_{CO}/g_{Cat}/h which showed highest FT rate compared with untreated by plasma and unprompted by Ru. Karaca et al [46] reported that CoPt/Al₂O₃-N1 catalyst has much higher cobalt-time yields, i.e. 8.4×10^{-5} mol_{CO}/g_{Cat}/h could be attributed to higher reducibility of smaller cobalt particles and higher concentration of cobalt active sites.

Martínez et al. [47] investigated a high surface area and a hierarchical macro-mesoporous structure γ -Al₂O₃ nanofibers supported 30 wt% Co-1.0 wt. % Ru catalyst used to elucidate the diffusional and dispersion effects during FTS compared to commercial alumina (Sasol). The benefits of using the macro-mesoporous nanofibrous support (high Co⁰ dispersion and fast CO transport rate through the liquid phase filling the pores) are manifested at high metal loadings (30 wt. % Co) where the nanofibrous catalyst displays the highest specific activity and productivity to diesel products.

Table 2. Fischer-Tropsch results obtained on undoped and doped SiC-based containing cobalt catalysts. Reaction conditions: $H_2/CO = 2$, pure syngas, total pressure = 40 atm.

Catalyst	T(°C)	GHSV (h ⁻¹)	CO Conversion n (%)	Product selectivity (%)				CTY ^a (10 ⁻⁵ mol _{co} /g _{Co} /s)	ASM ^b
				CO ₂	CH ₄	C ₂ -C ₄	C ₅₊		
10Co/SiC	215	2850	26.9	0	2.9	1.6	95.5	4.0	0.19
	220	2850	28.8	0	3.7	2.0	94.3	4.3	0.21
	225	2850	32.3	0	4.5	2.4	93.1	4.8	0.23
	230	2850	35.4	0.1	5.4	2.9	91.6	5.3	0.24
10Co/TiO ₂ -SiC	215	2850	33.9	0	3.2	1.5	95.3	5.0	0.24
	220	2850	37.0	0	3.9	1.7	94.4	5.5	0.26
	225	2850	43.4	0	4.5	1.9	93.6	6.5	0.30
	230	2850	50.5	0.2	5.9	2.2	91.7	7.5	0.35
30Co/TiO ₂ -SiC	215	2850	57.7	3.1	4.7	0	92.2	2.9	0.40
	220	2850	68.3	2.7	4.7	0	92.5	3.4	0.47
	230	3800	61.8	3.1	6.2	0.1	90.6	4.1	0.56
30Co-Ru/SiC-E [20]	230	3800	47	3.0	5.5	0.0	91.5	2.9	0.43

^a Cobalt-Time-Yield (molar CO conversion rate per g atom Co per hour)

^b FTS rate (Mass C₅₊ per g catalyst per hour)

Table 3. Comparison of FTS catalytic performance of the SiC-based catalysts with the other cobalt containing catalysts reported in the literature.

Catalyst	Reaction temperature (°C)	CO Conversion (%)	Product selectivity (%)				CTY ^x (10 ⁻⁵ mol _{co} /g _{Co} /s)	Ref
			CO ₂	CH ₄	C ₂₋ C ₄	C ₅₊		
10Co/TiO ₂ - SiC	220	37.0	0	3.9	1.7	94.4	5.5	This work
	230	50.5	0.2	5.9	2.2	91.7	7.5	
30Co/TiO ₂ - SiC	220	68.3	2.7	4.7	0	92.5	3.4	This work
	230	61.8	3.1	6.2	0.1	90.6	4.1	
Co-Ru/SiC- E ^a	230	47	3.0	5.5	0.0	91.5	2.9	[20]
20Co- 2Ca/SiC ^b	220	31.1	0.2	1.0		98.8	1.6	[22]
	250	50.9	0.3	1.6		98.2	2.7	
12Co- 2Ca/SiC ^b	250	59.3	0.3	1.1		98.5	4.8	[22]
S100 ^c	220	<15		34	-	36	3.0	[48]
IEN8 ^d	210	65	2.8	-		76.1	3.7	[13]
	250	84	5.8	-		74.0	19.2	
10Co/TiO ₂ ^e	220	30-35	-	16.7	-	72.2	3.3	[49]
CoRu/SiC- P60 ^f	220	38	-	24.9	30.4	44.7	2.5	[45]

CoPt/Al ₂ O ₃ -N ^g	220	39	-	8.0	-		8.4	[46]
1Ru- 30Co/Al ₂ O ₃ _nf ^h	220	c.a.40	-	13.8	13.2	< 73	4.9 (6.2)	[47]

[a] Reaction conditions: GHSV = 3800 h⁻¹, P= 40 bar, H₂/CO=2; [b] Reaction conditions: GHSV = 6000Ncm³/g_{cat}/h, P= 20 bar, H₂/CO=2; [c] Reaction conditions: P= 1 bar, Flow rate= 4.5ml/min, [d] Reaction conditions: P= 35 bar, CO/H₂/N₂ = 33/66/6; [e]Reaction conditions: GHSV = 3 NL/g_{cat}/h, P= 20 bar, H₂/CO=2; [f] Reaction conditions: P = 1 bar, 500 mg catalysts, T = 493 K, GHSV = 1800 ml/(g h)⁻¹, H₂/CO = 2.[g] T = 493 K, P = 20 bar, H₂/CO = 2, GHSV = 14000 ml/(g h)⁻¹. [h] T = 493 K, P = 2.0 MPa, H₂/CO = 2. Data in parenthesis correspond to initial activity.[X] Cobalt-Time-Yield (molar CO conversion rate per g atom Co per hour)

The 10Co/SiC and 10Co/TiO₂-SiC catalysts also exhibit an extremely high stability as a function of the FTS test duration according to the results presented in Figure 10. Almost no deactivation is observed on the catalyst up to 100 h on stream which indicates that deactivation linked with cobalt surface oxidation or sintering is unlikely to occur under the reaction conditions used in the present work.

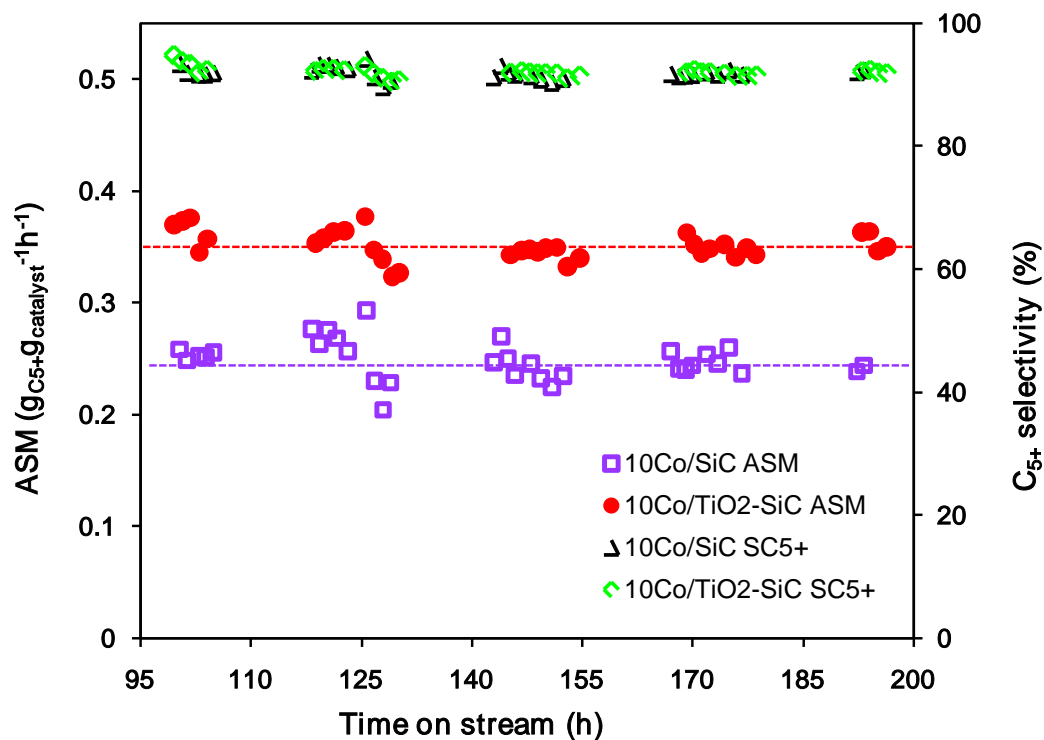


Figure 10. FTS performance and stability of the 10Co/SiC and 10Co/TiO₂-SiC catalyst as a function of time on stream at 230 °C. Reaction conditions: H₂/CO molar ratio = 2, pure syngas, total pressure = 40 bar, GHSV = 2850 h⁻¹

3.5 Chain growth factor (α) from the linear portion of the hydrocarbon

The chain growth factor (α) on the catalysts was calculated and the results are presented in Figure 11. The chain growth factor (α) is obtained from the curve of $\ln(W_n/n)$ against n , where n is the chain length, W_n is the weight fraction of hydrocarbon with carbon numbers n . According to the results one can state that the chain growth factor (α) is relatively high on both catalysts, i.e. 0.92 for 10Co/SiC and 0.92 for TiO₂ doping catalyst, which is in good agreement with the relatively high C₅₊ selectivity obtained on both catalysts.

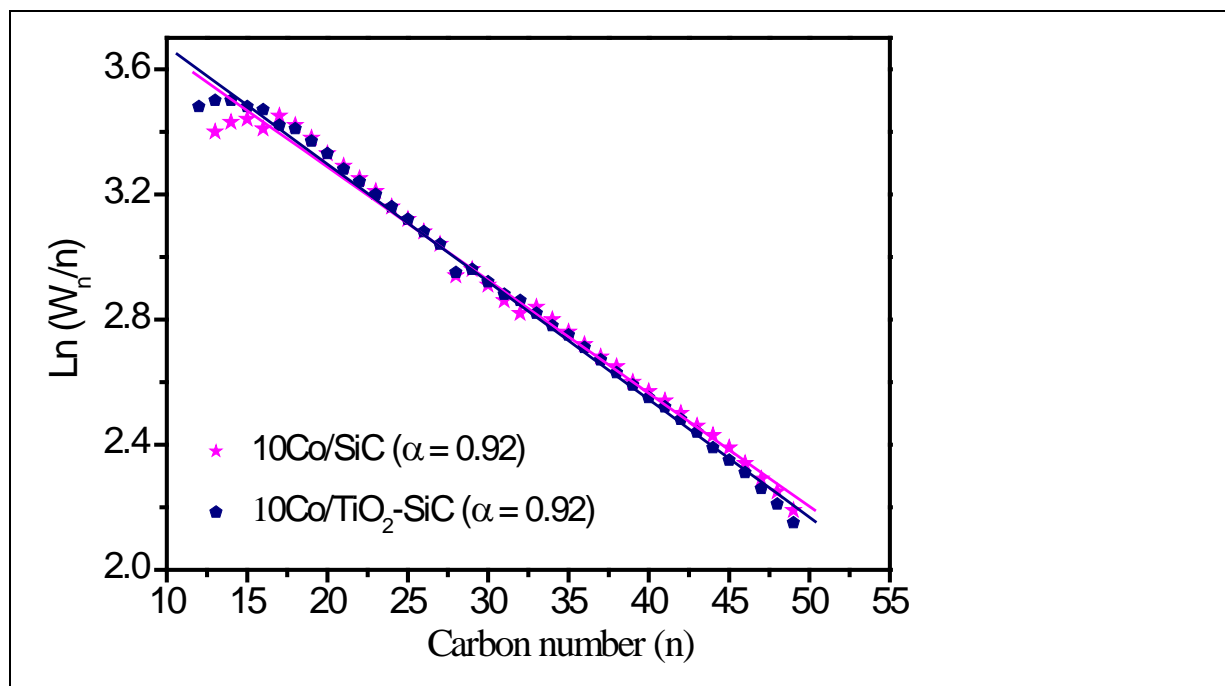


Figure 11. Calculated chain growth factor (α) from the linear portion of the liquid hydrocarbons recovered after FTS tests on the Co/SiC and Co/TiO₂-SiC catalysts.

3.6 Influence of the cobalt loading

In the industrial process the metal loading is generally high at around 30 wt. % in order to ensure a highest CO conversion per pass and to avoid costly recycling of the unreacted products. To study in depth the FTS performance of TiO₂-SiC support, the 30 wt. % cobalt loading was introduced to obtain higher hydrocarbon products per weight of catalyst. Increasing the active phase loading per unit weight of catalyst will inevitably decrease the STY value and thus, the comparison of the FTS performance between both cobalt-based catalysts with different cobalt loadings will be carried out using a specific activity, i.e. ASM representing the weight of liquid hydrocarbon formed per gram of catalyst per hour [$\text{g}_{\text{C}_{5+}} \cdot \text{g}_{\text{catalyst}}^{-1} \cdot \text{h}^{-1}$], instead of the cobalt time yield value as before. Figure 12 illustrates the influence of temperature (215 °C and 220 °C) on the activity of 10 wt. % and 30 wt. % cobalt on TiO₂-SiC catalysts. On the high loaded catalyst the FTS activity approaching a specific rate of $0.47 \text{ g}_{\text{HC}} \cdot \text{g}_{\text{catalyst}}^{-1} \cdot \text{h}^{-1}$ which is among the highest specific rate reported for an unpromoted cobalt catalyst. The FTS activity on the 30Co/TiO₂-SiC catalyst under more severe reaction conditions, i.e. 230 °C and 3800 h⁻¹, is also evaluated and the results are presented in Figure 12 and Table 2. The specific rate steadily increased to $0.59 \text{ g}_{\text{HC}} \cdot \text{g}_{\text{catalyst}}^{-1} \cdot \text{h}^{-1}$ with a relatively higher C₅₊ selectivity, i.e. 91 %. It is also worthy to note that the specific

rate obtained on the unpromoted 30Co/TiO₂-SiC catalyst is also relatively high and more stable compared to those promoted by noble metal obtained on the Co-Re/Al₂O₃, Co-Re/SiO₂ and Co-Re/TiO₂ catalysts as reported by Tsakoumis et al. [50]. The most active catalyst reported in the work of Tsakoumis et al. [50] is the Co-Re/Al₂O₃ with an initial reaction rate of about 0.56 g_{CH₂}·g_{catalyst}⁻¹·h⁻¹ followed by a rapid deactivation down to 0.45 g_{CH₂}·g_{catalyst}⁻¹·h⁻¹ after about 22 h on stream. It is also worth mentioning that the 30Co/TiO₂-SiC catalyst has been run for more than 200 h under different reaction conditions.

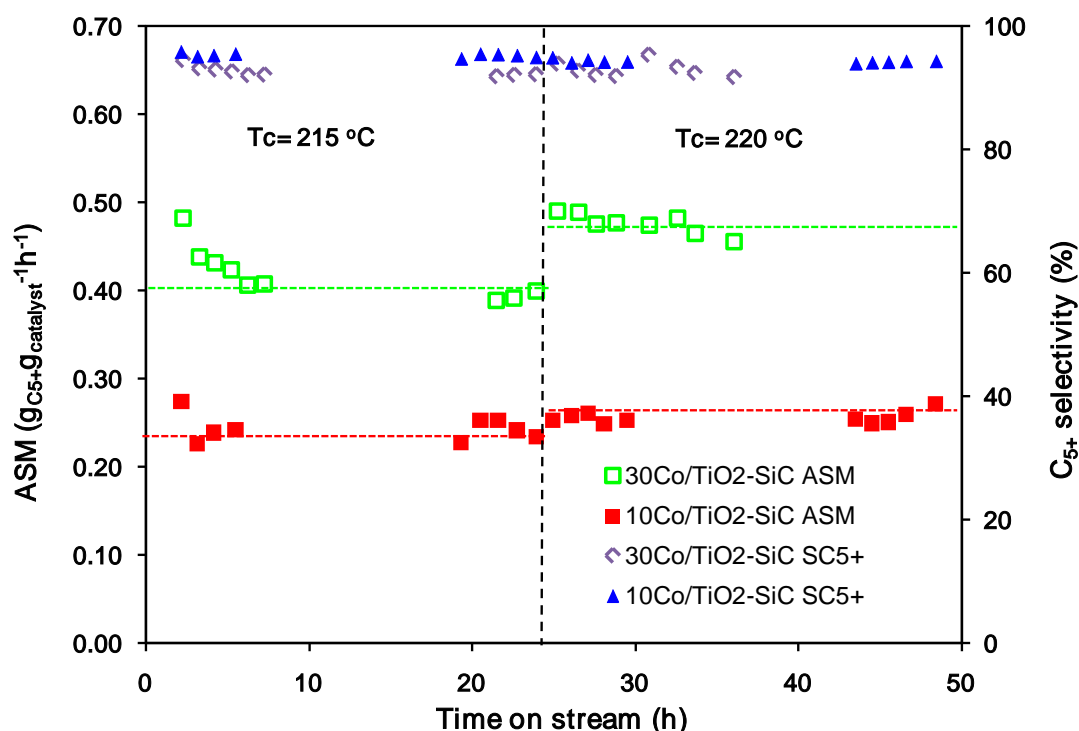


Figure 12. FTS activity and C₅₊ selectivity as functions of time on stream on 10Co/TiO₂-SiC and 30Co/TiO₂-SiC catalysts. Reaction conditions: H₂/CO molar ratio = 2, pure syngas, total pressure = 40 bar, GHSV = 2850 h⁻¹

The stability of the Co/TiO₂-SiC catalyst under FTS conditions was also evaluated with time on stream under optimized FTS conditions, i.e. high space velocity and high reaction temperature, and compared with the one obtained on an undoped SiC containing a cobalt phase promoted with 0.1 wt. % of ruthenium (Figure 13). According to the results the TiO₂ doped SiC-based catalyst exhibits a higher FTS performance than the undoped one promoted with noble metal. The FTS activity remains also stable for about 30 h on stream and confirms the relatively high stability of the catalyst promoted with TiO₂.

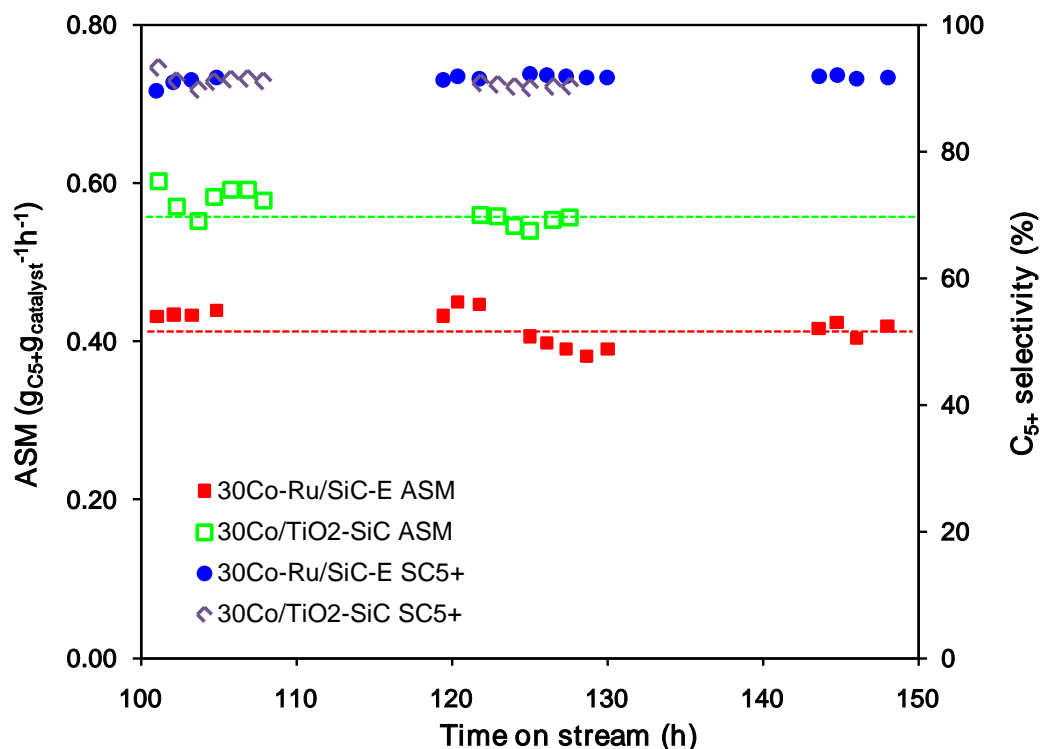


Figure 13. FTS activity and C₅₊ selectivity as functions of time on stream on 30Co/TiO₂-SiC and Co-Ru/SiC-E [20] catalysts. Reaction conditions: H₂/CO molar ratio = 2, pure syngas, total pressure = 40 bar, GHSV (STP) = 3800 h⁻¹, reaction temperature = 230 °C.

4. Conclusion

Silicon carbide doped with TiO₂ with high specific surface area, ca. 100 m²·g⁻¹, can be efficiently employed as support for the cobalt phase in the Fischer-Tropsch synthesis (FTS) reaction. The medium metal-support interaction between the cobalt precursor and TiO₂ leads to the formation of small cobalt particles with enhanced FTS activity compared to the same catalyst supported on the undoped SiC support. Indeed, such small metal particles with a large fraction of surface atoms significantly contribute to the enhancement of the conversion rate of reactants into products. The intermediate product evacuation thus reduces the gradient concentration of the H₂ and CO next to the active site and prevents the formation of light products, while keeping the liquid hydrocarbon selectivity in a high range even at high conversion rate. The meso- and macro-porosity of the support also prevents deactivation of the catalyst by pore plugging due to the formation of carbonaceous residues. Finally, SiC-

based catalysts exhibit a relatively high specific rate along with a high liquid hydrocarbon selectivity compared to those previously reported in the literature.

References

-
- [1] A. Y. Khodakov, W. Chu, P. Fongarland, *Chem. Rev.* 107, (2007) 1692-1744.
- [2] M. E. Dry, *Catal. Today* 71, (2002) 227-241.
- [3] A. Y. Khodakov, *Catal. Today* 144, (2009) 251-257.
- [4] D. Leckel, *Ener. Fuels* 23 (2009) 2342-2358.
- [5] Q. Zhang, J. Kang, Y. Wang, *ChemCatChem.* 2 (2010) 1030-1058.
- [6] C. Perego, R. Bortolo, R. Zennaro, *Catal. Today* 142(2009), 9-16.
- [7] J. I. Yang, J. H. Yang, H. J. Kim, H. Jung, D. H. Chun, H. T. Lee, *Fuel* 89, (2010) 237-243.
- [8] N. Tsubaki, S. Sun, K. Fujimoto, *J. Catal.* 199, (2001) 236-246.
- [9] R. Oukaci, A. H. Singleton, J. G. Goodwin Jr. *Appl. Catal. A* 281 (1999) 129-144.
- [10] S. Storsaeter, O. Borg, E.A. Blekkan, B. Totdal, A. Holmen, *Catal Today.* 100 (2005) 343-347.
- [11] O. Borg, P.D.C. Dietzel, A.I. Spjelkavik, E.Z. Tveten, J.C. Walmsley, S. Diplas, S. Eri, A. Holmen, E. Ryttera, *J Catal.* 259 (2008) 161-164.
- [12] G. L. Bezemer, P. B. Radstakea, U. Falke, H. Oosterbeek, H. P. C. E. Kuipers, A. J. van Dillen, K. P. de Jong, *J. Catal.* 237, (2006) 152-161.
- [13] G. L. Bezemer, J. H. Bitter, H. P. C. E. Kuipers, H. Oosterbeek, J. E. Holewijn, X. Xu, F. Kapteijn, A. J. van Dillen, K. P. de Jong, *J. Am. Chem. Soc.* 128, (2006) 3956-3964.
- [14] S. Zarubova, S. Rane, J. Yang, Y.D. Yu, Y. Zhu, D. Chen, A. Holmen, *Chemsuschem.* 4 (2011) 935-942.

- [15] G. Jacobs, Y. Ji, B.H. Davis, D. Cronauer, A.J. Kropf, C.L. Marshall Appl. Catal. A 333 (2007) 177-191.
- [16] M. Vob, D. Borgmann, G Weldler, J. Catal. 212 (2002) 10-21.
- [17] G.Jacobs, T.K. Das, Y. Zhang, J. Li, G. Racoillet, B.H. Davis, Appl. Catal. A 281, (2002) 233-263.
- [18] Y. Wang, D. P. Vanderwiel, A. L. Y. Tonkovich, Y. Gao, E. G. Baker, US Patent 7,045,486, Battle Memorial Institute, 2006.
- [19] M. Lacroix, L. Dreibine, B. de Tymowski, F. Vigneron, D. Edouard, D. Bégin, P. Nguyen, C. Pham, S. Savin-Poncet, F. Luck, M. J. Ledoux, C. Pham-Huu, Appl. Catal. A : Gen. 397, (2011) 62-72.
- [20] B. de Tymowski, Y. Liu, C. Meny, C. Lefèvre, D. Begin, P. Nguyen, C. Pham, D. Edouard, F. Luck, C. Pham-Huu, Appl. Catal. A : Gen. 419-420 (2012) 31-40.
- [21] A. R. De la Osa, A. De Lucas, J. L. Valverde, A. Romero, I. Monteagudo, P. Coca, P. Sanchez, Catal. Today 167,(2011) 96-106.
- [22] A. R. De la Osa, A. De Lucas, A. Romero, J. L. Valverde, P. Sanchez, Fuel 90, (2011) 1935-1945.
- [23] A. R. De la Osa, A. De Lucas, J. Diaz-Maroto, A. Romero, J. L. Valverde, P. Sanchez, Catal. Today 187, (2012) 173-182.
- [24] H. M. Torres Galvis, J. H. Bitter, C. B. Khare, M. Ruitenbeek, A. Iulian Dugulan, K. P. de Jong, Science 17 (2012) 835-838.
- [25] C. Lesaint, W.R. Glomm, O. Borg, S. Eri, E. Rytter and G. Oye, Appl. Catal. A 351 (2008) 131-135
- [26] T. Witoon, M. Chareonpanich, J. Limtrakul, Fuel Process. Technol., 92 (2011) 1498-1505

-
- [27] H. Xiong, M. A. M. Motchelaho, M. Moyo, L. L. Jewell, N. J. Coville, *J. Catal.* 278, (2011) 26-40.
- [28] P. Nguyen, Ch. Pham, *Appl. Catal. A* 391 (2011) 443-454.
- [29] F. Diehl, A. Y. Khodakov, *Oil & Gas Sci. Technol.* 64 (2009) 11-24.
- [30] G. Jacobs, P. M. Patterson, Y. Zhang, T. Das, J. Li, B. H. Davis, *Appl. Catal. A* 233 (2002) 215-226.
- [31] S. Storsæker, Ø. Borg, E. A. Blekkan, A. Holmen, *J. Catal.* 231 (2005) 405-419.
- [32] Ø. Borg, S. Eri, E. A. Blekkan, S. Storsæter, H. Wigum, E. Rytter, A. Holmen. *Journal of Catalysis* 248 (2007) 89-100
- [33] Ø. Borg, E.A. Blekkan, S. Eri, D. Akporiaye, B. Vigerust, E. Rytter, A. Holmen, *Top. Catal.* 45, (2007) 39-43.
- [34] A. Tavasoli, R. Malek Abbaslou, M. Trepanier, A.K. Dalai, *Appl. Catal. A* 345 (2008) 134–142.
- [35] A.R. De la Osa, A. De Lucas, A. Romero, J.L. Valverde, P. Sánchez, *Fuel* 90, (2011) 1935-1945.
- [36] A.R. De la Osa, A. De Lucas, A. Romero, J.L. Valverde, P. Sánchez, *Catalysis Today* 176 (2011) 298– 302
- [37] P.A. Chernavskii, A.Y. Khodakov, G.V. Pankina, J.-S. Girardon, E. Quinet, *Appl. Catal. A* 306 (2006) 108-119.
- [38] X. Zhu, X. Lu, X. Liu, D. Hildebrandt and D. Glasser, *Ind. Eng. Chem. Res.* 21 (2010), 10682–10688
- [39] E. Rytter, S. Eri, T. H. Skagseth, D. Schanke, E. Bergene, R. Myrstad, A. Lindvag, *Ind. Eng. Chem. Res.* 46 (2007) 9032-9036

- [40] S. Krishnamoorthy, M. Tu, M. P. Ojeda, D. Pinna, E. Iglesia, *J. Catal.* 211 (2002) 422-433
- [41] E. Iglesia, *Appl. Catal. A* 161 (1997) 59-78
- [42] E. van Steen, M. Claeys, *Chem. Eng. Technol.* 31 (2008) 655-666
- [43] C. Aaserud, A. M. Hilmen, E. Bergene, S. Eri, D. Schanke, A. Holmen, *Catal. Lett.* 94 (2004) 171-176.
- [44] J. P. den Breejen, A. M. Frey, J. Yang, A. Holmen, M. M. van Schooneveld, F. M. F. de Groot, O. Stephan, J. H. Bitter, K. P. de Jong. *Top Catal* 54, (2011) 768–777
- [45] J. Hong, W. Chu, P. A. Chernavskii, A.Y. Khodakov. *Journal of Catalysis* 273 (2010) 9–17
- [46] H. Karaca, O. V. Safonova, S. Chambrey, P. Fongarland, P. Roussel, A. Griboval-Constant, M. Lacroix, A. Y. Khodakov. *Journal of Catalysis* 277 (2011) 14–26
- [47] A. Martínez, G. Prieto, J. Rollán, *Journal of Catalysis* 263 (2009) 292–305
- [48] T.M. Eggenhuisen, J.P. Den Breejen, D. Verdoes, P.E. De Jongh, KP de Jong. *JACS*, 132 (2010) 18318-18325
- [49] K. Jalama, J. Kabuba, H. Xiong, L. L. Jewell. *Catalysis Communications* 17 (2012) 154–159
- 50 N. E. Tsakoumis, M. Ronning, Ø. Borg, E. Rytter, A. Holmen, *Catal. Today* 154 (2010) 162-182.

Conclusion and Perspectives

The present work focus on the use of a new type of support, namely silicon carbide (β -SiC), with medium to high specific surface area containing cobalt active phase for the Fischer-Tropsch synthesis (FTS). The FTS process has become one of the most important processes for producing synthetic fuel from natural gas during the last decade in order to compensate the decrease of the crude oil reserves. In this present work, all the tests were carried out in a fixed bed configuration where heat transfer is a crucial problem to be solved in order to maintain the liquid hydrocarbon selectivity. The influence of several parameters, i.e. the thermal conductivity of the support, the nature of the impregnated solvent, the pore size of the support and the doping of the support, was investigated in order to check-out the most appropriate catalyst for this high mass and heat transfer reaction. The different conclusions are summarized below.

Influence of the support conductivity and pore size. The results obtained indicate that the Co-based catalyst supported on SiC carrier in a foam shape, with mesopores and medium thermal conductivity, exhibits a relatively high catalytic performance for the FTS process along with a high selectivity towards liquid hydrocarbons compared to the one supported on an insulator alumina support. On an insulator support, Al_2O_3 foam coated with a thin layer of $\gamma\text{-Al}_2\text{O}_3$, the FTS activity and intrinsic C_5+ selectivity, at medium CO conversion, are similar to those obtained on the SiC support with higher thermal conductivity. However, at higher reaction temperature a large difference in terms of the C_5+ selectivity is observed between the tested catalysts, i.e. 80 % for the SiC-based catalyst and only 54 % for the Al_2O_3 -based catalyst. Such low C_5+ selectivity on the Al_2O_3 -based catalyst is attributed to the presence of local hot spots, which are likely to be generated under these severe reaction conditions, on the catalyst surface which induce secondary cracking reactions leading to the formation of light products instead of long chain waxes. These results indicate that the catalyst surface temperature control can be achieved in an easy way on the SiC-based, due to its high intrinsic thermal conductivity, compared to the insulator support based on alumina. It is also worthy to note that the influence of the mesopores of the support on the liquid hydrocarbon selectivity has also been reported by different authors in the literature. However, in our present study the two catalysts have the same pore size distribution and thus, such influence could be phased out to explain the high selectivity on the SiC-carrier.

The FTS activity can be further improved by supporting the cobalt phase on a hybrid support, i.e. $\gamma\text{-Al}_2\text{O}_3$ coated SiC carrier, which provides higher cobalt dispersion. It is striking

to point out the fact that on such hybrid support the C5+ selectivity is completely different compared to that which was observed on the Al₂O₃-based catalyst, i.e. 80 % for the Al₂O₃-SiC compared to 54 % on the Al₂O₃. These results are attributed to the presence of an underlying conductive SiC matrix which acts as a heat dissipating structure allowing a better homogenization of the catalyst surface temperature and prevents local hot spots formation leading to the selectivity degradation. It is the first time that this support effect is reported. Experiments are underway to measure the radial and axial heat dispersion within the SiC foam structure, under conditions as close as possible to those encountered under the FTS test, in order to get more insight about the possible thermal conductivity effect of the SiC foam support for the FTS performance. The influence of the foam window size on the CO conversion and C5+ selectivity is also underway. Work is also on going to evaluate the FTS performance on this SiC-based catalyst in a more conventional shape, i.e. grains size with granulometry ranged between 0.125 and 0.250mm, in a high aspect ratio tubular fixed-bed reactor, i.e. inner diameter × length, 6mm × 200mm, with a higher space velocity, i.e. 3800 h⁻¹ STP, and will be presented soon.

The chemical inertness of the SiC support also allows one to perform an efficient active phase and support recovery by a simple acid treatment at room temperature. Elemental analysis carried out on the recovered support confirms the complete removal of the metal active phase after the acid treatment. The recovered support can also be fully re-used without any loss in term of catalytic activity and selectivity. This result is of great economical interest as it allows the recovery of the expensive and toxic metal active phase and the disposal of solid supports which is environmentally unacceptable.

Influence of the nature of the impregnated solvent. In this chapter the influence of the impregnated solvent on the active phase dispersion and catalytic performance for the FTS process was investigated. The cobalt was promoted with trace amount of ruthenium in order to decrease the reduction temperature which prevents excessive sintering of the active phase.

Cobalt supported on silicon carbide catalyst prepared via an incipient wetness impregnation using ethanol as solvent exhibits an extremely high FTS activity along with a high S_{C5+} selectivity under severe FTS conditions, i.e. high temperature (235 °C) and high gaseous space velocity (ca. 3800 h⁻¹). The high FTS activity was linked to the large pore size of the catalyst which provides a high escape rate for the product, reducing by such a way the pore plugging by heavy liquid hydrocarbons, and facilitating high access of the reactant to the

active sites located within the pore. The relatively high S_{C_5+} selectivity could be attributed to the thermal conductivity of the support which prevents hot spot formation or gradient temperature inside the catalyst bed which could promote the formation of light products. The Co–Ru/SiC-E catalyst also exhibits an extremely high FTS stability over more than 400 h. ^{59}Co zero field NMR analysis carried out on the catalysts indicates that while the overall fcc Co to hcp Co ratio does not change significantly upon the solvent that is used, the ethanol solvent seems to promote a much larger amount of small size (< 8 nm) Co particles. These small particles have a large surface-to-volume ratio and could be responsible for the enhanced FTS activity. The NMR analysis also evidences for the first time the quantitative determination of the formation of an alloy between Co and Ru when using ethanol as the impregnation solvent. Work is on going to determine quantitatively the relative concentration of the different cobalt species present in the sample, by varying the acquisition temperature from 4 to 77 K and to correlate these values with the FTS activity.

Influence of the titanium doping. In this chapter silicon carbide doped with titanium oxide was used as a new support for cobalt phase. The titanium was used as a doping and was introduced directly into the ceramic precursor matrix before carburization process. The resulting solid contains a mix of silicon carbide and titanium carbide which was further converted into TiO_2 doped SiC material after a calcinations step in air at 550°C .

This silicon carbide doped with TiO_2 possesses a relatively high specific surface area, ca. $100\text{ m}^2\cdot\text{g}^{-1}$, and was further employed as support for the cobalt phase in the Fischer-Tropsch synthesis (FTS) reaction. The medium metal-support interaction between the cobalt precursor and TiO_2 leads to the formation of small cobalt particles (5-15 nm) with enhanced FTS activity compared to the same catalyst supported on the undoped SiC support (30-40 nm). These small cobalt particle size lead to a significant enhancement of the FTS performance compared to that obtained on the undoped catalyst with bigger active phase particle size. Indeed, such small metal particles with a large fraction of surface atoms significantly contribute to the enhancement of the conversion rate of reactants into products. Indeed, the characteristics of the surface atoms are significantly different from atoms in deeper layers such as bond distances, geometries and bonding energies are altered by the reduced local coordination at the surface. The adequate pore size distribution of the support, i.e. meso- and macro-pores contribution, also facilitates the evacuation of the intermediate products, keeping the active sites more available for reactants. The intermediate product evacuation thus reduces the gradient concentration of the H_2 and CO next to the active site and prevents the formation

of light products, while keeping the liquid hydrocarbon selectivity in a high range even at high conversion rate. The meso- and macro-porosity of the support also prevents deactivation of the catalyst by pore plugging due to the formation of carbonaceous residues. Finally, SiC-based catalysts exhibit a relatively high specific rate along with a high liquid hydrocarbon selectivity compared to those previously reported in the literature for the FTS process.

Perspectives

The interplay between the different parameters have allowed us to develop one of the most active and selective catalyst for the FTS process. The results obtained allow us to propose several perspectives in order to optimize this new type of catalyst to bridge the gap between the laboratory scale development and pre-industrialization process.

The first one will concern the influence of promoter, i.e. Ru or Pt, on the catalytic performance of the FTS process. The support is the most active one developed during this work, namely the SiC doped with TiO₂. It is expected that the presence of the promoter will help in the dispersion of cobalt particles which provide a better FTS performance and also a higher stability as a function of time on stream.

The second one will be focused on the improvement of the support effective surface area by introducing a superstructure consisted with 1D nanocarbons such as nanofibers or nanotubes with higher specific surface area without any micropores. It is expected that such hybride support will provide a higher dispersion of the active phase, either pure or promoted with trace amount of noble metal, and thus a better catalytic performance, without a problem linked with mass transfer due to the lack of micropores.

Finally, the morphology of the support, foam or extrudates, will be also investigated in order to anticipate the transfer from the laboratory scale to the industrial development.

We will also focus our attention on the development of a new characterization technique which was implemented within this work, namely the ⁵⁹Co NMR technique. The results obtained have shown that this technique can be efficiently applied to determine the active phase particle size as a function of the catalyst pretreatment. It is expected that this technique will provides great opportunities for establishing a detailed understanding of the

catalyst structure and the catalytic activity in order to develop a more rational design of the FTS catalysts.

Fischer Tropsch synthesis on conductive on silicon carbide based support

Résumé

La synthèse de Fischer-Tropsch (SFT) permet la transformation d'un mélange de gaz de synthèse, i.e. H_2 et CO , issu des différentes matières premières (charbon, gaz naturel ou biomasse) en hydrocarbures synthétiques. Les catalyseurs généralement utilisés en SFT sont à base de fer ou de cobalt supporté sur alumine ou silice. Dans ce travail, le carbure de silicium (SiC) a été proposé comme nouveau support de remplacement pour la SFT.

Les résultats obtenus ont montré que les catalyseurs à base de cobalt supporté sur du SiC , contenant essentiellement des mésopores, sont actifs et sélectifs pour la réaction de SFT par rapport aux catalyseurs traditionnels supportés sur alumine ou silice. L'activité en SFT peut être améliorée en utilisant de l'éthanol comme solvant d'imprégnation ou en ajoutant un promoteur tel que le ruthénium. Le dopage du support de départ par du TiO_2 contribue également à une forte augmentation de l'activité en SFT grâce à la formation de petites particules de cobalt présentant une activité en SFT plus élevée. La forte interaction entre le TiO_2 et le cobalt permet également d'améliorer d'une manière considérable la stabilité du catalyseur.

Mots clés: Synthèse Fischer-Tropsch, carbure de silicium, cobalt, catalyse

Résumé en anglais

The Fischer-Tropsch synthesis (FTS) allows the transformation of a mixture of synthesis gas, i.e. H_2 and CO , into valuable liquid hydrocarbons. The catalysts generally used in FTS are based on iron or cobalt supported on alumina or silica. In the present work, silicon carbide (SiC) has been proposed as a replacement media to traditional supports.

The results obtained indicate that the mesoporous SiC containing cobalt catalyst exhibits a good FTS activity and an extremely high selectivity towards liquid hydrocarbons compared to other FTS catalysts supported on alumina or silica. The FTS activity on the Co/SiC catalyst can be improved by changing the impregnation solvent or by promoting the cobalt phase with trace amount of noble metal. The doping of the SiC support with TiO_2 phase also significantly improves the FTS activity keeping a similar high selectivity thanks to the formation of small cobalt particles in contact with the TiO_2 phase.

Keywords: Fischer-Tropsch synthesis, silicon carbide, cobalt, catalysis